

DLIO
7
6
ER-68-69-18
p. 2

UNIVERSITY OF COLORADO
LIBRARY

LABORATORY MEASUREMENTS OF AIR FLOW OVER WIND
WAVES FOLLOWING THE MOVING WATER SURFACE

Po-cheng Chang

December 1968

LIBRARIES
JUL 14 1971
COLORADO STATE UNIVERSITY

LABORATORY MEASUREMENTS OF AIR FLOW OVER WIND

WAVES FOLLOWING THE MOVING WATER SURFACE

Po-cheng Chang

Colorado State University

Fort Collins, Colorado

December 1968

CER68-69PcC18

ABSTRACT

LABORATORY MEASUREMENTS OF AIR FLOW OVER WIND WAVES FOLLOWING THE MOVING WATER SURFACE

This dissertation presents a laboratory study of the dynamic properties of air flow over small wind-generated water waves. Through the measurements of mean velocity profiles, turbulent fluctuation profiles and energy spectra, the detailed structure of turbulent wind immediately above and between the crests of progressive water waves has been examined.

A self-adjusting probe positioner was designed, which allowed a velocity sensor (a hot wire anemometer) to measure instantaneous air velocities at a fixed distance from a moving water surface with waves of a dominant frequency, 2 to 3 Hz. With the aid of a digital computer, the desired parameters of air flow were obtained by a statistical technique which was developed to sample and average simultaneous recordings of water surface displacements and instantaneous air velocities.

The statistical properties of water surface which include wave spectra, probability distributions of water surface elevation and its time derivatives, give good agreement with the results obtained by previous investigators. The waves investigated have the ratio of wave celerity and air friction velocity on the average close to one. For those waves, the effect of the moving surface seems to cause little deviation in the dynamic properties of the velocity field from those found over solid boundaries.

Mean properties of the turbulent air flow referred to the mean water level were obtained by continuous sampling of the air flow over many waves with a sensing probe either at a fixed distance from the mean water level (fixed probe measurement) or at a constant distance from the moving water surface (moving probe measurement).

It was found that for continuously averaged measurements the fixed probe yielded results which deviate less from the local mean than the moving probe results. This holds for the mean velocity distributions and especially for the turbulent quantities.

The results of local air properties indicate that, on the average, air flow separates from the wavy water surface just behind crests and reattaches somewhere on the windward face of the next wave. The measured turbulent quantities consistently show the characteristics of a separated air flow. The separation phenomenon suggests that, without some modification, the Benjamin-Miles' shearing flow mechanism is inapplicable to the growth of fully developed small water waves. The observed flow configuration tends to support the separation mechanism of energy transfer originally outlined by Jeffreys, and later explored further by Stewart.

This study demonstrates the usefulness of using a wave following probe to obtain a more complete description of the dynamic properties of both air and water near the interface. In principle, the methods developed here could be used to further explore the properties of air flow over undulating surfaces, including the determination of the local Reynolds stresses.

Po-cheng Chang
Fluid Mechanics Program
Civil Engineering Department
Colorado State University
Fort Collins, Colorado 80521
December 1968

ACKNOWLEDGMENTS

The author wishes to express his deep gratitude to Dr. Erich J. Plate for his help, guidance and encouragement during the course of this investigation, and to Dr. George M. Hidy for his constant interest and many valuable suggestions.

Messrs. Arpad Gorove and Robert Atchley, technicians in CSU Fluid Mechanics and Diffusion Laboratory, helped in design and construction of the moving probe. Mr. Thomas L. Davis of NBS at Boulder provided assistance in the analog to digital conversion of the data. Mrs. Lois Niemann did the computer programming required for the data reduction. Mr. Kuo Shyong Su helped with data collection and Mr. Tzu-shen Lin assisted in reducing the data. Miss Hanae Akari prepared the figures and Mrs. Mary Fox and Mrs. Alta Defenbaugh typed the thesis. Their help is greatly appreciated. Without it, this work would not have been possible.

For their comments and critical review of the dissertation, gratitude is expressed to Dr. Jack E. Cermak, Dr. Daryl B. Simons and Dr. Samuel W. Marshall who served on the dissertation committee.

Special thanks are given to Mr. Thomas L. Davis and the National Bureau of Standards for the free use of the Analog to Digital Data Conversion System at Boulder. Financial support for this research was provided by the National Science Foundation in connection with its contract with the National Center for Atmospheric Research, and its grant No. GK-188 to Colorado State University.

TABLE OF CONTENTS

<u>Chapter</u>		<u>Page</u>
	LIST OF TABLES	ix
	LIST OF FIGURES.	x
	LIST OF SYMBOLS.	xiii
I	INTRODUCTION	1
	1.1 Purpose	1
	1.2 Literature Review	3
	1.2.1 Wave generation by wind.	3
	a. Theoretical background.	3
	b. Experimental background	7
	1.2.2 Air flow over water waves.	8
II	OBSERVATIONAL CONSIDERATIONS	11
	2.1 Notation.	11
	2.2 Interpretation of Air Flow Measurements over a Moving Water Surface.	11
	2.3 Velocities Obtained from Moving Probe Experiments	14
	2.3.1 Measured mean and turbulent quantities . .	17
	2.3.2 Separation of $\overline{u_o'^2}$ from $\overline{\hat{u}_o^2}$	17
	2.3.3 Estimation of turbulent energy spectrum from moving probe measurements	18
	2.4. Observation of Local Flow Properties.	19
	2.4.1 Average dominant waves	20
	2.4.2 Local air flow properties.	22
III	APPARATUS, EXPERIMENTAL PROCEDURE AND DATA REDUCTION TECHNIQUES	25
	3.1 The Wind Tunnel Flume Combination	25

TABLE OF CONTENTS - Continued

<u>Chapter</u>		<u>Page</u>
	3.2 Measurements of Water Surface Elevations.	27
	3.3 Measurements of the Mean Velocity and Turbulent Fluctuations of Air by a Sensor Fixed in Space	29
	3.4 Measurements of Air Velocity by the Moving Probe	32
	3.4.1 The system for the self-adjusting positioner	32
	3.4.2 Dynamic calibration of the self-adjusting positioner	36
	3.4.3 Data collection procedure.	41
	3.4.4 Digitization of analog data.	45
	3.4.5 Statistical sampling and averaging of digital data	46
IV	EXPERIMENTAL RESULTS	49
	4.1 Geometry and Statistical Properties of the Water Surface	49
	4.1.1 Probability distributions of water surface elevation and their rates of change.	51
	4.1.2 The frequency spectra of wind waves.	54
	4.1.3 Average dominant waves	56
	4.2 Properties of the Turbulent Air Flow over Water .	59
	4.2.1 Simultaneous visual records of turbulent air and water waves.	59
	4.2.2 Mean velocities.	66
	a. Local mean velocity profiles.	66
	b. Mean velocity profiles with reference to the mean water level	72
	4.2.3 Longitudinal turbulent fluctuation	76

TABLE OF CONTENTS - Continued

<u>Chapter</u>		<u>Page</u>
	a. Local $\sqrt{u'^2}$ profiles.	76
	b. Longitudinal $\sqrt{u'^2}$ profiles with reference to the mean water level . . .	81
	4.2.4 Turbulent energy spectra	86
	a. Local energy spectra.	86
	b. Energy spectra of longitudinal velocity fluctuations over mean water surface. .	94
V	DISCUSSION	100
	5.1 General Characteristics of the Water Surface Serving as the Lower Boundary of Air Flow	100
	5.1.1 Symmetry of wind wave shape.	101
	5.1.2 Properties of the frequency spectra of wind waves	103
	5.2 Turbulent Air Flow over Water	104
	5.2.1 Separation and the streamline pattern. . .	104
	a. The consequences of separation.	109
	5.2.2 Comparison of measured local velocity profiles with other experiments.	112
	5.3 Comparison of Experimental Results with Existing Theoretical Models.	115
VI	CONCLUSIONS.	119

LIST OF TABLES

<u>Table</u>		<u>Page</u>
1	Local Mean Velocity Data of Case 1	69
2	Local Mean Velocity Data of Case 2	69
3	Local $\sqrt{u'^2}$ Data of Case 1	79
4	Local $\sqrt{u'^2}$ Data of Case 2	79

LIST OF FIGURES

<u>Figure</u>		<u>Page</u>
1	Schematic diagram for the procedure of fixed probe measurement and moving probe measurement over a perturbed surface	13
2	Schematic diagram for the procedure of determining average dominant waves and local air velocity properties	21
3	Schematic diagram of the Colorado State University wind-water tunnel	26
4	Schematics and block diagrams of the capacitance bridge	28
5	Calibration curves of capacitance wave gauge, probe positioner and hot wire anemometer	30
6	Control electronics of self-adjusting positioner	33
7	Mechanical system of self-adjusting positioner	34
8	Schematic diagram of the control principle of self-adjusting positioner	34
9	Spectrum of water waves, spectrum of probe positions, and cospectrum and quadrature spectrum of water waves and probe positions	39
10	Gain and phase lag of the transfer function of self-adjusting probe positioner; and the normalized covariance of water waves and probe positions	40
11	Simultaneous Brush recorder traces of water waves and probe positions	42
12	Block diagram of the data collection system	43
13	Time record of water surface displacements	50
14	Probability distributions of water surface displacements and their time derivatives	52
15	Energy spectra of water waves	55
16	Average dominant wave (I)	57
17	Average dominant wave (II)	58

LIST OF FIGURES - Continued

<u>Figure</u>		<u>Page</u>
18	A set of average dominant waves (I)	60
19	A set of average dominant waves (II)	61
20	Simultaneous records of turbulent air and water waves. . .	62
21	Local mean velocity profiles (I)	67
22	Local mean velocity profiles (II).	68
23	Confidence band of the local mean velocity profile	70
24	Comparison of air velocity profiles at different positions along the waves.	73
25	Mean velocity profiles above the mean water level.	74
26	Local turbulent RMS profiles (I)	77
27	Local turbulent RMS profiles (II).	78
28	Turbulent intensity profiles above the mean water level. .	82
29	Variation of mean velocity at a given point along the water waves.	85
30	Correlation of air and water motions	87
31	Local turbulent energy spectra	88
32	Inferred energy spectrum	92
33	Turbulent energy spectrum measured with a fixed probe. . .	95
34	Turbulent energy spectrum measured with a moving probe . .	97
35	Turbulent energy spectrum corrected for wave-probe induced fluctuations	99
36	Comparison of normalized average waves with sine wave and trochoidal wave	102
37	Streamline pattern over wind generated waves (I)	106
38	Streamline pattern over wind generated waves (II).	107

LIST OF FIGURES - Continued

<u>Figure</u>		<u>Page</u>
39	Possible configuration of streamlines above progressive water waves	110
40	Air velocity profiles above wavy surface (from Schooley, Motzfeld and Bonchkovskaya)	113

LIST OF SYMBOLS

<u>Symbol</u>	<u>Definition</u>
a	Wave amplitude
A,B	Real value constants
c	Phase speed of wave
Co	Cospectrum
Coh	Coherency or normalized covariance
e	Voltage
E	Energy of fluid
f	Frequency in Hz ; subscript denotes the quantities associated with fixed probe measurement
g	Gravitational acceleration
h	Unit impulse function
H (s)	Transfer function
\bar{H}	Average wave height
K	Wave number
o	Subscript denotes the quantities associated with moving probe measurement
P	Probe positions
\bar{P}	Average wave period
Q	Quadrature spectrum
R	Correlation function
s	Jeffreys' sheltering coefficient
S	Energy spectrum function
t	Time
u,v,w	Velocity component in x, y and z directions, respectively
u*	Friction velocity

LIST OF SYMBOLS - Continued

<u>Symbol</u>	<u>Definition</u>
u_p	Water particle velocity due to wave
u_s	Water surface velocity due to wind driven current
u', v'	Turbulent fluctuations in x and y directions, respectively
u''	Velocity fluctuation with respect to sample mean
\hat{u}	Wave-probe induced velocity fluctuation
u_∞	Free stream velocity
x	Longitudinal downstream direction
y	Vertical direction from the mean water level
z	Lateral direction
α, β, γ	Real value constants
δ	Boundary layer thickness
ξ	Vertical distance from moving water surface
η	Water surface perturbation above mean water level
ρ	Fluid density
ν	Kinematic viscosity
ω	Frequency defined as $2\bar{\lambda}f$
κ	Von Karman universal constant = 0.40
τ	Time delay
ϕ	Phase angle
ψ	Stream function
$\bar{\lambda}$	Average wave length
ϵ	Dissipation rate
σ	Standard deviation

Any other symbols which do not appear in this list will be described whenever they first appear in the text.

Chapter 1

INTRODUCTION

1.1 Purpose

The problems involved in air-water interaction such as momentum, heat and mass transfer across the interface are complicated by the fact that the interface boundary is not prescribed but deforms continuously and irregularly as a consequence of the dynamic interaction of the air and water. During the past 50 years, a number of theoretical and empirical efforts have been made to relate the water waves to the wind. These efforts have met with partial success. Further theoretical progress can be expected only when the characteristics of the wind field above and very close to the water surface have been determined in more detail experimentally.

With this in view, Deacon (1963) appealed for "as serious a study of the flow of turbulent air over a water surface as is made of the flow of air over the wings of an aircraft". Stewart (1967) pointed out the "crying need" for measurements in the air below the level of the wave crests. Thus far such experiments have not been performed because the difficult experimental techniques required by the undulating boundary were not available.

In an attempt to improve the available experimental methods for measuring air flow over water waves, a new technique has been developed, and is described in this dissertation. A self-adjusting probe positioner was designed, and the data taken using it were then analyzed for statistical properties of the air flow with a digital computer. The servo-controlled probe positioner made it possible to measure with a hot wire

anemometer the instantaneous air velocity at a fixed distance from the surface. By digitizing the signals of the hot wire anemometer and the water wave gauge and by sampling and averaging simultaneous recordings of instantaneous air velocities and water surface displacements one can obtain the statistical structure of turbulent air near the moving water surface.

This technique is applied to a study of the dynamic properties of air flow over small wind-generated water waves in a wind-tunnel flume. Specifically, mean velocity profiles, turbulent fluctuation profiles, and energy spectra at various positions along a defined average wave are obtained. From these results, the flow field above the water surface is reconstructed and its interaction with the waves is inferred. Certain statistical properties of the water surface are calculated to specify the characteristics of the lower boundary for the air flow. Included are such properties as the probability distribution of the water surface and of the first and second time derivatives of water surface elevation, as well as wave amplitude spectra.

Also included in this study is a discussion of the overall mean properties of the air flow with reference to the mean water level. These properties are obtained by continuous sampling of the air flow over many waves with a sensing probe either at a fixed distance from the mean water level or at a constant distance from the moving water surface. The results are compared to those obtained by previous investigations over both water and solid surfaces. There also is included a discussion of the contributions of local mean velocity fluctuation to the experimentally observed mean turbulent fluctuation, as measured by the moving probe.

Finally, the applicability of the existing theoretical models of wave generation by wind are briefly examined by comparing the underlying physical assumptions with the experimental results of this study.

1.2 Literature Review

1.2.1 Wave generation by wind

a. Theoretical background.--Several hypotheses have been proposed to explain the physical processes involved in the generation of waves by wind. Each hypothesis ignores one or more aspects of the problem and only attempts to describe a certain stage of wave growth. Since energy can be transferred from the air to the surface through the action of the normal pressure fluctuations in the air or by the shearing stress at the interface, the problem can be treated either as a stochastic process or a stability problem.

The group of hypotheses which explains the growth of waves in terms of stochastic fluctuations of the normal pressure have been advanced by Eckart (1953) and Phillips (1957). The other group of hypotheses considers the wave growth as a consequence of the instability of a small perturbation applied to the air-water interface. This group includes the work of Helmholtz (1868), Kelvin (1871), Wuest (1949), Lock (1954), Jeffreys (1925), Benjamin (1959) and Miles (1957, 1959, 1962a, 1962b, 1967).

Among the theories mentioned above only the models of Jeffreys, Phillips and Miles-Benjamin are of realistic interest to the generation of water waves by turbulent wind. Therefore, only these mechanisms will be described further. For comprehensive surveys of the other theories, the reader is referred to Ursell (1956), Kinsman (1965), Phillips (1966), Shemdin and Hsu (1966), and Drake (1967).

(i) Jeffreys' separation mechanism.--By analogy to flow separation near the downstream region of a bluff body, Jeffreys (1925) divided the energy transfer rates from the wind to the waves into two parts: (a) form drag associated with flow separation in the lee of the wave crest and, (b) tangential stresses associated with skin friction. Neglecting the reaction of skin friction, Jeffreys postulated a "sheltering coefficient", s , to account for the flow separation.

In Jeffreys' mathematical model, a complicated air-water interface $\eta(x, t)$ has been idealized into a simple harmonic wave train of length $2\pi/k$, traveling with a phase speed c , written as

$$\eta = a \cos k(x - ct) \quad (1-1)$$

where t is time, and a amplitude. Only the periodic component of wind-exerted pressure in phase with the wave slope is considered in the calculation of work done by the wind on the wave. This is

$$s \rho_a (u_\infty - c)^2 \frac{\partial \eta}{\partial x} \quad (1-2)$$

where ρ_a is air density and u_∞ is free stream velocity. Jeffreys indicated that $s < 1$, but no method of calculating the coefficient was given.

The work done by the wind on the water is then

$$\frac{dw}{dt} = s \rho_a (u_\infty - c)^2 c \int \int (\partial \eta / \partial x)^2 dx dy \quad (1-3)$$

(ii) Phillips resonance mechanism.--Phillips (1957) suggested that energy may be transferred to the water by the direct resonance action of the normal pressure fluctuations in the air with free modes of oscillation in the water. The water was assumed to be

inviscid and thus irrotational. There is no coupling between air and water motion; i.e., the statistical properties of the pressure fluctuations are assumed to be independent of the wave generated by the air flow itself. Wave growth is a result of a resonance between the water wave components and the pressure fluctuations having the same wave lengths and wave speed. Under such conditions, the predicted growth rate is linear in time, or, for a steady wind, with fetch.

(iii) Miles-Benjamin shear flow mechanism.--Using the same pressure distribution as Jeffreys, neglecting the viscous effects in the air and water and assuming no interaction between the turbulent components in the air and in the water, Miles (1957) formulated a wave generation mechanism which does not consider flow separation. The feedback of waves induces a linear coupling between the water surface and the aerodynamic pressure, but the air flow causing the waves to grow is considered not to be altered appreciably by the motion of the wavy surface.

The chosen free surface profile, η , is a sinusoidal function expressed in complex notation as

$$\eta = \exp [i k (x - ct)] , \quad ka \ll 1 \quad (1-4)$$

Following Miles (1957), the aerodynamic pressure P_a is assumed to have the form

$$P_a = \rho_a u_1^2 k a [\alpha \cos k (x - ct) - \beta \sin k (x - ct)] \quad (1-5)$$

where α and β are dimensionless pressure coefficients which are in-phase and out-of-phase with the surface wave respectively, u_1 is a reference speed for the air. The resulting total energy growth is then

$$E = E_0 \exp (2/g \rho_a / \rho_w k^2 u_1^2 \beta x) \quad (1-6)$$

where E_0 is energy at $t=0$ or $x=0$, ρ_w is the mass density of water, and g is the gravitational acceleration. Only the out-of-phase pressure component β transmits energy from the air flow to the wave and the growth rate is exponential. On the basis of the inviscid Orr-Sommerfeld equation, Miles (1957) obtained an approximate solution of β for a shear flow with logarithmic velocity distribution. The magnitude of β depends on $\frac{u''(y_c)}{u'(y_c)}$, where $u'(y_c)$ and $u''(y_c)$ are, respectively, the first and second derivatives of the mean velocity profile $u(y)$ at the critical layer y_c where the mean air velocity equals the phase speed of the surface wave.

If Jeffreys' mechanism is expressed in terms of growth rate, it is given by

$$E = E_0 \exp \left[2/g \rho_a/\rho_w k^2 (u_\infty - c)^2 s x \right] \quad (1-7)$$

Although Jeffreys' sheltering coefficient s must be determined empirically, it is believed s is greater than β so that a larger exponential growth rate is expected for separation mechanism.

Miles inviscid theory has been explained physically by Lighthill (1962). According to Lighthill, Miles' mechanism requires a vortex distribution such that an enclosed streamline pattern (a "cat's eye") appears over the wave crest in the neighborhood of the critical height in the reference system of $u-c$.

On the basis of observation that the air flow does not seem to be wave-like at a short distance above the waves, Stewart (1967) argues that Miles' model cannot be correct and proposed a streamline pattern, in Lighthill's $u-c$ reference system, where the Lighthill cat's eye is pulled away from crests down into troughs. Therefore, an eddy will

exist only between and below the crests. Thus, the transfer of momentum and growth of the waves is caused by a kind of separation mechanism.

Miles (1960) in a later paper incorporated Phillips' mechanism into his inviscid model in an attempt to give a comprehensive model over the complete spectrum of waves. Miles (1962) also considered the possibility of energy transfer by a shear flow to short surface waves through the viscous Reynolds stresses in the close vicinity of the surface and over a certain range of the spectrum, through resonance between the water waves and the air Tollmein-Schlichting waves. This mechanism has also been considered by Benjamin (1959). This viscous mechanism of Benjamin and Miles is applicable to the waves with critical layer in the air and very close to the water surface. In this study, $c/u^* \approx 1$, the critical layer lies on the average in the laminar sublayer, thus only the Benjamin-Miles shear flow mechanism is relevant to the waves investigated here.

b. Experimental background.--Many experiments have been made in an attempt to verify the reviewed hypotheses, and to provide information to expand the theoretical models. The experiments of Stanton et al. (1932), Motzfeld (1937), Thijsse (1951), Bonchkovkaya (1955), Larras and Claria (1960) have been aimed at verifying the underlying assumptions of Jeffreys' model. They simulated the air flow over water by blowing air over stationary, solid, and sinusoidal surface and measured pressure distribution above the boundary. All of the above experiments, with the exception of Thijsse's results, gave sheltering coefficients too small to generate waves. Because these experiments disregard all dissimilarities of the dynamics of energy transfer between water surface and a solid boundary, an experimental verification of Jeffreys' model is still missing.

The most direct approach to test the theories of Phillips and Miles is to compare the theoretical growth rate with that obtained from spectral measurements. Such measurements have been performed by Cox (1958), Hamada (1963), Holmes (1963), Hidy and Plate (1966), Wiegell and Cross (1966), Bole and Hsu (1967), and Plate et al. (1968). Shemdin and Hsu (1966), on the other hand, have examined Miles's (1957) theory directly by measuring the perturbed pressure distribution with a sensor following the waves. By comparing the experimental results with the theoretical models, the agreement between theories and experiments is still far from satisfactory. In general, no direct evidence is found for turbulent pressure fluctuations to be responsible for the wave generation. Miles (1962) viscous shear flow mechanism is only applicable to very short fetches after the first visible wave, and the exponential growth rates are consistently greater than that predicted by Miles (1957) inviscid theory. Many investigators attribute the growth rate discrepancies from Miles (1957) theory to flow separation but none of them have submitted any direct experimental evidence for the existence of separation.

The deficiencies of the wind wave generation theories are partly due to a very incomplete state of knowledge of aerodynamic properties of air flow near the air-water interface. It is therefore the purpose of this study to explore the detailed structure of air flow above waves. A short review of the known properties of air flow over the water mainly in the aspect of the experimental work is given below.

1.2.2 Air flow over water waves

Miles (1957) assumed a logarithmic air velocity profile above the mean water level in his shear flow model, and also a wave pattern

which was so low in amplitude that it did not penetrate the viscous sublayer. In marine physics the logarithmic profile has been used as a working formula to describe the air flow in the atmospheric boundary over water. Stewart (1961), in considering the effect of the transfer of momentum to surface waves from wind blowing over water, was led to a contrary conclusion, suggesting that the mean velocity profiles near the water surface need not be logarithmic below the critical layer where $u = c$. Miles (1965), from quantitative calculations, found the effect due to the Stewart's momentum transfer to be small. This discussion seems to be the first time the profiles of air flow over water has drawn serious consideration, by accounting the dynamic properties of a deformable boundary.

Recently laboratory studies of Hidy and Plate (1966), Plate and Hidy (1967), Shemdin and Hsu (1966), Hess (1968), Plate *et al.* (1968) and geophysical studies of Takeda (1963), Hamblin (1965), Weiler (1966), have indicated that the velocities near the surface are greater than expected from the corresponding logarithmic form drawn through the upper portion of the profiles. The logarithmic profiles seem to hold only during the very early stages of wave growth. Phillips (1966) and Shemdin (1967) suggested that the technique of measuring mean velocities with a fixed probe above wavy water surface requires correction for the effects of shifting streamlines and of wave-induced perturbation. However, both Shemdin and Phillips predict that the measured velocity distribution would be lower than the logarithmic distribution while the duration of the actual profile is in the opposite direction. The shape of the observed profiles has thus not been explained as yet.

The structure of turbulence in the air above the water has been investigated only recently. The geophysical studies of Grant et al. (1962), Pond et al. (1963), Pond et al. (1966) and Weiler (1966) provide some preliminary information on the turbulent structure above the sea through various correlation and spectral calculations from data on the air velocity field. Measurements in the laboratory have been performed by Hess et al. (1968), Karaki and Hsu (1968) and Plate et al. (1968). Those investigations generally show no strong difference in u' and v' that would distinguish the turbulent structure of air flow over the water from that over the flat plate. Only the shearing stresses show a marked departure from shearing flow over solid surface and over water waves.

All of the experimental data mentioned above were taken with a probe fixed relative to mean surface by continuous sampling, and thus yield information which is of little use in defining the details of the air flow pattern near the water surface. Before the investigation of this study, Schooley's (1963) local mean velocity profiles at several positions along water waves appear to be the only measurements concerning the instantaneous local properties near the air-water interface. This type of data yields flow configuration in the vicinity of air-water interface, which give a direct test of the validity of theoretical models. It seems appropriate therefore to investigate the boundary layer over water in more detail with particular attention to the region close to water surface.

Chapter II

OBSERVATIONAL CONSIDERATIONS

The properties of air flow over a moving water surface can be observed from several different points of view. In this chapter the differences in measurements with a fixed probe and a probe which follows the wave motion will be discussed, and methods developed for obtaining the velocity parameters for the two different reference coordinate systems, will be described.

2.1 Notation

An orthogonal Cartesian coordinate system (x,y,z) will be used to specify the positions in the physical space. x is the longitudinal downstream direction, and the original $x = 0$, is located at the downstream edge of the aluminum plate that covers the water near the inlet of the tunnel. y is the vertical direction taken upwards from the mean water level. z is the lateral direction. For the measurements taken with respect to the moving water surface, the distance from the point of measurement to the moving water surface is defined as ξ . The velocity components are (u,v,w) .

2.2 Interpretation of Air Flow Measurements over a Moving Water Surface

Three types of measurements can be performed to determine the air velocity field above progressive water waves. The first type of measurement, which will be called fixed probe measurement, is made at a fixed point relative to a fixed reference frame. The height of this point is defined as the average distance above the mean water level. Quantities obtained for this case are identified by the subscript f . The main portion of previous measurements over water have been taken

by this method. The second type of measurement, which will be called moving probe measurement, and denoted by the subscript 0, is made at a point that has a fixed distance from the moving water surface at any instant. The third type of measurement, which will be called short time local measurement, is made at a point that has a defined position with respect to the crest of a particular wave.

The first two types of measurements yield overall mean properties of air over a wavy surface containing many Fourier components. Both pertain to the same mean water level, but the air flows encountered by them are different. This is illustrated in Fig. 1.

These two reference frames can be made the same by suitable transformations of coordinates. Suppose the surface wave-form is described by the real part of the following equation

$$\eta = a \exp [ik(x - ct)] \quad (2-1)$$

Then the transformation between the two frames of reference is:

$$x = x'; y = y' + a \exp(ikct); z = z'; t = t' \quad (2-2)$$

where (x,y,z,t) and (x',y',z',t') are the space and time coordinates in both the fixed and the moving frames respectively. Shemdin and Hsu (1967) have shown that a function $f(x,y,z,t)$ can be described by

$$f(x,y,z,t) = f[x(x',y',z',t), y(x',y',z',t'), z(x',y',z',t'), t(x',y',z',t')] . \quad (2-3)$$

It follows that

$$\frac{\partial f}{\partial x} = \frac{\partial f}{\partial x'} ; \frac{\partial f}{\partial y} = \frac{\partial f}{\partial y'} ; \frac{\partial f}{\partial z} = \frac{\partial f}{\partial z'} ;$$

$$\frac{\partial f}{\partial t} = \frac{\partial f}{\partial t'} - ikac \exp [ikct] \frac{\partial f}{\partial y'} \quad (2-4)$$

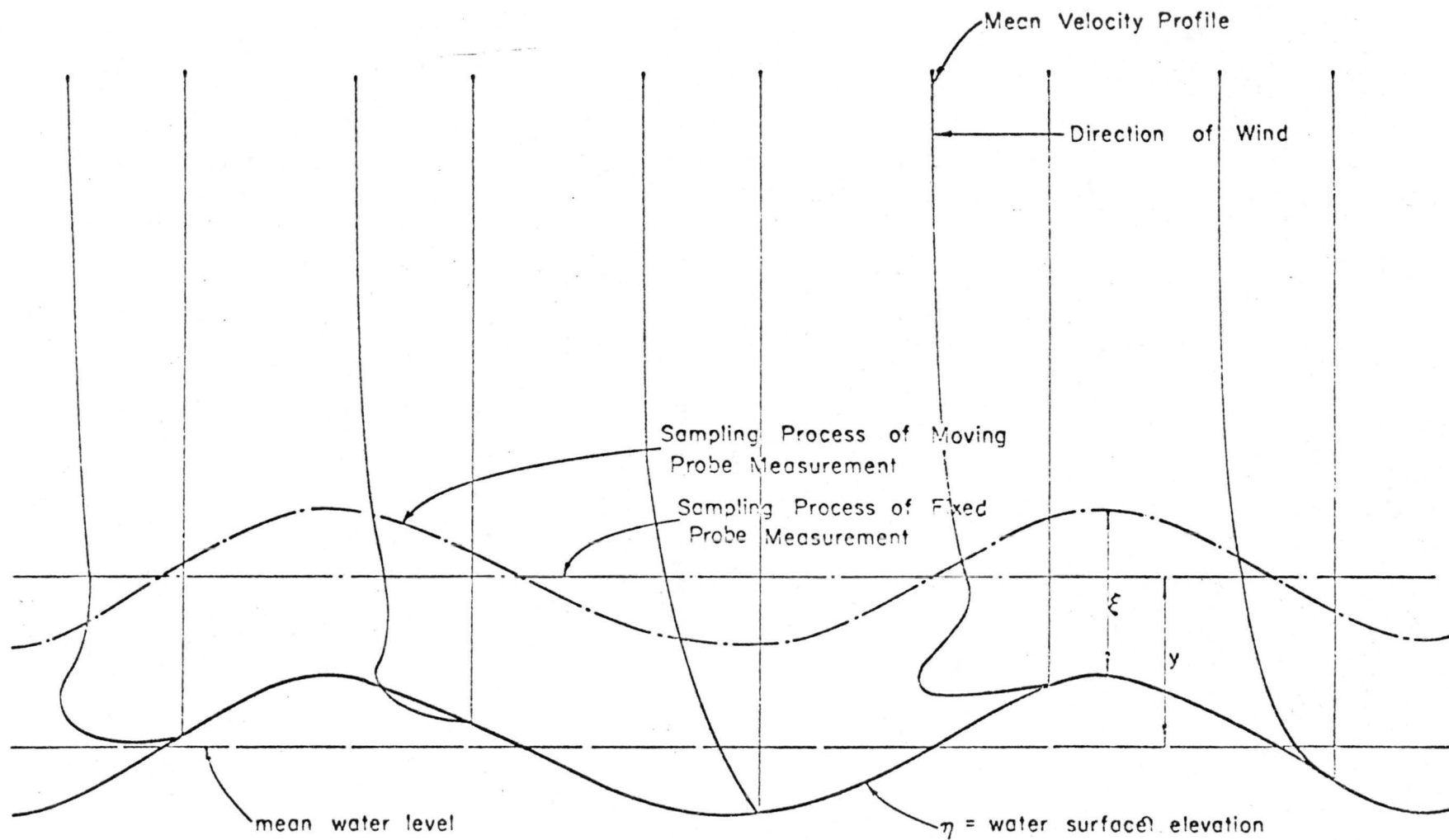


Fig. 1. Schematic diagram for the procedure of fixed probe measurement and moving probe measurement over a perturbed surface.

Shenkin and Hsu (1967), also concluded that the solutions of the linearized boundary-value problem of infinitesimal waves, such as that obtained by Miles (1957), are equally valid for the flow field in a fixed or a moving frame of reference, since the Orr-Sommerfeld equation and the boundary conditions for a flow are the same in both situations.

The local properties of air flow can be obtained from the moving reference frame by the simultaneous measurements of the instantaneous velocities and water surface displacements, with suitable sampling and averaging. Before the detailed procedure of determining the local properties can be described, the concept of moving probe measurements needs to be further explored. In the following the primes of the space and time coordinates in the moving frame will be dropped and the y' will be replaced by ξ . The coordinates of the moving reference system become (x, ξ, z, t) .

2.3 Velocities Obtained from Moving Probe Experiments

The instantaneous velocity of air in the direction of wave propagation as obtained by a moving probe consists of a time mean \bar{u}_0 , a random component due to turbulence u'_0 , a velocity component \hat{u}_0 , due to inviscid streamline displacement and due to mean velocity variation along probe motion. Thus,

$$u(x, \xi, z, t) = \bar{u}_0(x, \xi, z) + u'_0(x, \xi, z, t) + \hat{u}_0(x, \xi, z, t) \quad (2-5)$$

Here the quantity \hat{u}_0 is highly organized and is assumed to have no correlation with turbulence. For fixed probe measurements, the instantaneous velocity can also be expanded into a similar expression, bearing in mind that the components at $y = \xi$ are not necessarily equal to the corresponding components of the moving probe measurements.

The contribution of the inviscid streamline displacement from potential flow theory would decay as e^{-ky} . Most of the contribution to \hat{u}_0 results, however, from mean velocity variations along probe motion and is due to the existence of velocity gradients, i.e., is a viscous effect. It must be determined experimentally. But at large distances away from the air-water interface the inviscid streamline squeezing is no longer important, and the mean velocity profiles can be considered stationary and spatially constant. Then, the magnitude of the velocity component due to probe motion can be estimated from an assumed velocity profile above mean water level. Let the velocity profile be described as

$$u(y) = \frac{u_*}{\kappa} \ln \frac{y}{y_0} \quad (2-6)$$

where u_* is friction velocity, κ von Karman's universal constant, and y_0 an effective roughness parameter. Then, the amplitude of \hat{u}_0 is equal to

$$\begin{aligned} \frac{1}{2}[u(y+a) - u(y-a)]_{y=\xi} &= \frac{u_*}{2\kappa} \ln \left[\frac{y+a}{y-a} \right]_{y=\xi} \\ &= \frac{u_*}{2\kappa} \ln \left[\frac{1+a/y}{1-a/y} \right]_{y=\xi} \end{aligned} \quad (2-7)$$

For $\frac{a}{y} < 1$, Eq. (2-7) may be expressed in a series:

$$\frac{u_*}{\kappa} \left[\frac{a}{y} + \frac{1}{3} \left(\frac{a}{y} \right)^3 + \dots \right]_{y=\xi} \quad (2-8)$$

Evaluating the rms of \hat{u}_0 from Eq. (2-8), one has

$$[\hat{u}_0^2]^{1/2} = 0.7 \frac{u_*}{\kappa} \left[\frac{a}{y} + \frac{1}{3} \left(\frac{a}{y} \right)^3 + \dots \right]_{y=\xi} \quad (2-9)$$

This component depends on the friction velocity and the ratio of the

amplitude of the water waves to the height of the probe above the mean water level. The component is independent of the wave frequency.

If a hot-wire probe is used as a sensing element in moving probe measurements, and the vertical distance traveled by the probe is denoted by $p(t)$, the velocity sensed by the wire held normal to the mean flow is

$$\hat{u}_o = (\bar{u}_o + u'_o + \hat{u}_o) \vec{i} + (v'_o + \hat{v}_o + \frac{dp}{dt}) \vec{j} \quad (2-10)$$

or

$$|\vec{u}_o| = [(\bar{u}_o + u'_o + \hat{u}_o)^2 + (v'_o + \hat{v}_o + \frac{dp}{dt})^2]^{1/2} \quad (2-11)$$

where $\frac{dp}{dt}$ is the probe velocity which is the rate of change of water surface elevation at the given point, i.e.,

$$\frac{dp}{dt} = -akc \sin kct \quad (2-12)$$

Equation (2-12) can be expanded as

$$\begin{aligned} |\vec{u}_o| &= [(\bar{u}_o + \hat{u}_o)^2 + 2(\bar{u}_o + \hat{u}_o)(u'_o) + (u'_o)^2 + (v'_o + \hat{v}_o + \frac{dp}{dt})^2]^{1/2} \\ &= (\bar{u}_o + \hat{u}_o) \left[1 + \frac{2(u'_o)}{(\bar{u}_o + \hat{u}_o)} + \frac{(u'_o)^2 + (v'_o + \hat{v}_o + dp/dt)^2}{(\bar{u}_o + \hat{u}_o)^2} \right]^{1/2} \quad (2-13) \end{aligned}$$

By the binomial expansion, Eq. (2-13) can be expressed in a series

$$|\vec{u}_o| = (\bar{u}_o + \hat{u}_o) \left[1 + \frac{(u'_o)}{(\bar{u}_o + \hat{u}_o)} + \frac{(u'_o)^2 + (v'_o + \hat{v}_o + dp/dt)^2}{2(\bar{u}_o + \hat{u}_o)^2} + \dots \right] \quad (2-14)$$

This expression can be approximated to the following, under the assumptions that $(\bar{u}_o + \hat{u}_o) \gg \hat{v}_o, u'_o, v'_o, \frac{dp}{dt}$; and that the high order terms can be neglected:

$$|\vec{u}_o| \approx |\bar{u}_o + u'_o + \hat{u}_o| \quad (2-15)$$

The result shows that the effect of probe-induced perturbation, $\frac{dy}{dt}$, is not important. From now on \hat{u}_0 will be designated as fluctuation due to the combination of wave and probe motions.

2.3.1 Measured mean and turbulent quantities

From Eq. (2-15) the mean velocity \bar{u}_0 , and the measured root-mean-square of velocity fluctuations $[\overline{u'_{om}}]^2$ obtained from continuous sampling by use of a hot wire at a fixed distance from the moving water surface, are equal to

$$\bar{u}_0(x, \xi, z) = \lim_{T \rightarrow \infty} \frac{1}{2T} \int_{-T}^T u_0(x, \xi, z, t) dt \quad (2-16)$$

and

$$\begin{aligned} [\overline{u'_{om}}]^2 &= \{ \overline{[(\bar{u}_0 + \hat{u}_0 + u'_0) - \bar{u}_0]^2} \}^{1/2} \\ &= [\overline{\hat{u}_0^2} + 2\overline{\hat{u}_0 u'_0} + \overline{u'^2_0}]^{1/2} \\ &= [\overline{\hat{u}_0^2} + \overline{u'^2_0}]^{1/2} \end{aligned} \quad (2-17)$$

since $\overline{\hat{u}_0 u'_0} \equiv 0$ according to assumption.

Eq. (2-17) indicates that the contribution of $\overline{\hat{u}_0^2}$ must be determined independently to separate $\overline{u'^2_0}$ from $\overline{\hat{u}_0^2}$. The presence of the \hat{u}_0 component also will be found in the spectral density if a long record of moving probe measurements is considered as a sample record of a stationary time series. A possible method of separating the turbulence from the probe and wave induced motions is considered in the next section.

2.3.2 Separation of $\overline{u'^2_0}$ from $\overline{\hat{u}_0^2}$

The turbulence can be separated from the measured quantity by correlating the components of velocity $u'_{om} = u'_0 + \hat{u}_0$ with the

simultaneous wave record, provided that the fluctuation \hat{u}_0 is linearly related to water surface undulation η , and turbulent motion u' is not correlated with the surface undulation. The experimental results which are shown later (p. 88) indicate that the phase shifts between \hat{u}_0 and η are less than 10° . With the linear assumption, we can express \hat{u}_0 as

$$\hat{u}_0(x, \xi, z, t) = b\eta(x, 0, z, t) \quad (2-18)$$

where $\eta(t)$ is water surface elevation and b is a transfer coefficient with dimension $[T]^{-1}$ then,

$$\overline{u_0 \eta} = \overline{u_0} \overline{\eta} = \sqrt{(\hat{u}_0)^2} \sqrt{\eta^2} \quad (2-19)$$

or

$$\begin{aligned} \frac{\overline{u_0 \eta}}{\sqrt{\eta^2} \sqrt{(\hat{u}_0 + u'_0)^2}} &= R_{\hat{u}_0 \eta}(\xi, 0) = \frac{\sqrt{\hat{u}_0^2}}{\sqrt{(\hat{u}_0 + u'_0)^2}} = \\ &= \frac{\sqrt{\hat{u}_0^2}}{\sqrt{u_{0m}'^2}} \end{aligned} \quad (2-20)$$

Consequently, $R_{\hat{u}_0 \eta}(\xi, 0)$ denotes the fraction of the measured turbulent intensity at a point which is associated with the wave and probe motions. The turbulent kinetic energy $u_0'^2$ then can be estimated from

$$\overline{u_0'^2} = \overline{u_{0m}'^2} - \overline{\hat{u}_0^2} = (1 - R_{\hat{u}_0 \eta}^2) \overline{u_{0m}'^2} \quad (2-21)$$

2.3.3 Estimation of turbulent energy spectrum from moving probe measurements

If the linear relation between \hat{u}_0 and η is extended to every Fourier component, we can separate the turbulent energy spectrum $S_{u_0' u_0'}(f)$ from the measured spectrum $S_{u_0 u_0}(f)$. This type of analysis

was adopted by Lubasik and Crosch (1963), and Bowden and White (1966) to separate the turbulence from orbital velocities associated with the waves themselves.

The cross spectrum of velocity u_o and water elevation η can now be assumed as

$$S_{u_o \eta} (f) = S_{\hat{u}_o \eta} (f) = b' (f) S_{\eta \eta} (f) \quad (2-22)$$

where $b' (f)$ is a transfer function. The spectrum of nearly periodic fluctuations associated with wave and probe motions is equal to

$$S_{\hat{u}_o \hat{u}_o} (f) = b'^2 (f) S_{\eta \eta} (f) \quad (2-23)$$

Combining Eq. 2-22 and Eq. 2-23, one finds

$$\frac{[S_{u_o \eta} (f)]^2}{S_{u_o u_o} (f) S_{\eta \eta} (f)} = \frac{b'^2 (f) S_{\eta \eta}^2 (f)}{S_{u_o u_o} (f) S_{\eta \eta} (f)} = \frac{S_{\hat{u}_o \hat{u}_o} (f)}{S_{u_o u_o} (f)} \quad (2-24)$$

This quantity is the coherency $\text{Coh}_{\hat{u}_o \eta}$ between velocity and surface elevation, which denotes the fraction of measured turbulent energy at a certain frequency which is associated with the wave and probe motions. By Schwartz's inequality, the coherency is always bounded by unity (Lumley and Panofsky, 1964). Its value is achieved only when the Fourier components of \hat{u}_o and η have proportional amplitudes throughout the ensemble. Once the coherency is known the spectrum of turbulence can be obtained from the relation:

$$S_{u_o' u_o'} (f) = S_{u_o u_o} (f) - S_{\hat{u}_o \hat{u}_o} (f) = [1 - \text{Coh}_{\hat{u}_o \eta} (f)] S_{u_o u_o} (f) \quad (2-25)$$

2.4 Observation of Local Air Flow Properties

As the lower boundary of air flow moves and the water surface is composed of a great number of wave components which are different

in size, shape, and velocity. Therefore, the characteristics of the air flow over a wave is of little statistical significance. Nevertheless, the wind generated waves consist of a pattern in which a particular wave appears repeatedly. These waves, called dominant waves constitute a well defined entity for which an associated velocity field can be defined. Individual waves of the "dominant" class deviate only slightly from a mean dominant wave, and the mean of the ensemble of these waves can be found from well known statistical methods, applied for example, to a sample of the n highest waves in a recording of water surface displacement. These waves may be identified in the record and the associated velocity field can be obtained from simultaneous wave and velocity records. The detailed procedure is described below.

2.4.1 Average dominant waves

Since the large amplitude dominant waves in a wave record usually have a better defined shape than other groups of waves, and the air flow above them is least affected by the neighboring waves, the average dominant waves are defined from a sample of the highest waves. To derive an average dominant wave, a sufficient number of the highest waves, say n , is picked from the record by scanning the wave peaks. The average dominant wave is obtained by aligning the peaks of the chosen highest waves at the same reference abscissa and averaging the ordinate values.

If the time of passage of the peak of each chosen wave, as measured by a wave gauge, is denoted by T_{pi} , then the average dominant wave, $\bar{\eta}$, can be found by convolving the water surface elevation record $\eta(t)$ with a Dirac delta function and obtaining the averages by writing (see Fig. 2 as follows:)

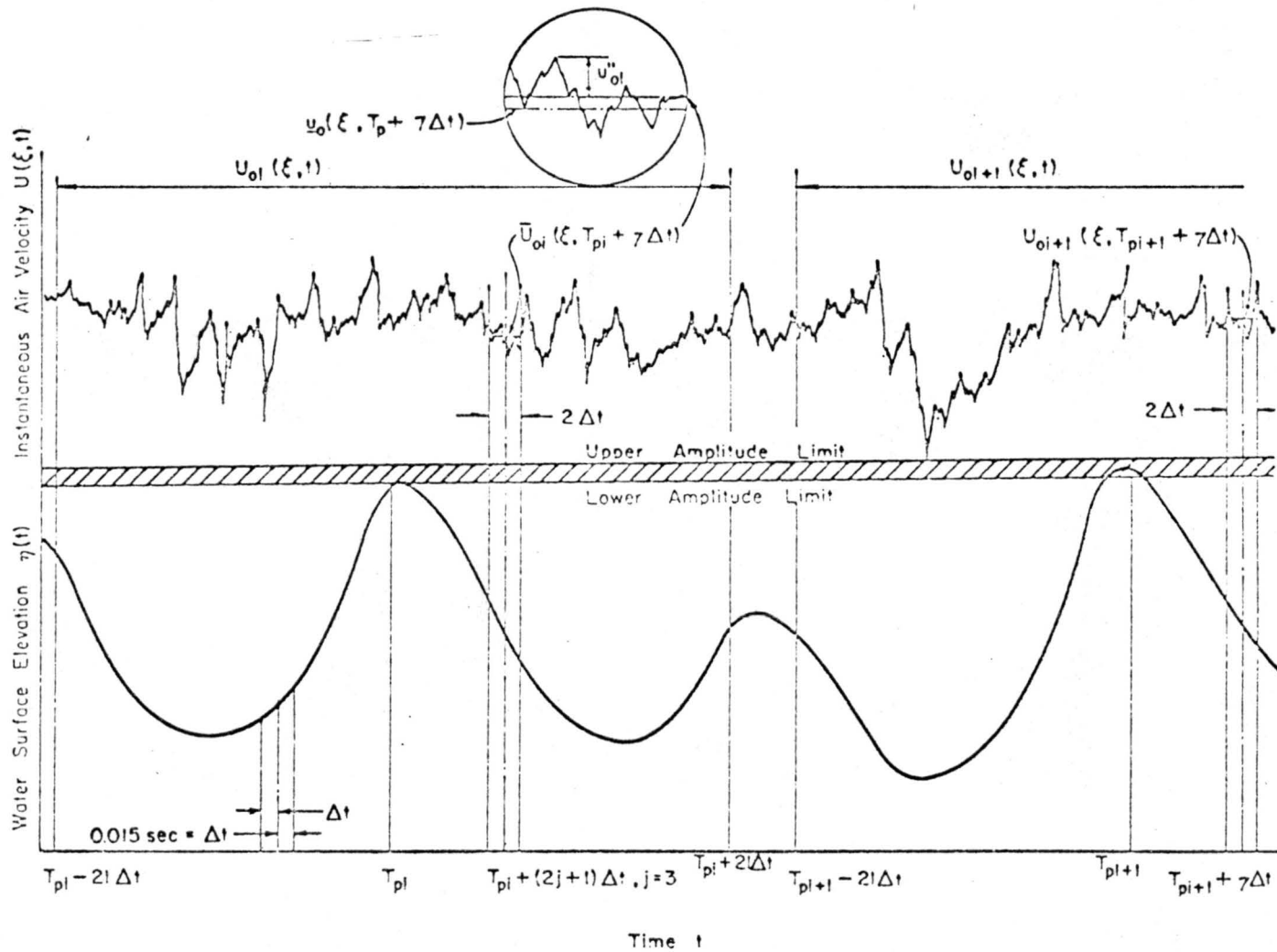


Fig. 2. Schematic diagram for the procedure of determining average dominant waves and local air velocity properties.

$$\bar{\eta}(T_p \pm j\Delta t) = \frac{1}{n} \sum_{i=1}^N \int_0^T \eta(t) \delta(T_{pi} \pm j\Delta t - t) dt \quad (2-26)$$

where T is the duration of wave record, Δt is the spacing of data points obtained in the process of digitizing the wave record, the under bar indicated the ensemble average defined as $\bar{\eta} = \frac{\sum \eta_n}{n}$, and $j = 0, 1, 2, \dots, q$ is chosen so that $q\Delta t$ is larger than a dominant wave period.

The resulting lowest average points on both sides of the peak are then defined as troughs, and the distance between them is defined as the average period. The average frequency, the reciprocal of the average period, will be equal to the dominant frequency associated with the spectral peak.

2.4.2 Local air flow properties

After a sample of dominant waves is obtained and identified in the digital record, the air velocity data corresponding to the chosen waves are determined over a specified time range at various positions above the water waves with respect to their crests, as shown in Fig. 2. Over this short piece of instantaneous velocity record, the mean, the turbulent intensity and the spectrum can be calculated. This time range $\Delta t'$ for short time averaging should be short enough to reveal local mean flow characteristics in the air and to avoid trend problems in spectral analysis. The so-called trend problems are due to the existence of a slowly varying component of velocity which always keeps the auto-correlation function from going to zero. On the other hand, the record should be long enough to include the fluctuating components in the frequency range of interest. The duration of this time range will be determined in the next chapter wherein $\Delta t'$ is chosen as $2\Delta t$.

The local mean velocity $\underline{u}_o [\xi, T_p \pm (2j + 1)\Delta t]$, at given points with respect to the peak of average dominant waves, is found by the following

$$\begin{aligned} \underline{u}_o [\xi, T_p \pm (2j + 1)\Delta t] &= \frac{1}{n} \sum_{i=1}^n \left(\pm \frac{1}{2\Delta t} \right) \int_{T_{pi} \pm 2j\Delta t}^{T_{pi} \pm (2j+2)\Delta t} u_{oi}(\xi, t) dt \\ &= \frac{1}{n} \sum_{i=1}^n \overline{u_{oi}} [\xi, T_{pi} \pm (2j + 1)\Delta t] \end{aligned} \quad (2-27)$$

where $u_{oi}(\xi, t)$ is the instantaneous velocity record corresponding to the i th chosen wave. The use of time $T_p \pm (2j+1)\Delta t$ is to identify the position of the velocity record with respect to the wave peak, not to show the "time" dependence of mean velocity at a certain point. We regard $\underline{u}_o [\xi, T_p \pm (2j+1)\Delta t]$ as equivalent to the velocity distribution $u_o(\xi, x)$ above a particular wave in a spatial base.

Each short time-local mean $\overline{u_{oi}}$ may deviate from ensemble local mean \underline{u}_o , the quantity $\frac{1}{n} \sum_{i=1}^n (u_{oi} - \underline{u})^2 = \sigma_a^2$ which will be called the variance of the short time mean. If the velocity deviation from the mean $\overline{u_{oi}} [\xi, T_{pi} \pm (2j+1)\Delta t]$ is denoted by $u''_{oi} [\xi, T_p \pm (2j+1)\Delta t]$, the ensemble mean of turbulent kinetic energy at a certain point is obtained from the following relationships (see Fig. 2):

$$\begin{aligned}
\overline{u_o'^2} [\xi, T_p \pm (2j+1)\Delta t] &= \frac{1}{n} \sum_{i=1}^n \left(\pm \frac{1}{2\Delta t} \right) \int_{T_{pi} \pm 2j\Delta t}^{T_{pi} \pm (2j+2)\Delta t} (\overline{u_{oi}'} + u_{oi}'' - \underline{u_o})^2 dt \\
&= \frac{1}{n} \sum_{i=1}^n \left(\pm \frac{1}{2\Delta t} \right) \int_{T_{pi} \pm 2j\Delta t}^{T_{pi} \pm (2j+2)\Delta t} (u_{oi}'')^2 dt + \frac{1}{n} \sum_{i=1}^n (\overline{u_{oi}'} - \underline{u_o})^2 \\
&= \overline{u_o''^2} [\xi, T_p \pm (2j+1)\Delta t] + \sigma_a^2 [\xi, T_p \pm (2j+1)\Delta t] \quad (2-28)
\end{aligned}$$

The second term is the variance of individual short time mean, in relation to ensemble mean, which represents the contribution of kinetic energy from the low frequency range.

In a similar manner, the ensemble mean $\underline{S_{u_o' u_o'}} [f, \xi, T_p \pm (2j+1)\Delta t]$ of turbulent energy spectrum at a point, in relation to the peak of the average dominant wave is obtained from the relation:

$$\underline{S_{u_o' u_o'}} [f, \xi, T_p \pm (2j+1)\Delta t] = \frac{1}{n} \sum_{i=1}^n S_{u_{oi}' u_{oi}'} [f, \xi, T_{pi} \pm (2j+1)\Delta t] \quad (2-29)$$

$S_{u_{oi}' u_{oi}'}$ is the spectral estimate from a single piece of short time record. The technique of Blackman and Tukey (1958) will be used to calculate $S_{u_{oi}' u_{oi}'}$.

For the above computations, quantities obtained from each individual piece of record are not very reliable. However, after an ensemble average of many estimates is obtained from the data over many almost identical waves, the reliability should be improved greatly. The reliability of estimations will be calculated in the next chapter.

Chapter III

APPARATUS, EXPERIMENTAL PROCEDURE AND DATA
REDUCTION TECHNIQUES

This chapter presents a detailed description of the facility and the associated instrumentation, actual experimental procedure, and the data reduction techniques. The experiments were performed in the wind tunnel flume combination at the Fluid Dynamics and Diffusion Laboratory of Colorado State University. The equipment consisted of the basic facility, the devices for measuring air velocity and turbulence, the water surface gauge, and the self-adjusting probe positioner.

3.1 The Wind Tunnel Flume Combination

The wind tunnel flume combination shown in Fig. 23, has been described in detail by Plate (1965). It consists essentially of a water tunnel over which a wind tunnel has been constructed so that the air flow joins the water surface tangentially. The tunnel is 0.61 meters wide by 0.76 meters high, and has a plexiglass test section about 12 meters long. The flume is hydraulically smooth everywhere. Sloping beaches of aluminum honeycomb at the outlet prevent reflection of water waves. A smoothly sanded aluminum plate standing on legs 10.6 cm above the floor of the tunnel was extended from the inlet of the tunnel to 5.0 m of the test section. At the junction point, the water was blocked by a vertical aluminum wall so that a standing body of water was obtained downwind from the edge of the plate. The water depth was adjusted in such a way that a continuous and smooth transition from the plate to the water surface was provided when the air was blowing. An axial fan controlled the air discharge

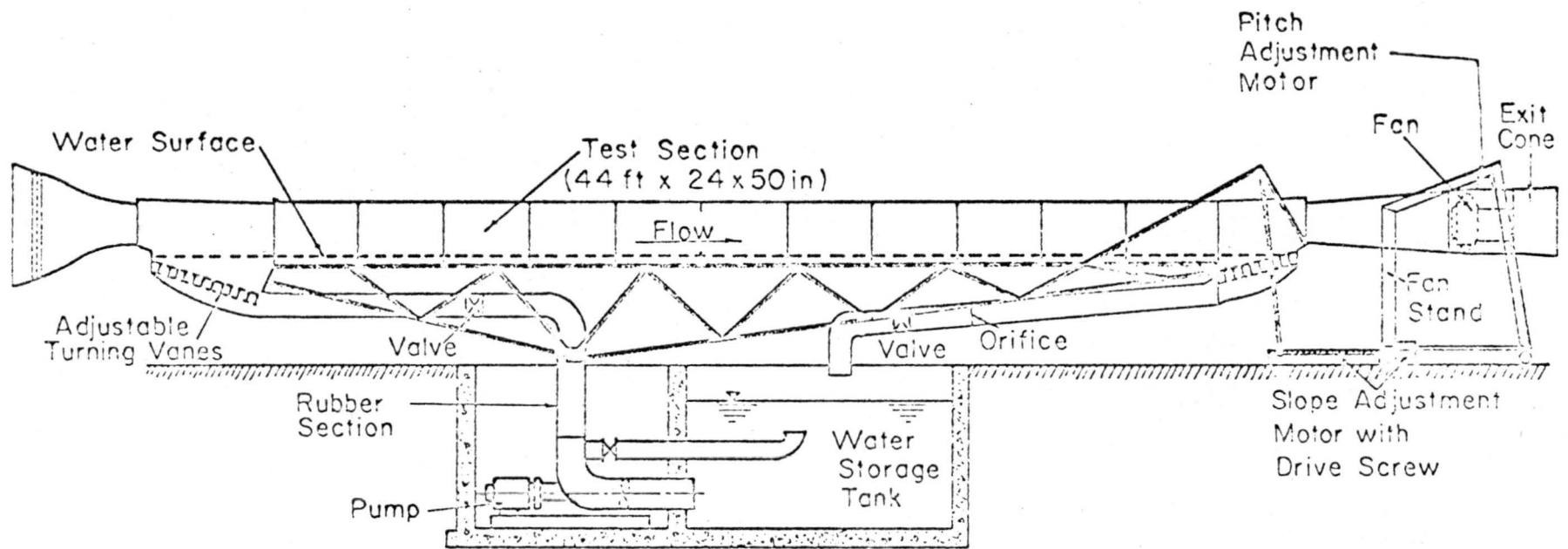


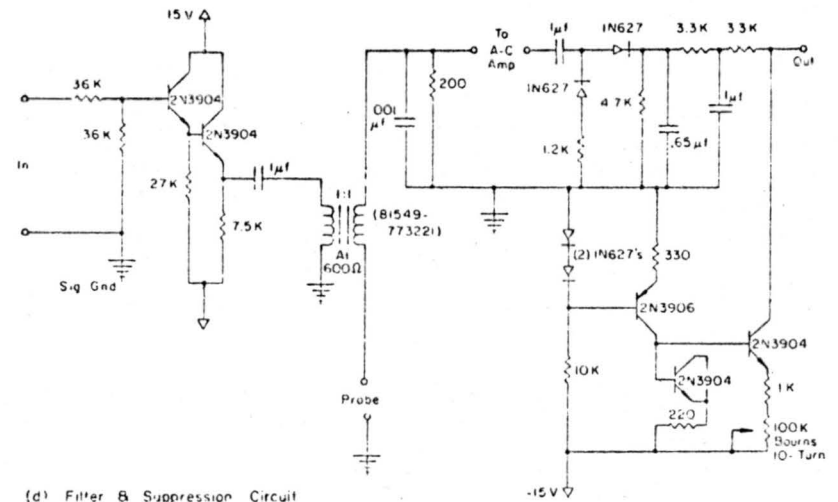
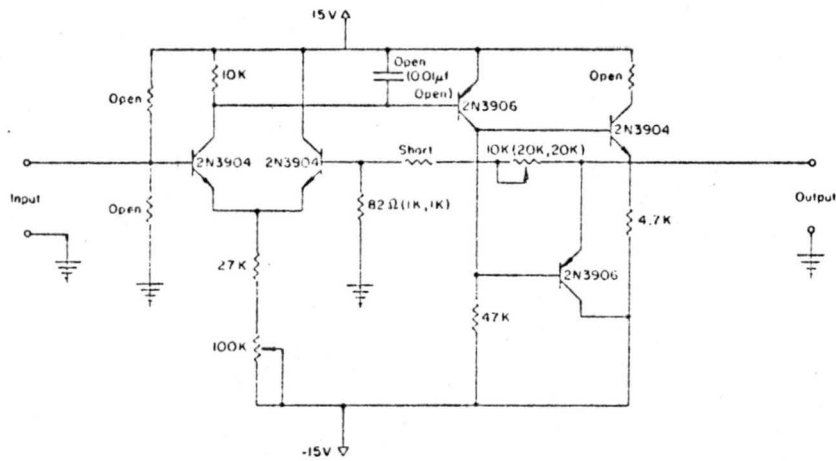
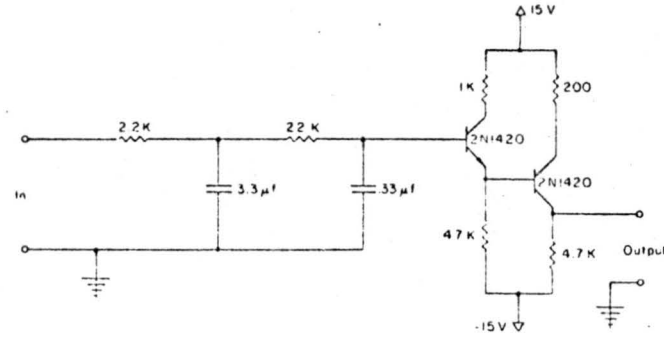
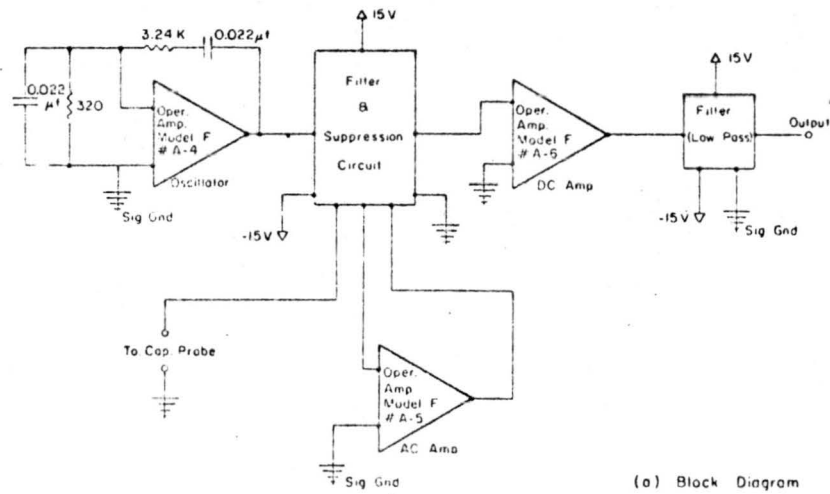
Fig. 3. Schematic diagram of the CSU wind-water tunnel

through the tunnel. The presence of the plate allowed the development of air flow to an equilibrium condition before approaching the water surface. Together with a set of fine mesh screens and a honeycomb at the tunnel inlet and just upstream of the outlet diffuser, it tended to ensure that various features in the air velocity field such as mean velocity profile turbulent intensity, scale, and distribution at the beginning of the water surface, corresponded to that obtained over a smooth flat plate (Hess, 1968).

3.2 Measurements of Water Surface Elevations

The displacement of the water surface was measured with a capacitance gauge and a measuring circuit which had been developed especially as a signal source for the self-adjusting probe positioner. The probe consisted of a 32 gauge nyclad insulated magnet wire which was stretched vertically across the tunnel in the center of the cross section. The copper wire and the water acted as two condenser plates with the insulation coating as the dielectric medium. The bare ends of the positive conductor were completely insulated from water with General Electric Company's RTV-108 Translucent Silicone Rubber to prevent any short circuits due to direct contact with the water.

The bridge is a solid state instrument which gives a varying D.C. voltage output proportional to water level. The D.C. level and the A.C. gain which control the sensitivity are controlled by two ten turn dial potentiometers on the front panel. The schematics and block diagrams of the capacitance bridge are shown in Fig. 4. The output of the Wien bridge oscillator is fed to the input of the zero suppression and filter board. The signal from the probe is applied to a low impedance transformer. The resulting signal is amplified by an A.C.



Note: The values in Parenthesis are for Models # 5 & # 6

Fig. 4. Schematics and block diagrams of the capacitance bridge.

amplifier (#A.5) and is then rectified by the diode and capacitor network of the filter and suppression board. The resulting D.C. voltage is amplified by the D.C. amplifier (#A.6) and fed through a low pass filter to become the output of the capacitance gauge.

The wires were calibrated before and after each series of experiments. The wetting effect caused by the wire insulation water absorption, which changed the calibration curve slightly, was practically eliminated by submerging it for more than one day. A linear relationship between water depth and the output voltage of the capacitance bridge was obtained by changing the water depth slowly and steadily. A typical calibration curve is shown in Fig. 5.

The output signal was fed to an Ampex F.M. tape recorder, type FR 1300. The analog data were then digitized for statistical analysis with a CDC 6400 digital computer. The detailed procedure will be described in the last section of this chapter.

3.3 Measurements of the Mean Velocity and Turbulent Fluctuations of Air by a Sensor Fixed in Space

Wind velocity profiles in reference to the mean water level were measured by a pitot-static tube fixed in space in conjunction with a Transonics Equibar Type 120, electronic micromanometer which had been calibrated against a standard water manometer. The actions of the wind on the water, which was initially at rest, resulted in a change in the mean water level from the initially horizontal condition. The change in the mean-water-level was determined from readings of piezometer taps spaced 1.22 meters apart along the floor of the tunnel. The difference was added to the original water level to yield the mean-water-level under the action of wind. A 0.318 cm O.D. pitot-static tube was mounted on a carriage which could be positioned anywhere in the tunnel. The

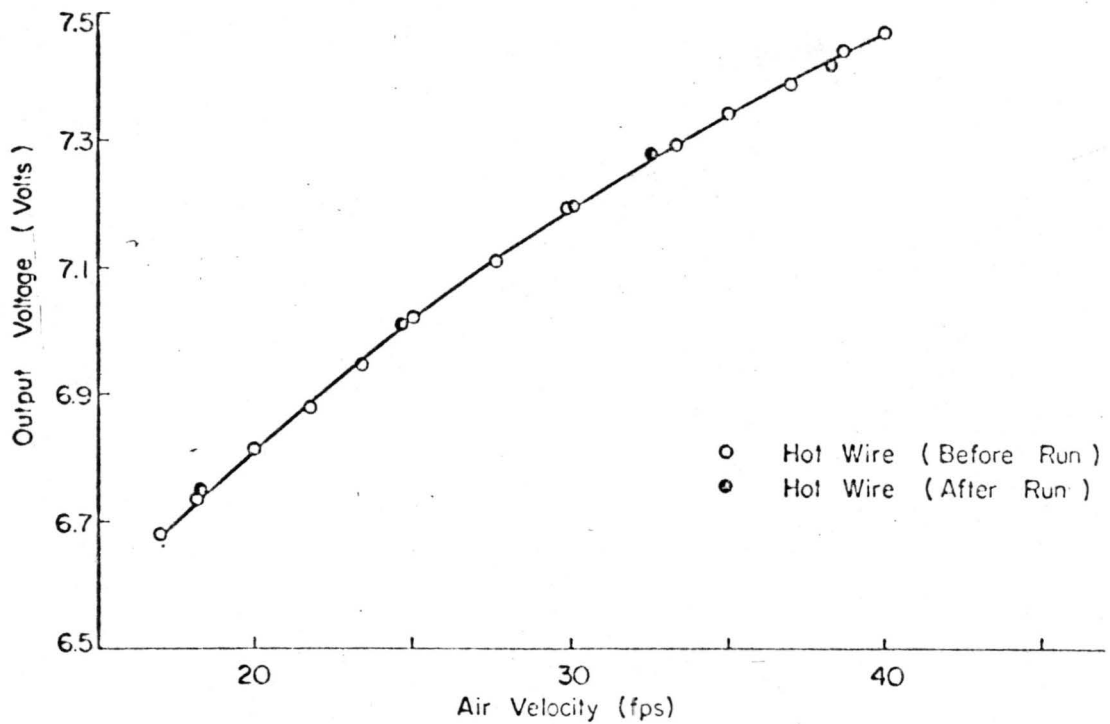
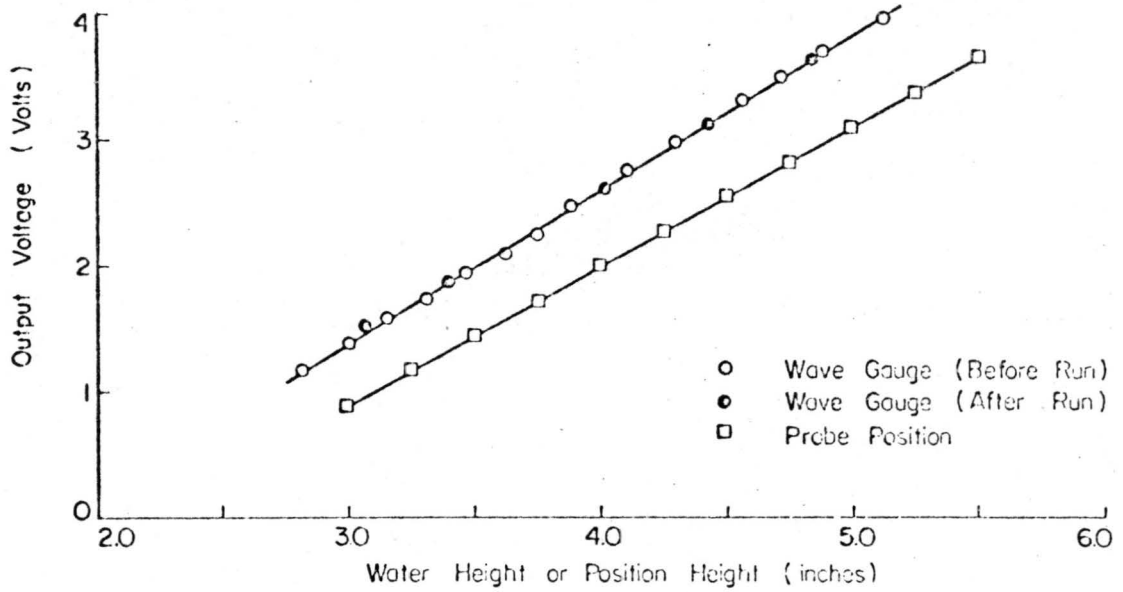


Fig. 5. Calibration curves of capacitance wave gauge, probe positioner and hot wire anemometer.

driving mechanism of the carriage allowed the probe to traverse vertically.

Velocity profiles were taken at two stations along the flume, one over the plate, the other one at 8.5 m from the downstream edge of the aluminum plate. The velocities were calculated from continuous plots of pressure difference versus time for one minute at various heights on a Moseley, Type 135, x-y plotter. All data in this study were taken at two reference velocities of 7.7 m/sec and 9.8 m/sec which are called case 1 and case 2 respectively. These reference velocities were measured by a pitot tube located 1.3 m upstream from the edge of the plate at a height of 30 cm above the plate. A constant value of air density was used to convert pressures into wind-stream velocity profiles.

Fluctuations in the longitudinal component of air velocity were measured with a constant temperature hot-wire anemometer, Disa Model 55 A01. The hot wire sensing element was made of 0.0005 cm diameter tungsten and was mounted on steel prongs held by a ceramic probe. The hot wire was calibrated against a standard pitot tube in the free stream at several mean velocities in the range of interest. A typical calibration curve is shown in Fig. 5. The pitot tube and the wire were mounted side by side in the tunnel, and care was exercised to assure that pitot tube and hot wire probe were separated by sufficient distance to prevent either one from disturbing the flow past the other. The best fit straight line was drawn to relate the square of the voltage output e^2 and the square root of corresponding air velocity \sqrt{u} :

$$e^2 = A\sqrt{u} + B .$$

The sensitivity, $\partial u/\partial e$, calculated from the above equation was then used to convert analog outputs back to actual physical quantities.

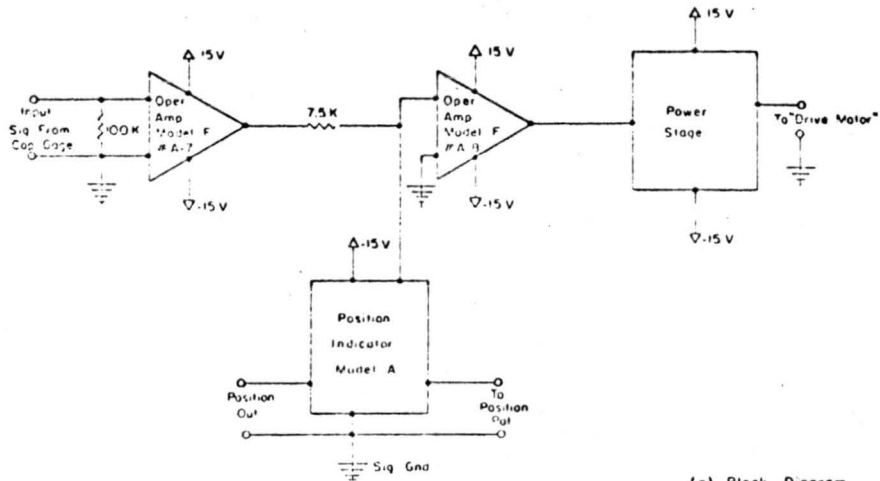
The anemometer output was read on a Bruel and Kjaer, Model 2416, true rms voltmeter, which measures 99% of the fluctuation signal above 2Hz, and the turbulent signal was recorded on an Ampex, Type FR 1300, tape recorder for spectral analysis. The spectra of these records were determined with a Bruel and Kjaer, Model 2109, analog spectrum analyzer with proportional one-third octave filters. The low frequency range of the spectrum was determined with a Technical Products, Type TP 627, spectrum analyzer which has constant band width filters of 2Hz with a continuously variable center frequency.

3.4 Measurements of Air Velocity by the Moving Probe

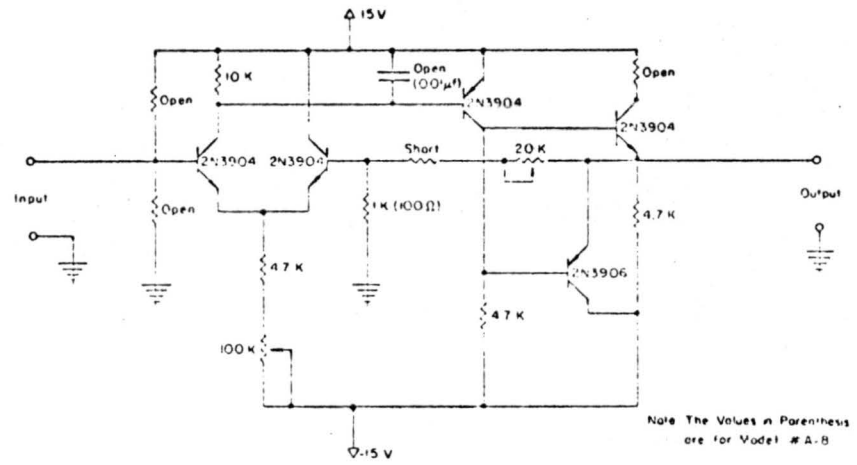
3.4.1 The system for the self-adjusting positioner

To measure air velocity above the interface of progressive wind waves under unsteady conditions, a servo-controlled probe positioner was developed. It consisted of a mechanical system and an electronic circuit, which allowed a velocity sensor to always measure velocities at a fixed distance from the water surface within small error limits. The self-adjusting probe positioner was built on a principle of a negative feedback control system. The signal from the capacitance wave gauge is the forcing input and the position of the probe is the response output. The control electronics and the mechanical system of the positioner are shown in Figs. 6 and 7, respectively.

The mechanical system consists of a hot-wire probe, a position potentiometer, a drive motor, a drive drum, and two nylon pulleys which are attached to a T-shape rigid brass rack. Efforts were made to minimize the weight of every moving component. A thin and rigid

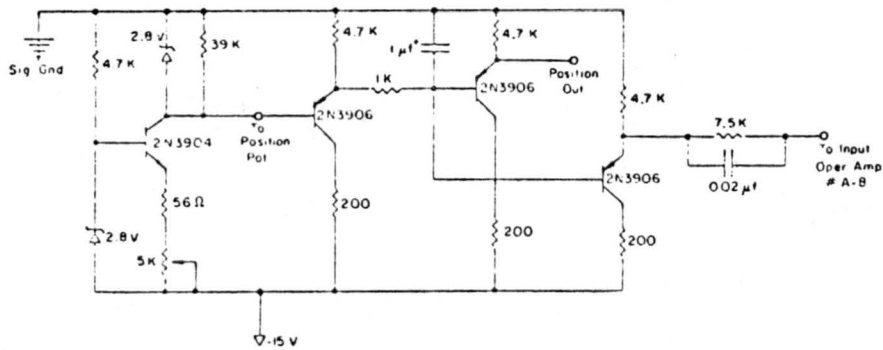


(a) Block Diagram

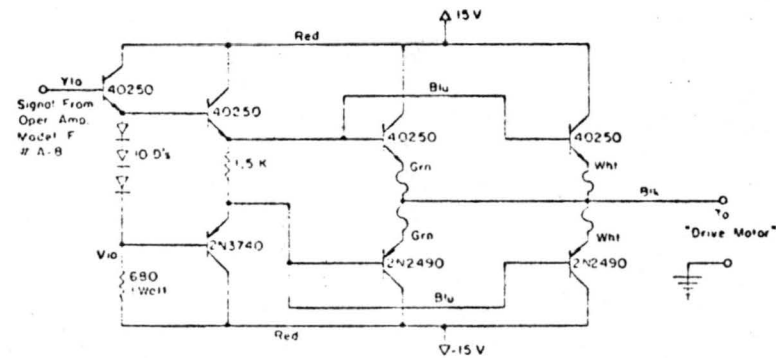


Note The Values in Parenthesis are for Model # A-B

(b) Operational Amplifier # A-7



(c) Position Indicator



(d) Power Stage

Fig. 6. Control Electronics of self-adjusting positioner.

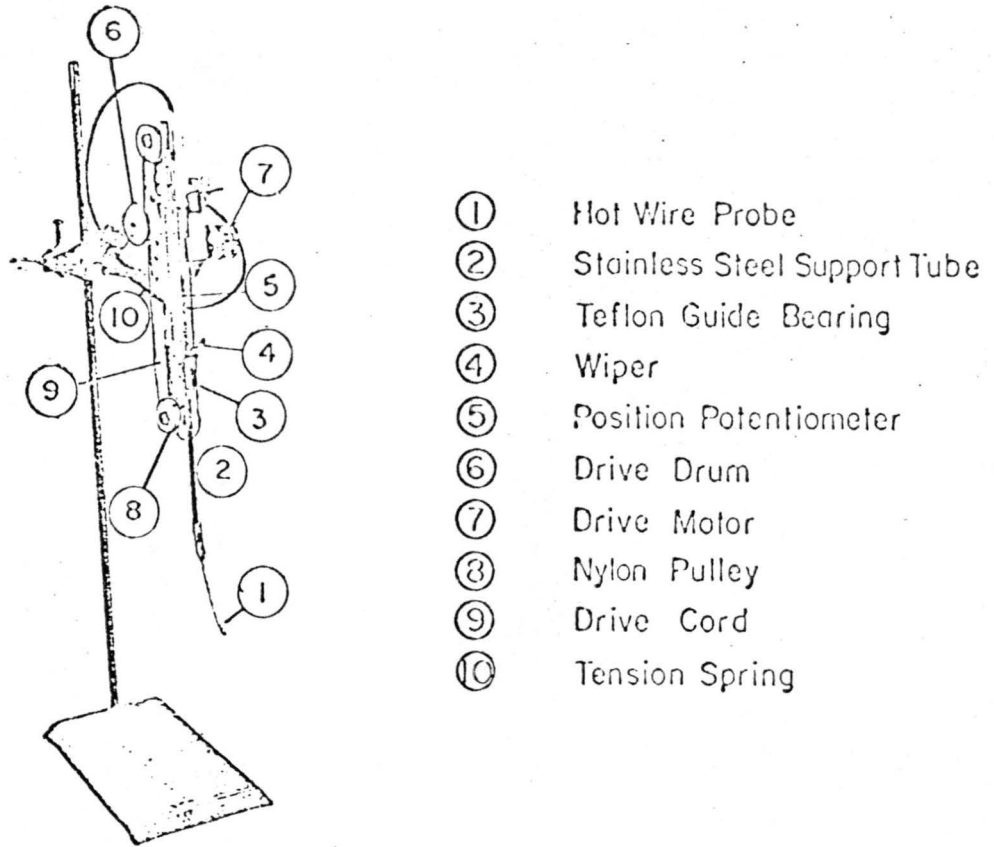


Fig. 7. Mechanical system of self-adjusting positioner.

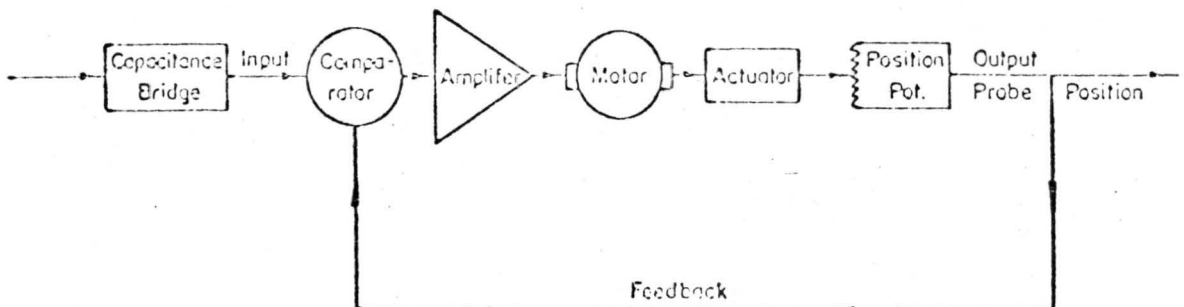


Fig. 8. Schematic diagram of the control principle of self-adjusting positioner.

ceramic hot-wire probe served as velocity sensor in this special experiment. The probe was inserted into a stainless steel support tube which could move freely up and down between two Teflon guide bearings. The position potentiometer was made of two brass resistive coils attached to a phenolic frame. The drive motor used was a Moseley, Type 10822, 12 volt D.C. motor as used in x-y plotters. The complete mechanical system was clamped to the carriage of the wind tunnel flume.

During the operation the relative elevation between the sensing probe and the perturbed water surface could be preselected by controlling the traverse position of the carriage and D.C. level of the capacitance gauge.

The principle of operation is shown schematically in the block diagram of Fig. 8. As soon as the water surface elevation changed, the comparator would detect an error voltage between the control voltage from the capacitance gauge and the potential coming from the position potentiometer. Through a power amplifier, this error voltage drove the motor in a way tending to restore the preselected relationships. The motor, accompanied with reduction gearing and friction clutch, actuated the rotary motion of the drive drum. A cord with tension springs over the drive drum and nylon pulleys in turn caused the wiper mounted on the support tube of the hot-wire probe to slide along the position potentiometer. The signal from the position potentiometer was again fed back to the comparator. In this fashion, the distance between the hot-wire probe and the instantaneous water surface was kept the same at all times.

A different design of a wave follower was used by Shemdin and Hsu (1966). This device was used to hold a pressure sensor at a fixed distance above mechanically generated waves. The basic principle of their oscillating device is similar to that of the self-adjusting probe positioner used in this study. Although Shemdin and Hsu did not give detailed information on the dynamic characteristics of their system, it is rather likely that the considerable inertia effects associated with their mechanical system restrict its applicability to simple mechanical waves where the phase lag between a sensor and water waves can be externally adjusted. For small wind waves, the dominant frequency is much higher and the dynamic response of a wave follower is required to cover a wide range of frequencies.

3.4.2 Dynamic calibration of the self-adjusting positioner

It was assumed that the feedback system of the probe positioner was linear. The signal for the water surface elevation from the capacitance gauge was the input to the system, and the signal for the position of probe positioner from the position potentiometer was the output. The ideal wave follower should follow water surface contours instantaneously without phase shift and without any amplitude attenuation or amplification. The dynamic characteristics of the real system could be evaluated from relationships between known inputs and outputs. The transfer function of the linear system was obtained from the cross correlation of water waves and positioner position. The input-output correlation function is the convolution of the input autocorrelation with the unit impulse function response (Plate, 1967).

$$R_{wp}(\tau) = \int_{-\infty}^{\infty} h(\sigma) R_{ww}(\tau-\sigma) d\sigma \quad (3-2)$$

where subscripts w and p denote the signals of water waves and probe position respectively. The correlation function of x and y variables is defined as

$$R_{xy}(\tau) = \lim_{T \rightarrow \infty} \frac{1}{2T} \int_{-\infty}^{\infty} x(t) y(t+\tau) dt \quad (3-3)$$

According to the convolution theorem of linear system, the Fourier transform of a convolution is the product of the Fourier transforms of the two convolved functions, but the Fourier transforms of $R_{wp}(\tau)$ are $2\pi S_{wp}(\omega)$, that of R_{ww} is $2\pi S_{ww}(\omega)$, and that of $h(\tau)$ is the transfer function $H(\omega)$. Here, $S_{wp}(\omega)$ and $S_{ww}(\omega)$ are cross spectrum of water waves and probe positions, and spectrum of water waves respectively. Mathematically, the cross spectrum $S_{xy}(\omega)$ is defined as

$$S_{xy}(\omega) = \frac{1}{2\pi} \int_{-\infty}^{\infty} R_{xy}(\tau) e^{-i\omega\tau} d\tau \quad (3-4)$$

Consequently

$$S_{wp}(\omega) = H(\omega) S_{ww}(\omega) \quad (3-5)$$

The gain $|H(\omega)|$ and phase angle $\phi(\omega)$ of the transfer function $H(\omega)$ were then determined from the input power spectrum $S_{ww}(\omega)$, and the cospectrum $Co_{wp}(\omega)$ and quadrature spectrum $Q_{wp}(\omega)$ of the output were determined respectively by Fourier transforming of the even and odd parts of the cross correlation function $R_{wp}(\tau)$, $E_{wp}(\tau)$ and $O_{wp}(\tau)$. The relationship among these functions is given by the following:

$$Co_{wp}(\omega) = \frac{1}{2\pi} \int_{-\infty}^{\infty} E_{wp}(\tau) \cos \omega\tau d\tau \quad (3-6)$$

$$Q_{wp}(\omega) = \frac{1}{2\pi} \int_{-\infty}^{\infty} O_{wp}(\tau) \sin \omega \tau \, d\tau \quad (3-7)$$

$$R_{wp}(\tau) = E_{wp}(\tau) + O_{wp}(\tau) \quad (3-8)$$

$$|H(\omega)| = \frac{1}{S_{ww}(\omega)} \sqrt{[Co_{wp}(\omega)]^2 + [Q_{wp}(\omega)]^2} \quad (3-9)$$

and

$$\phi(\omega) = \tan^{-1} \frac{Q_{wp}(\omega)}{Co_{wp}(\omega)} \quad (3-10)$$

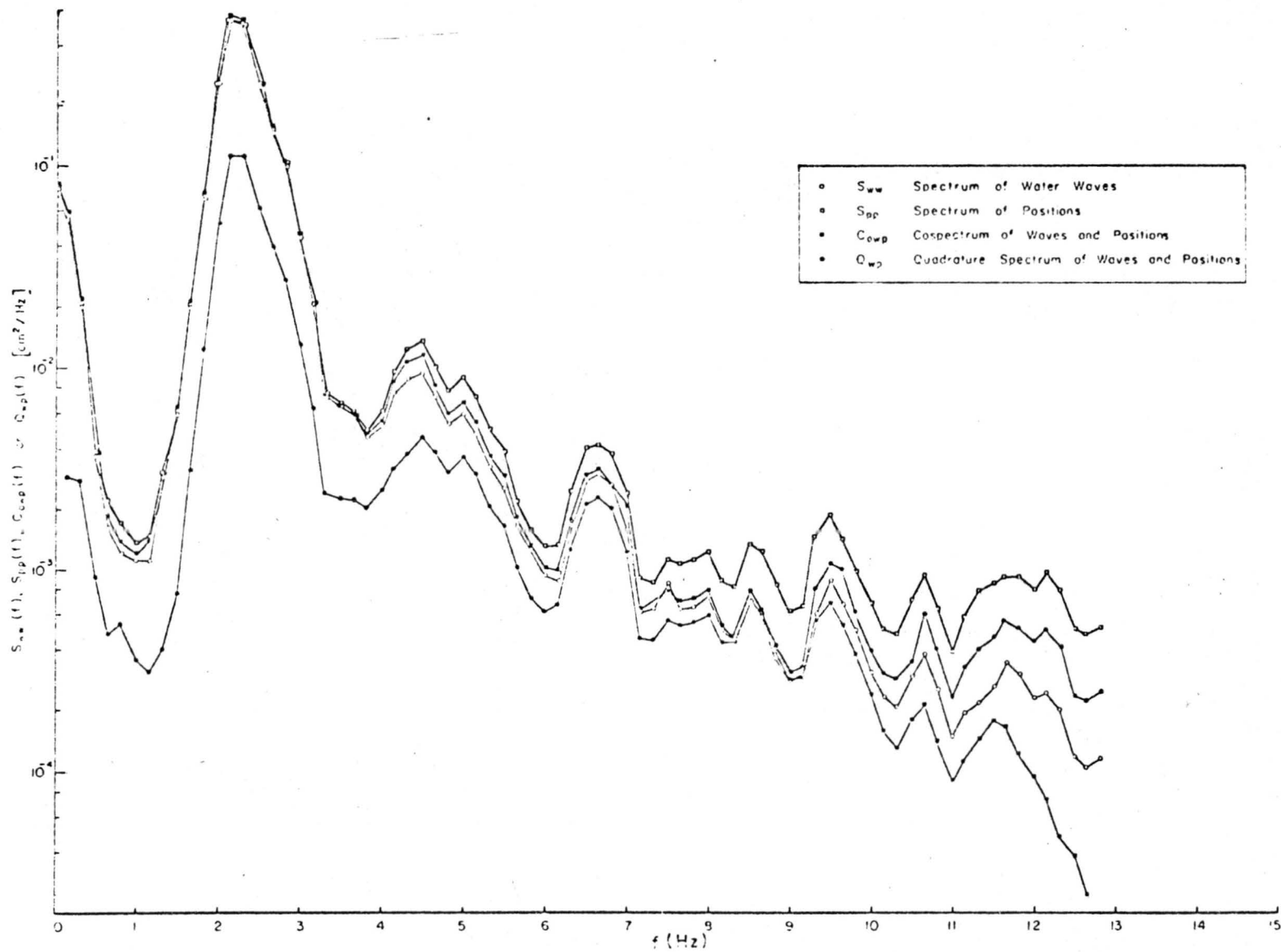


Fig. 9. Spectrum of water waves, spectrum of probe positions, and cospectrum and quadrature spectrum of water waves and probe positions.

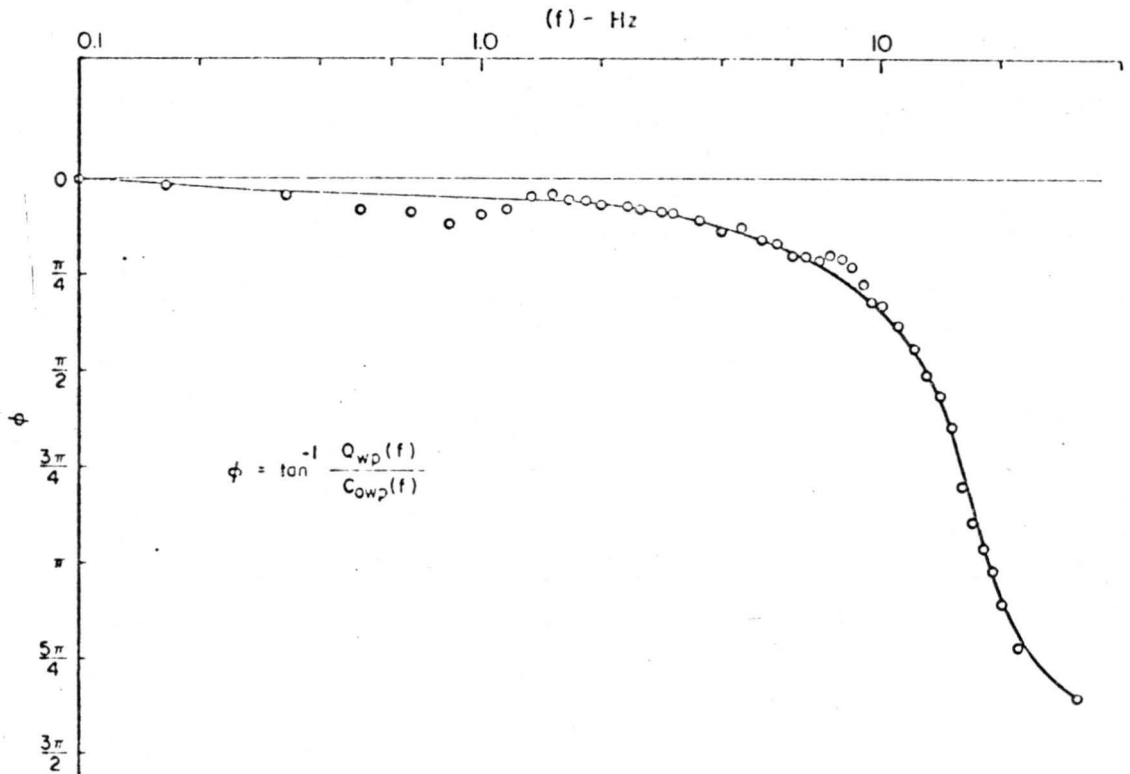
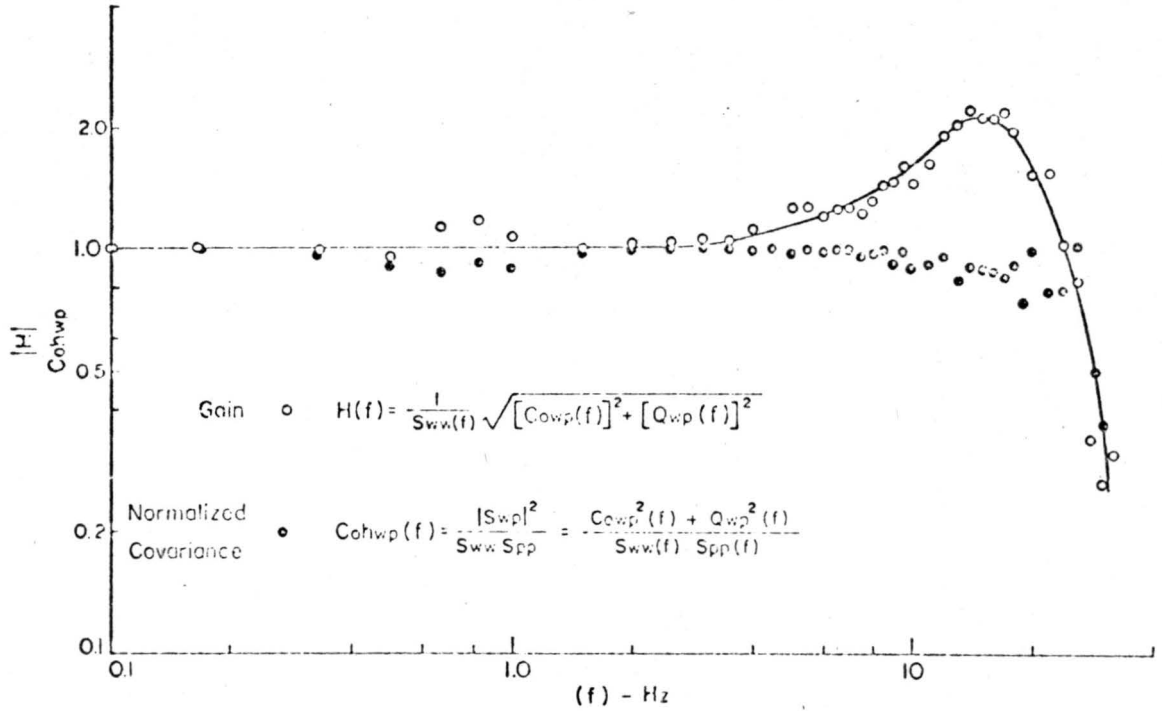


Fig. 10. Gain and phase log of the transfer function of self-adjusting probe positioner; and the normalized covariance of water waves and probe positions.

An example of such a calculation is shown in Figs. 9 and 10. The data was taken during actual experimental measurements.

The results indicate that in the neighborhood of the dominant frequency of the wave spectrum, 2.2 Hz, the gain of amplitude is within 5% and the phase lag is less than 0.05π . These errors are mainly due to inertia effects of the mechanical system. The bump in gain at frequencies around 15 Hz could easily be reduced by adjusting the damping coefficient of the system. It was considered that the appearance of this bump would not affect the performance of the self-adjusting positioner at the chosen experimental conditions.

The square of the spectral correlation, that is, the squared coherence was defined as:

$$\text{Coh}_{wp}(\omega) = \frac{|S_{wp}|^2}{S_{ww} S_{pp}} = \frac{C_{wp}^2(\omega) + Q_{wp}^2(\omega)}{S_{ww}(\omega) S_{pp}(\omega)} \quad (3-11)$$

This relation is also shown in Fig. 10. The simultaneous Brush recorder traces of the signals of water waves and positions in Fig. 11 demonstrate visually the excellent performance of the self-adjusting positioner over the waves of interest.

3.4.3 Data collection procedure

To measure air velocities at a fixed distance from the instantaneous water surface, simultaneous records of air velocities, water surface elevations, and locations of probe positioner were required. A block diagram of the data collection system is shown in Fig. 12.

Before any actual measurements were made, the hot wire probe, the wave capacitance probe, and the position potentiometer were carefully calibrated. The principle of the feedback system of the self-

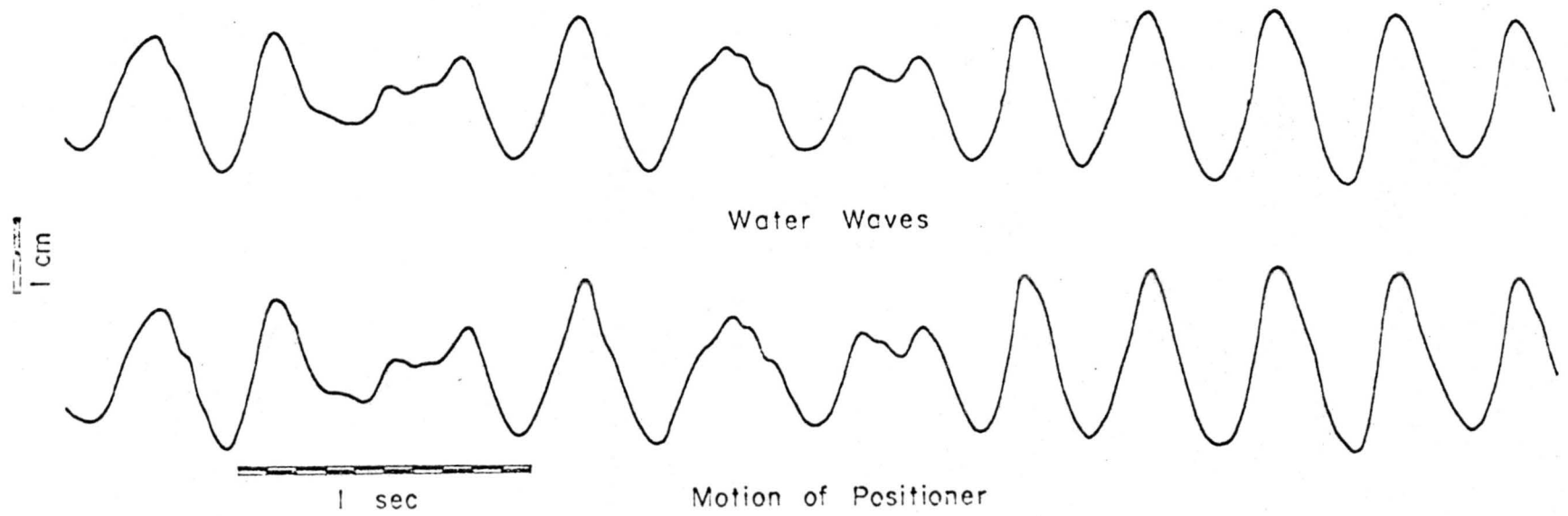


Fig. 11. Simultaneous brush recorder traces of water waves and probe positions.

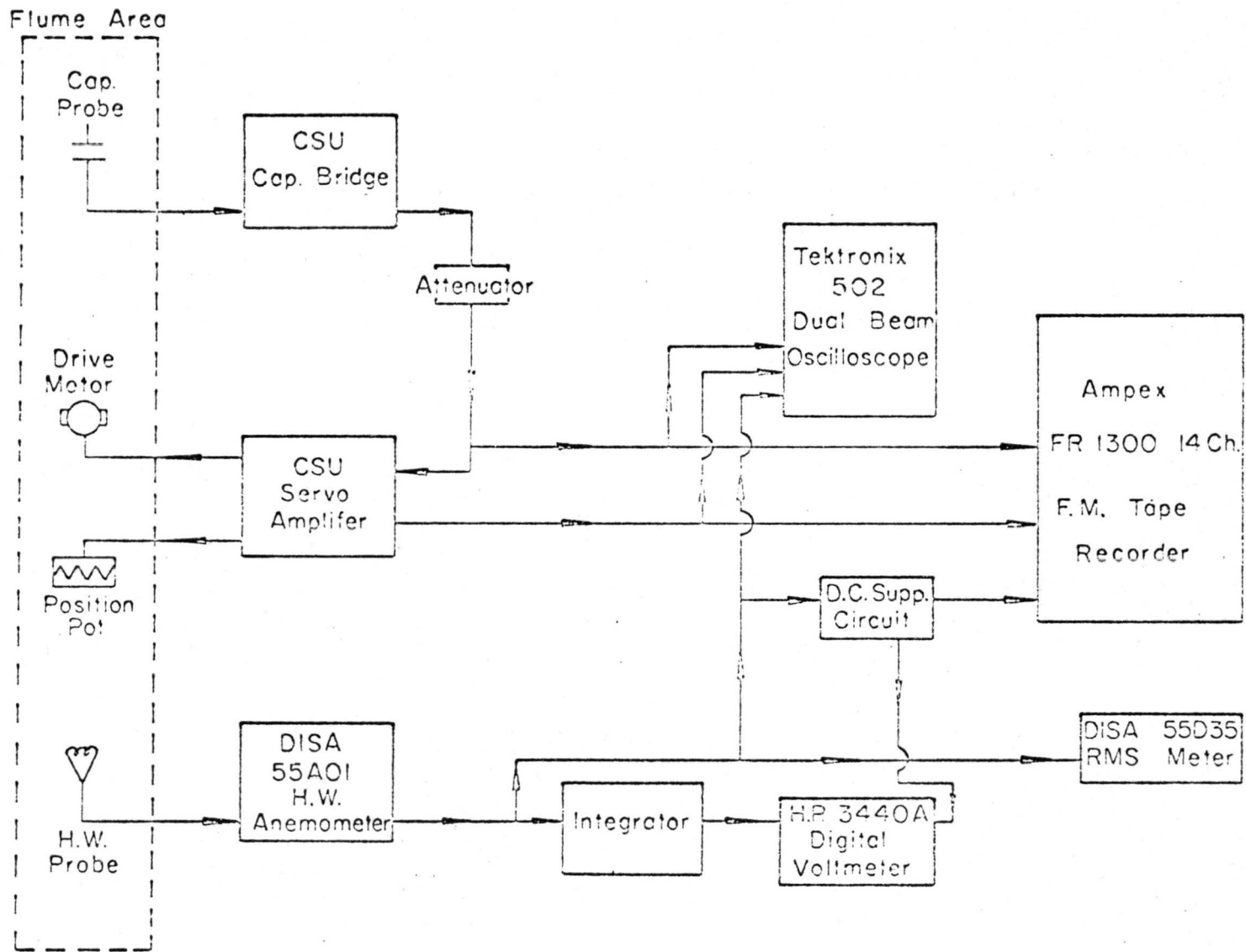


Fig. 12. Block diagram of the data collection system.

adjusting positioner is to maintain a preselected relation by always attempting to eliminate the error voltage. Hence, the sensitivities of wave gauge and position potentiometer should be the same, so that the difference between the real physical quantities, the distance between probe and water surface, could be maintained. An attenuator was introduced to regulate the sensitivity of the wave gauge to get identical changes in water surface elevation and the probe positioner.

The mean D.C. output of the hot wire anemometer, which gave the mean air velocity at a fixed height above the instantaneous water surface, was read directly from a digital voltmeter through an electronic integrator. The time mean of velocity fluctuations was obtained with a Disa, Type 55035, RMS voltmeter, which has a built-in time integrator and measures 99% of fluctuation signal in the range of 1 Hz and 400 KHz. The integration time constant used in measurement was 30 sec. Since the D.C. level carried by the hot wire anemometer exceeded the dynamic range of the Ampex FM tape recorder, a known D.C. level was bucked out with a suppression circuit, so that the signal could be recorded properly and recovered later for data analysis.

At every chosen height with respect to instantaneous water level, the signals of air velocity, water waves, and positions of moving probe were recorded simultaneously on magnetic tapes at the speed of 30 ips for 5 minutes. Each piece of recording was called a "run". The intervals of heights among runs were chosen in such a way that the mean velocity of turbulent air in the vicinity of the air-water interface could be mapped out. The smallest height intervals were 0.25 cm.

The lowest elevation above the water which could be obtained with the probe position was about 1 cm. Below this height, occasional water droplets began to disturb the hot wire signal. For each case there were 36 runs.

3.4.4 Digitization of analog data

Continuous magnetic recordings of air velocities, water waves, and probe positions at fixed heights above instantaneous water surface, were digitized by the Analog to Digital Data Conversion System (ADDCS). Model 751, produced by the Electronic Engineering Company of California for the National Bureau of Standards, Boulder, Colorado.

This unit can convert data at rates up to 40KHz and prepare magnetic tapes in a format compatible with CDC 6400, CDC 6600, IBM 7090, etc. Recording may be either low density (200 characters per inch) or high density (556 characters per inch). Block length may be preset to contain a maximum of 1024 digits.

On the CDC 6400 of Colorado State University, which was used for digital sampling and computation, the maximum blocking factor is 512 60-bit central memory words per physical record, of which 510 words are data items. Based on the specifications of the units and the range of interests in data analysis, the 5 KHz sampling rate, high density recording, and a block length of 90 60-bit words were chosen.

For every run, simultaneous analog recordings of 3 signals from hot wire, capacitance probe, and position potentiometer were digitized in sequence for 2 minutes; i.e., every signal was digitized at the rate of 1667 points/sec. resulting in 200,000 total data points with 0.0006 sec. spacing between points.

3.4.5 Statistical sampling and averaging of digital data

In the digital analysis, all quantities were always converted back first to their real physical values through proper calibrations before any sampling or calculation was made. Hence, the signal distortion which might arise from the nonlinearity of hot wire anemometer for other techniques will not be encountered. This technique had previously been used by Karaki (1968).

By treating the whole record of digital data for a run as a sample record of a stationary time series, one can analyze many statistical properties of the air and water motions. The results of this analysis such as probability distributions, statistical moments, various correlation functions, and energy spectra will be discussed in the following chapters. The mathematical and physical foundations for analyzing these random data will be described with the presentation of results.

The technique for the computation of spectral density functions was the same as that used by Hidy and Plate (1966), who essentially followed the method discussed by Blackman and Tukey (1958). The digital data of the water waves were first pre-smoothed by using the mean of every twenty-five data points. This filtering process retains the real energy produced by the water waves, but removes most of the noise picked up by the signal during the measuring, recording, and digitizing process; the interval between average data is still only 0.015 sec. and the energy contained in frequencies greater than the folding frequency of 30 Hz is not believed to be significant. The maximum lag t_{\max} was chosen at $t_{\max} = 100\Delta t$ yielding degrees of

freedom $q = 2\left(\frac{200,000}{25 \times 100} - \frac{1}{4}\right) = 160$. The final results have an 80% confidence band of approximately $\pm 15\%$. For the calculation of the spectra of air velocity fluctuations, the number of maximum lag was 400. For each spectral estimate, there were 1000 degrees of freedom with a resulting 80% confidence band of $\pm 5\%$. These figures were obtained from Blackman and Tukey (1958) under the assumption that the ensemble of spectral estimates is given by a chi-square distribution.

The most important information obtained from these data relates to the local properties of air at different heights and positions with respect to water waves. The local mean velocity, turbulent intensity, and energy spectrum, at a specified point with respect to the peak of an average dominant wave, were calculated with the statistical method which was developed in Section 3 of Chapter II. In the actual data reduction process, the sample number n was chosen as 20, and the time spacing Δt as 0.015 sec. The time range $\Delta t'$ for calculating local air flow properties was $2\Delta t = 0.03$ sec.; which was equivalent to approximately one-twelfth wave period and contained 50 digitized data points. The maximum number of lags for local turbulent spectrum calculations was chosen as 25, yielding a frequency range from 33.3 Hz to 833.3 Hz. The reliability of estimating the local properties through the ensemble averaging is discussed in the following section.

If the 20 short pieces of record are assumed equivalent to a single record with $20 \Delta t'$ duration, the degree of freedom for local spectrum calculation, will be equivalent to $q = 2\left(\frac{20 \times 0.03}{25 \times 0.0006} - \frac{1}{4}\right) = 80$. Under the assumption that the ensemble of spectral estimates is given by a chi-square distribution, the result will have an 80% confidence band of $\pm 20\%$. Since each piece of short record is independent of the

others, the reliability of the experimental result would actually be better than the calculated variation of $\pm 20\%$. We may expect the same confidence band for the turbulent intensity estimations. For the mean velocity, if 20 events of local mean velocity approximately obey a normal probability law, we will have 80% confidence that the sample averages will be within $\pm 0.28\sigma$ of the ensemble average, where σ is the standard deviation.

Chapter IV

EXPERIMENTAL RESULTS

The experimental investigations performed in this study were restricted to a fixed fetch where wind generated waves were fully developed in the sense of Plate et al. (1968) and the average ratio of wave celerity and air friction velocity is close to one. In this stage of growth, only wave components with spectral densities lower than the limit denoted by Phillips equilibrium curve (to be explained later) tend to increase with fetch so that the wave spectrum is maintained near equilibrium in the high frequency range of the spectrum. The typical geometry of the water surface which specifies the lower boundary for the air flow is presented first.

4.1 Geometry and Statistical Properties of the Water Surface

A typical record of surface displacements is shown in Fig. 13. Such records demonstrate how the water surface displacements vary continuously and irregularly with time. The waves appear in groups which usually contain about 8 waves of nearly constant frequency. The appearance of a modulation envelope means that the waves oscillate many times while their maximum amplitude slowly decreases and then increases as a consequence of the interference among several Fourier components.

To describe the geometry of water surface undulation, the probability distributions of water surface elevations, their rates of change, and frequency spectra of waves were calculated.

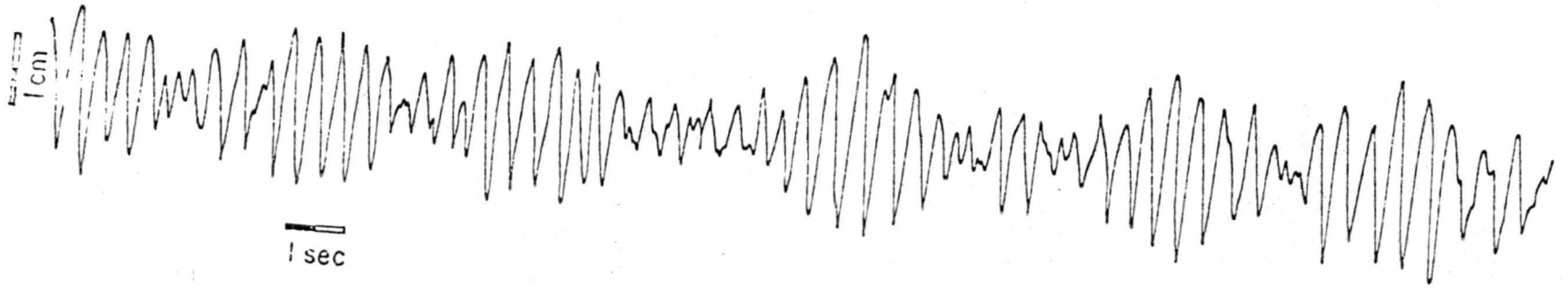


Fig. 13. Time record of water surface displacements.

4.1.1 Probability distributions of water surface elevation and their rates of change

Measured probability distribution of water elevations are shown in Figs. 14a and 14b. The probability density is plotted against units of standard deviation. Two sets of data represented by different symbols are presented for each case. The solid lines represent the Gaussian distribution.

The results consistently show that the water surface displacement is only approximately Gaussian. This fact may indicate a weak interaction among different frequency components. The various Fourier components can no longer be considered as linearly independent (Phillips, 1966), thus violating the conditions required by the central limit theorem for the tendency toward a Gaussian distribution. Kinsman (1960) found empirically that the Gram-Charlier distribution gave a better description of the water surface displacements. The Gram-Charlier series:

$$P(\gamma) = \left(\frac{1}{\sqrt{2\pi}}\right) e^{-1/2 r^2} \left(1 + \frac{1}{6} m_3 H_3 + \dots\right) \quad (4-1)$$

is shown by the broken curve in Fig. 14. This form of distribution also gives a slightly better representation of the data. Here, r is equal to $\eta/(\overline{\eta^2})^{1/2}$, $H_3 = r^3 - 3r$ is the Hermite polynomial of degree 3, and m_3 is the skewness $m_3 = \overline{\eta^3}/(\overline{\eta^2})^{3/2}$.

In Figs. 14c and 14d, the probability distributions of the rate of change of the water surface displacement $\partial\eta/\partial t = \eta_t$, at a fixed fetch are drawn. The rate of change of the water elevations at a fixed fetch represents the vertical velocity of water particles at the surface. Compared with the distribution for water surface

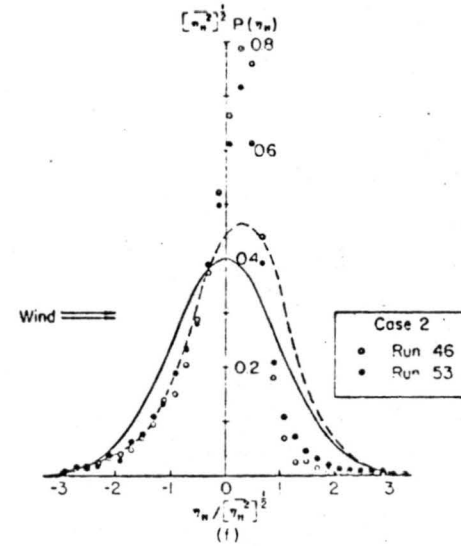
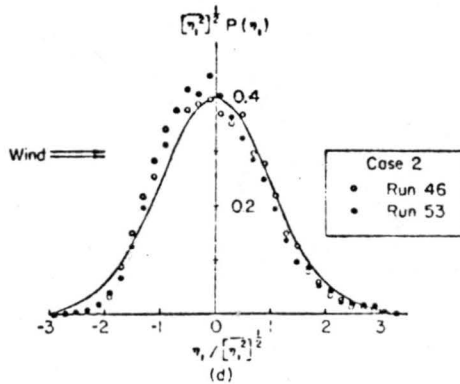
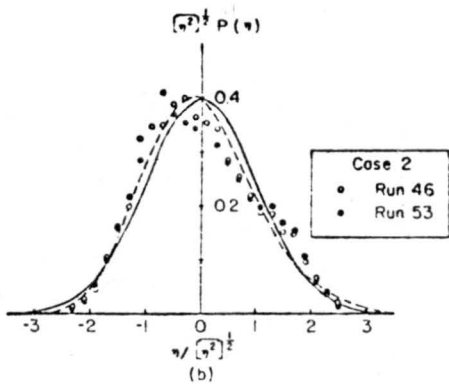
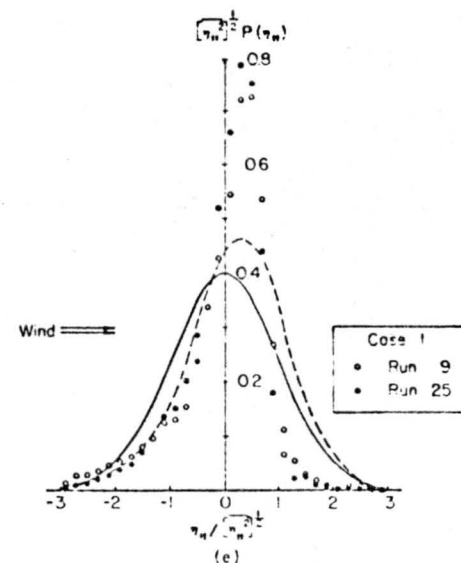
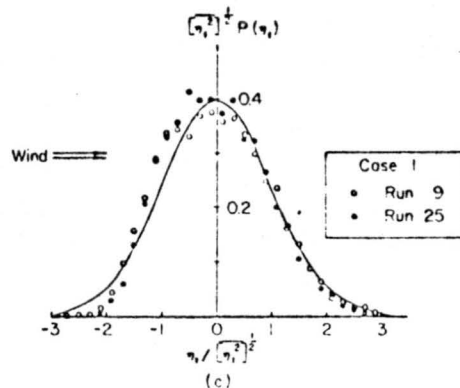
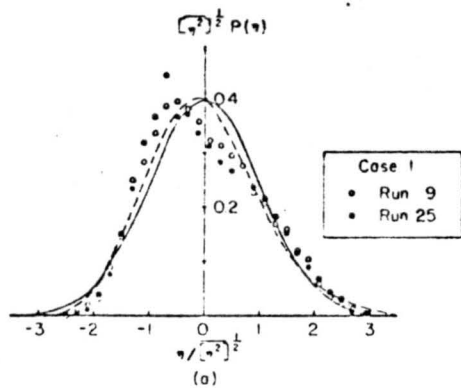


Fig. 14. Probability distributions of water surface displacements and their time derivatives.

displacement, the distribution of vertical velocity is closer to Gaussian distribution.

The spatial slope $\partial\eta/\partial x$ of the wave train seems to be a better quantity to reveal the nonlinear effects in the shorter components and the significance of the ripples for the air-water energy transfer (Phillips 1967). Although it is not possible to obtain spatial slopes from single capacitance wire measurements, its distribution still can be inferred from that of vertical acceleration, $\partial^2\eta/\partial t^2 = \eta_{tt}$. The vertical acceleration of an elementary wave, $a \cdot \cos(kx - 2\pi ft)$, has an amplitude of $(2\pi f) a$. For gravity waves, this equals gka . The spatial slope has an amplitude ka . Therefore, the distribution of acceleration (in units of g) and of slope (in radians) are equivalent.

The probability distributions of the vertical acceleration or the inferred spatial slope are shown in Figs. 14e and 14f. Here a Gaussian distribution is no longer a proper approximation. The most probable vertical acceleration appeared as a narrow and sharp peak, and is not zero but 0.1 g , directed downward. The acceleration is taken as positive in the down-wind direction. From the point of view of spatial slope, the most probable value of $\partial\eta/\partial x$ is about 6 degrees, with the azimuth of ascent pointing downwind. This result agrees in general with Cox and Munk's (1954) results. They measured the surface slopes directly from sun glitter on the sea surface and their results are reproduced in the figure with a broken line. In the present study, the most probable value observed is much higher than theirs. Such a discrepancy might be the result of the contribution from capillary ripples which are comparatively significant in producing surface slope for laboratory wind waves.

Plate et al. (1968), in deriving the -5 envelope for the dominant waves of the spectra, postulated that the maximum acceleration is a fraction of the gravitational acceleration, $\alpha'g$. It is interesting that the average standard deviation of vertical acceleration obtained in this study is 344 cm/sec^2 , which is equivalent to $0.34g$, which agrees well with semi-empirical value of $\alpha' = 0.29$.

4.1.2 The frequency spectra of wind waves

The spectral energy function $S_{\text{WW}}(f)$ is the Fourier transform of the calculated autocorrelation function for water waves. The laboratory water wave spectrum has been studied extensively by such investigators as Hidy and Plate (1966), Sutherland (1967), Plate et al. (1968). The techniques of digitizing and filtering employed by this study, however, assured a set of better data than those obtained in other experiments for spectral estimations.

The results are shown in Fig. 15. The local maxima appear at frequencies close to twice and triple that of the dominant peak frequency f_m . The best fit power law has been drawn over three distinct regions at high frequency and of spectra, i.e., $f_m < f < 2f_m$, $2f_m < f < f_c$ and $f > f_c$. Here f_c , about 8 Hz in this study, denotes the frequency where surface tension and the dissipation caused by viscosity became important. The resulting slopes in a double logarithmic plot are -8 or -9, -5 and -3 for the indicated three regions respectively.

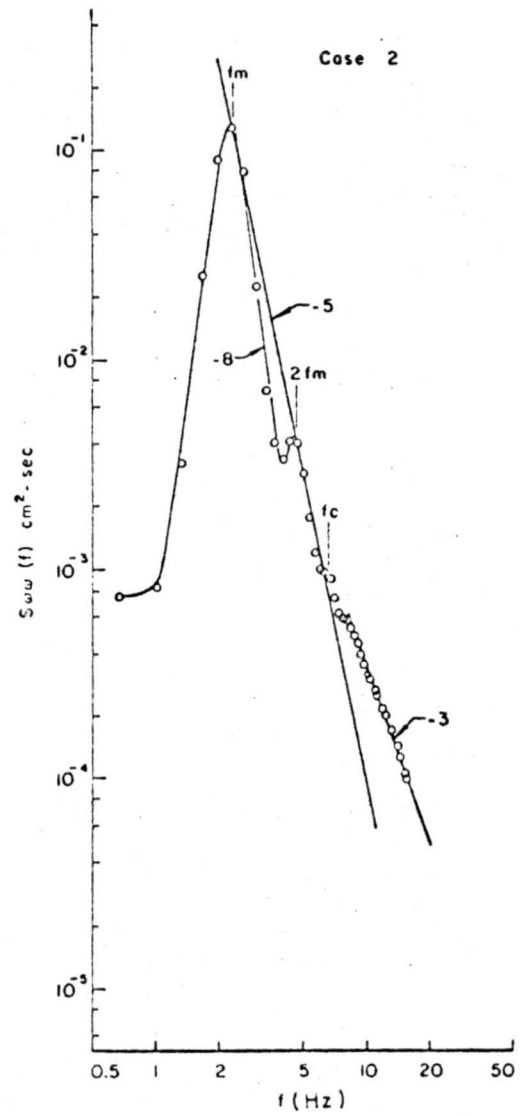
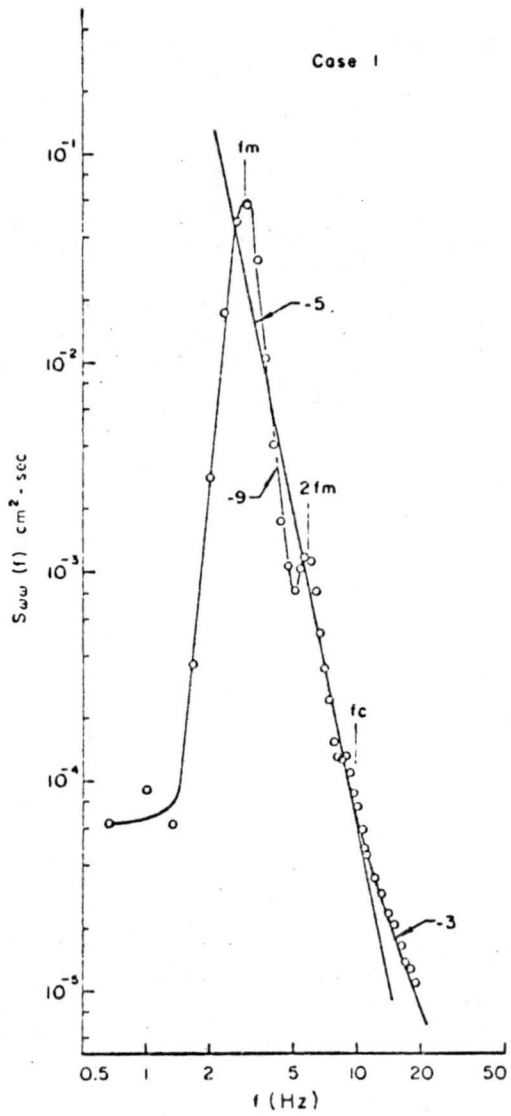


Fig. 15. Energy spectra of water waves.

4.1.3 Average dominant waves

Average dominant waves were defined experimentally according to the procedure described in Section 3 of Chapter II. These are the waves above which local properties of air flow are investigated. Two typical average dominant waves with confidence band of estimation are shown in Figs. 16 and 17. The positions along the waves are designated by numbers, so that they can easily be referred to later.

The time axis can be converted to a space axis by introducing the phase velocity, which is 0.5 m/sec and 0.65 m/sec computed from gravity wave theory based on \bar{H} and \bar{p} for case 1 and case 2 respectively. As far as the local air velocity properties above water waves are concerned, the space and time presentations would not show any difference.

There is little difference between the levels of the troughs on windward and leeward sides of waves. Their elevations are represented by a mean value. The distances are defined as follows: average wave height \bar{H} = distance (crest, trough); average wave period \bar{p} = distance (windward trough, leeward trough); \bar{p}_w = distance (crest, windward trough); \bar{p}_c = distance (crest, leeward trough). In case 1, \bar{H} is 1.8 cm, and \bar{p} , 0.33 sec. In case 2, \bar{H} is 2.7 cm, and \bar{p} , 0.42 sec. By introducing phase velocities from gravity wave theory, the corresponding calculated wave lengths are 16.5 cm and 27.3 cm, yielding the steepness \bar{H}/λ , 0.092, for the first case and 0.10 for the second case. The ratio of the average slopes on both sides, i.e., $\bar{\lambda}_w/\bar{H} \div \bar{\lambda}_L/\bar{H} = \bar{\lambda}_w/\lambda_L = \bar{p}_w/\bar{p}_L$, approximately equals to 1.25. The average frequencies, reciprocals of the average period, which are 3 Hz and 2.4 for cases 1 and 2 respectively, just equal the dominant frequencies associated with their spectral peaks.

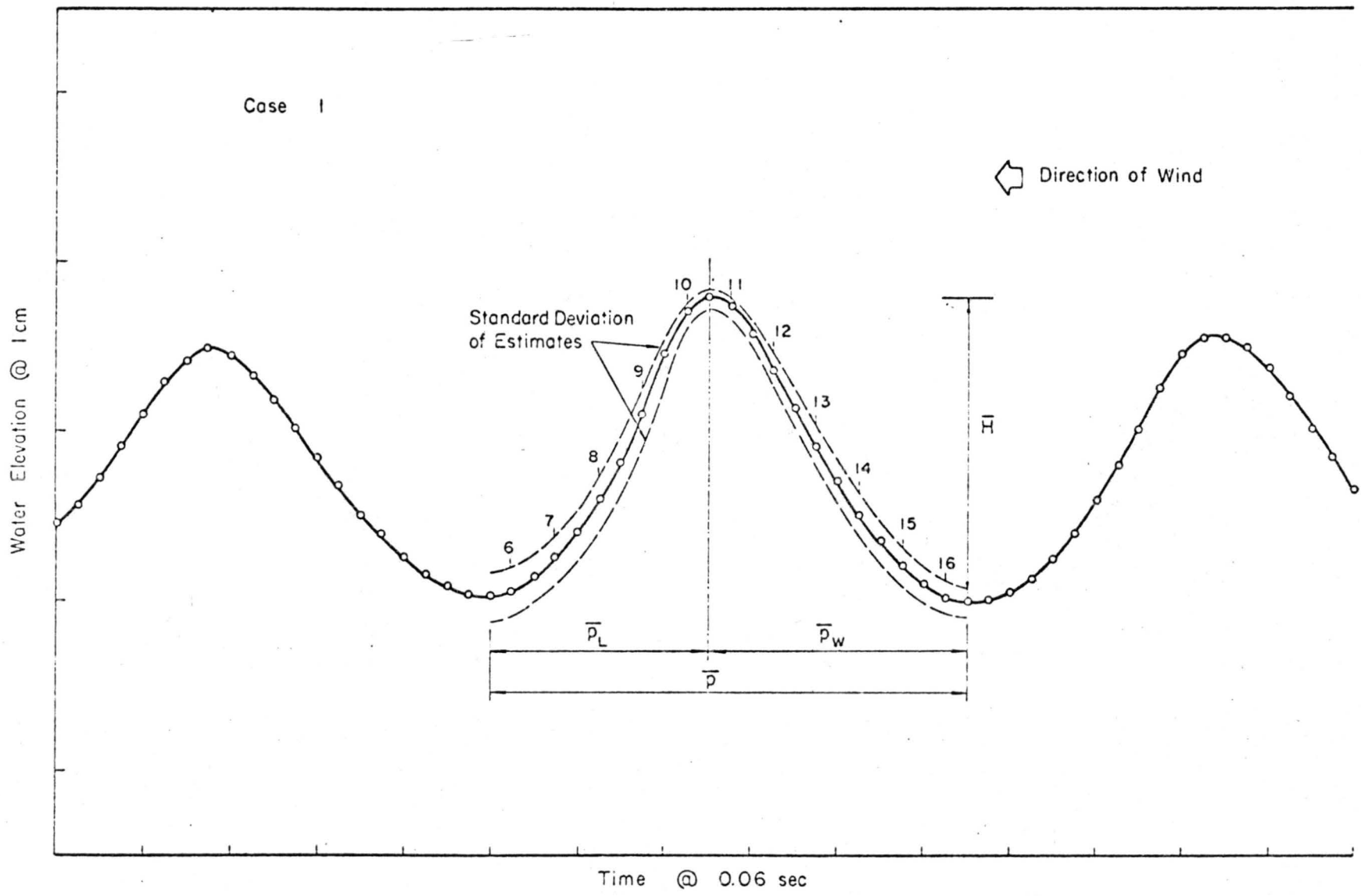


Fig. 16. Average dominant wave (I).

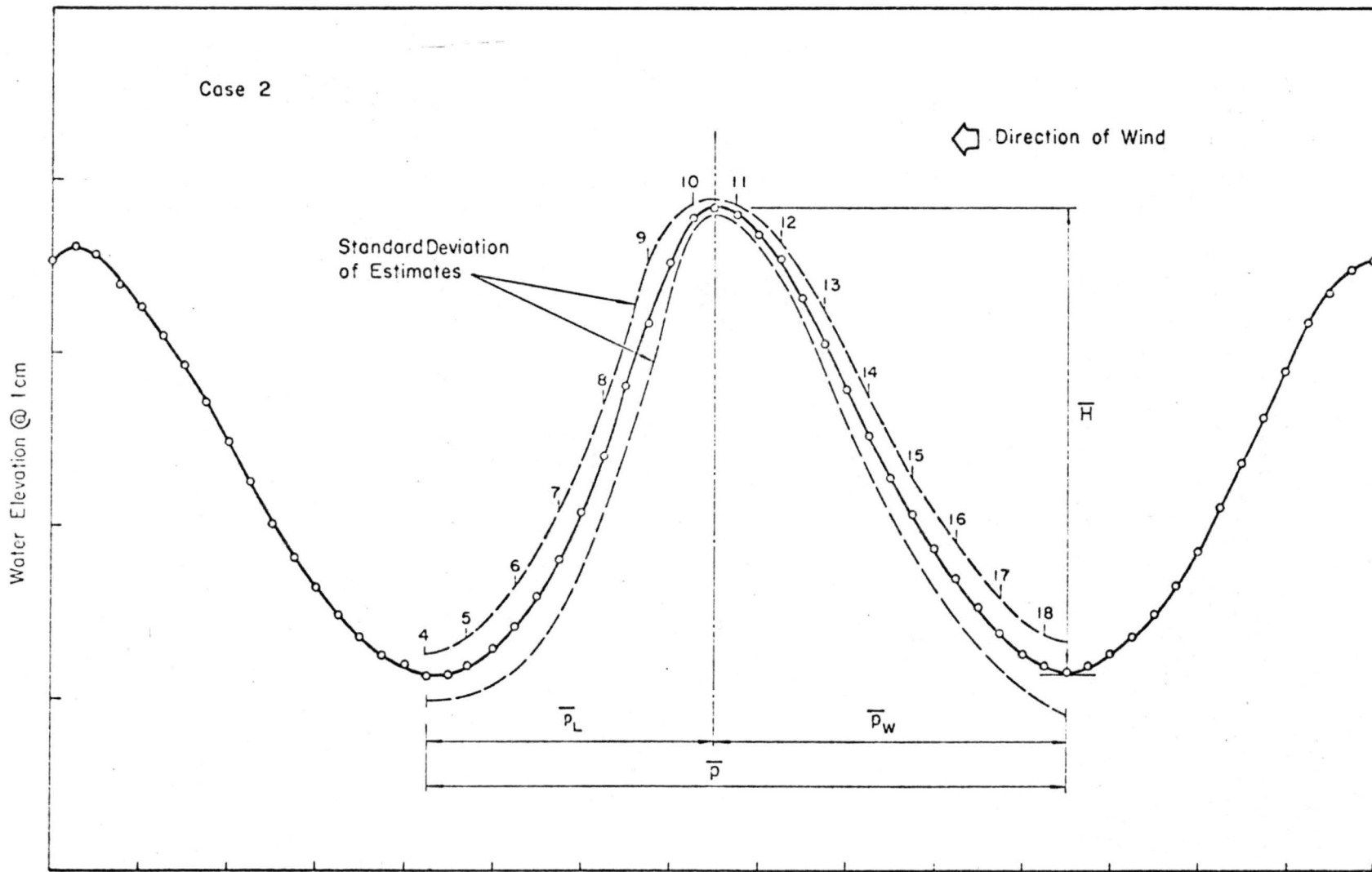


Fig. 17. Average dominant wave (II).

Although the ripples riding over the dominant waves do not appear in the profiles of the average waves, their influence on the air flow properties are still retained. The reason is that the air velocity data were taken before the averaging process was applied to obtain average dominant wave.

The set of average design waves calculated from several different runs are considered to be the same. Ten average design waves for each case are superimposed on each other in Fig. 18 and Fig. 19. The only difference results from the different D.C. levels of the capacitance probe.

4.2 Properties of the Turbulent Air Flow over Water

In this section, the measured properties of air flow over the water are presented, which include the mean velocity, RMS of turbulent fluctuation and energy spectrum. The local properties over average dominant waves are given first. The overall mean properties over the mean water level, for both fixed probe and moving probe references are then inferred from the local values. The inferred values are compared with those obtained directly by continuous sampling over many different wind waves. In this manner, the self-consistency of the experimental data are checked.

4.2.1 Simultaneous visual records of turbulent air and water waves

Figure 20 shows a typical set of simultaneous time records of water surface displacement and instantaneous air velocity taken with a moving probe. The sequence of records were taken with the Brush strip chart recorder as function of different heights from the instantaneous shape of the water surface under the conditions of case 2.

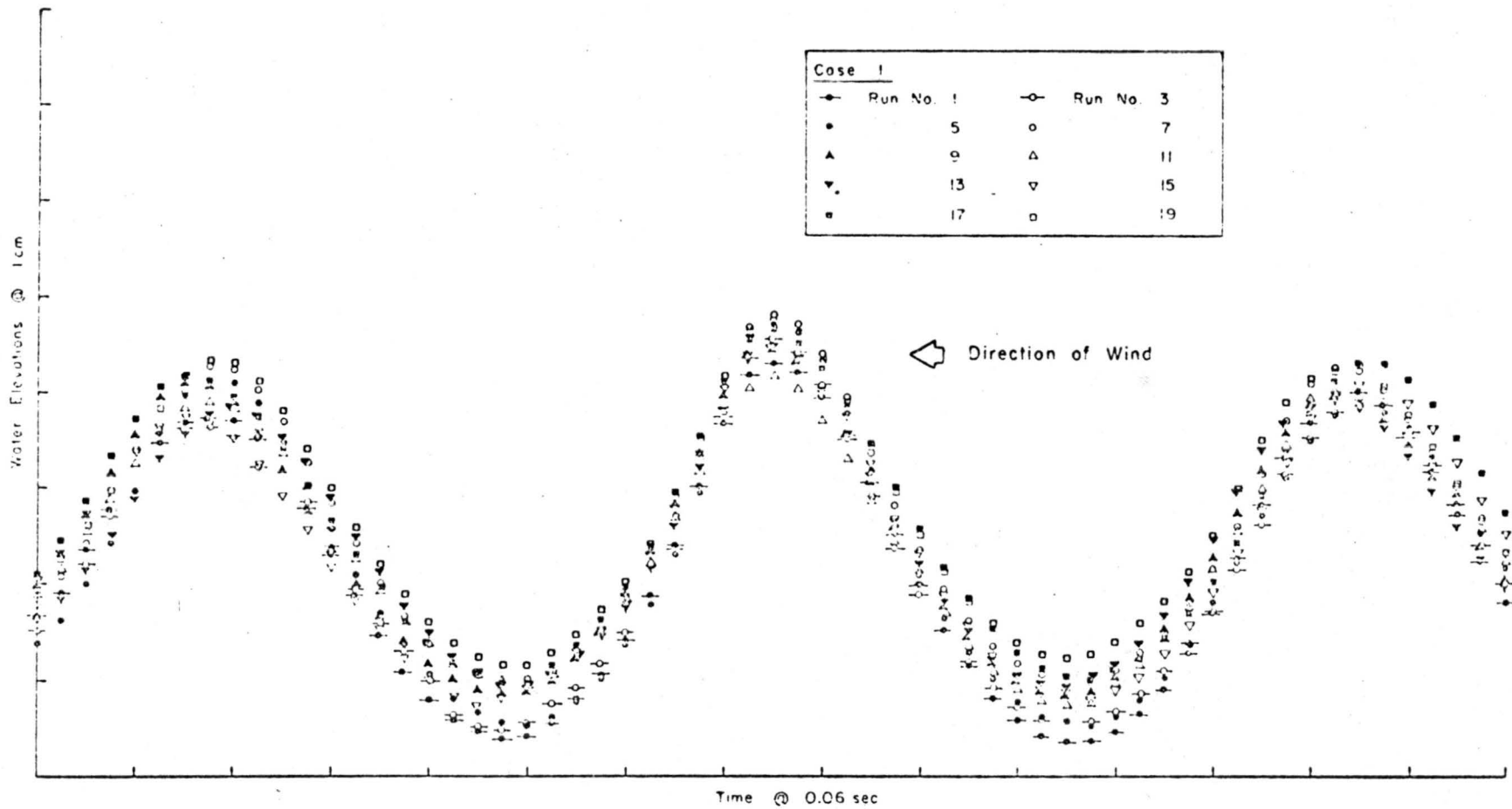


Fig. 18. A set of average dominant waves (I).

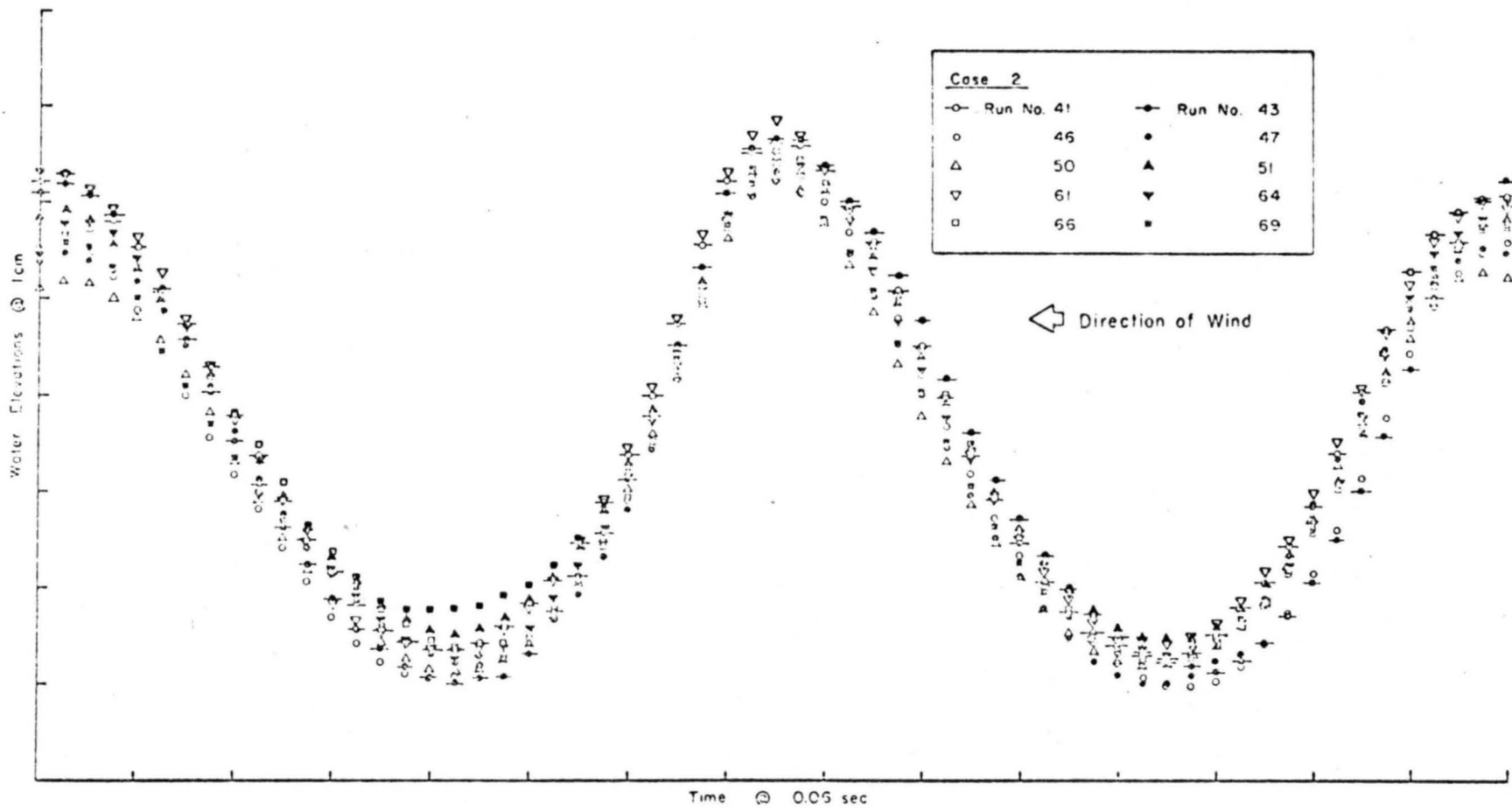


Fig. 19. A set of average dominant waves (II).

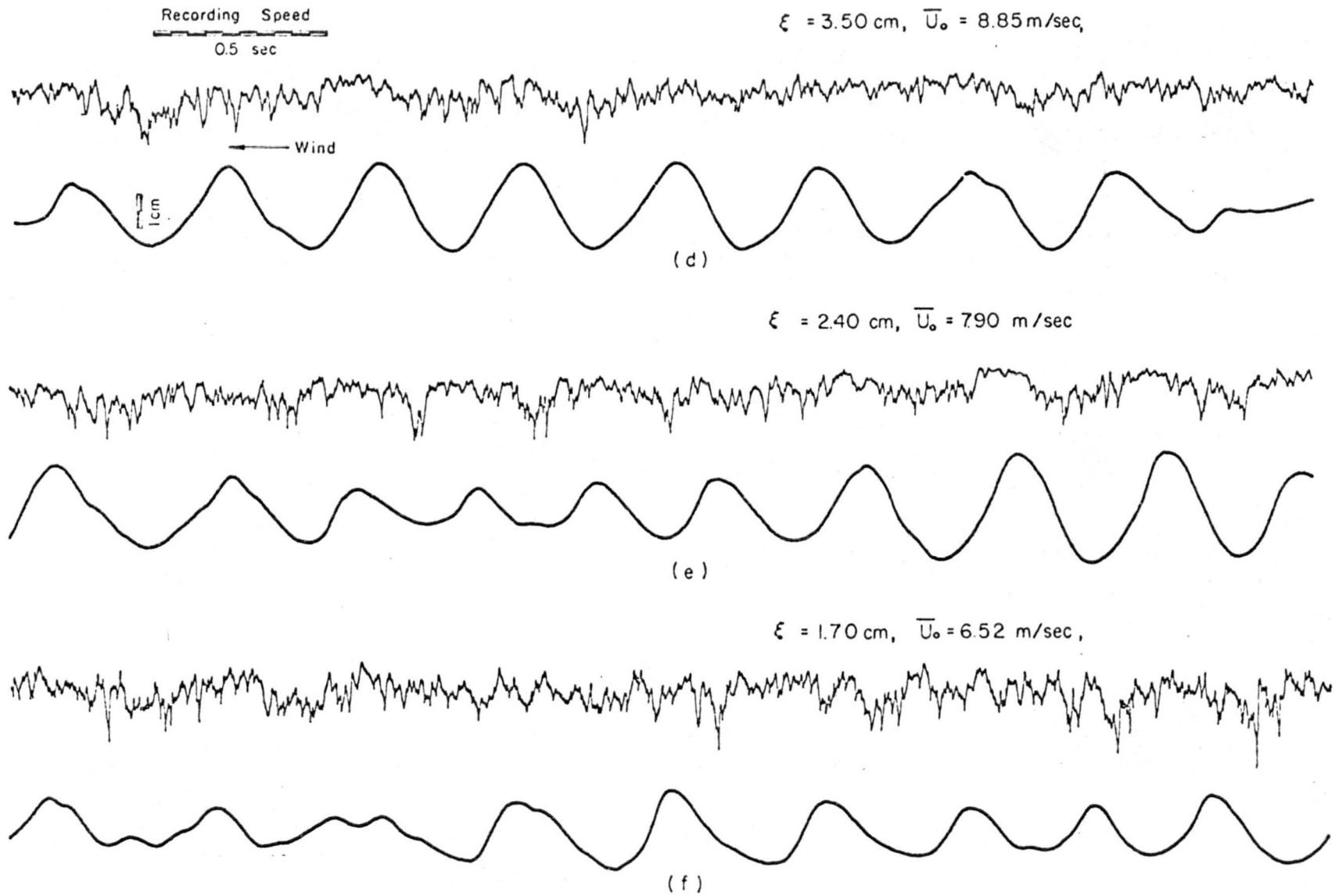


Fig. 20. Continued.

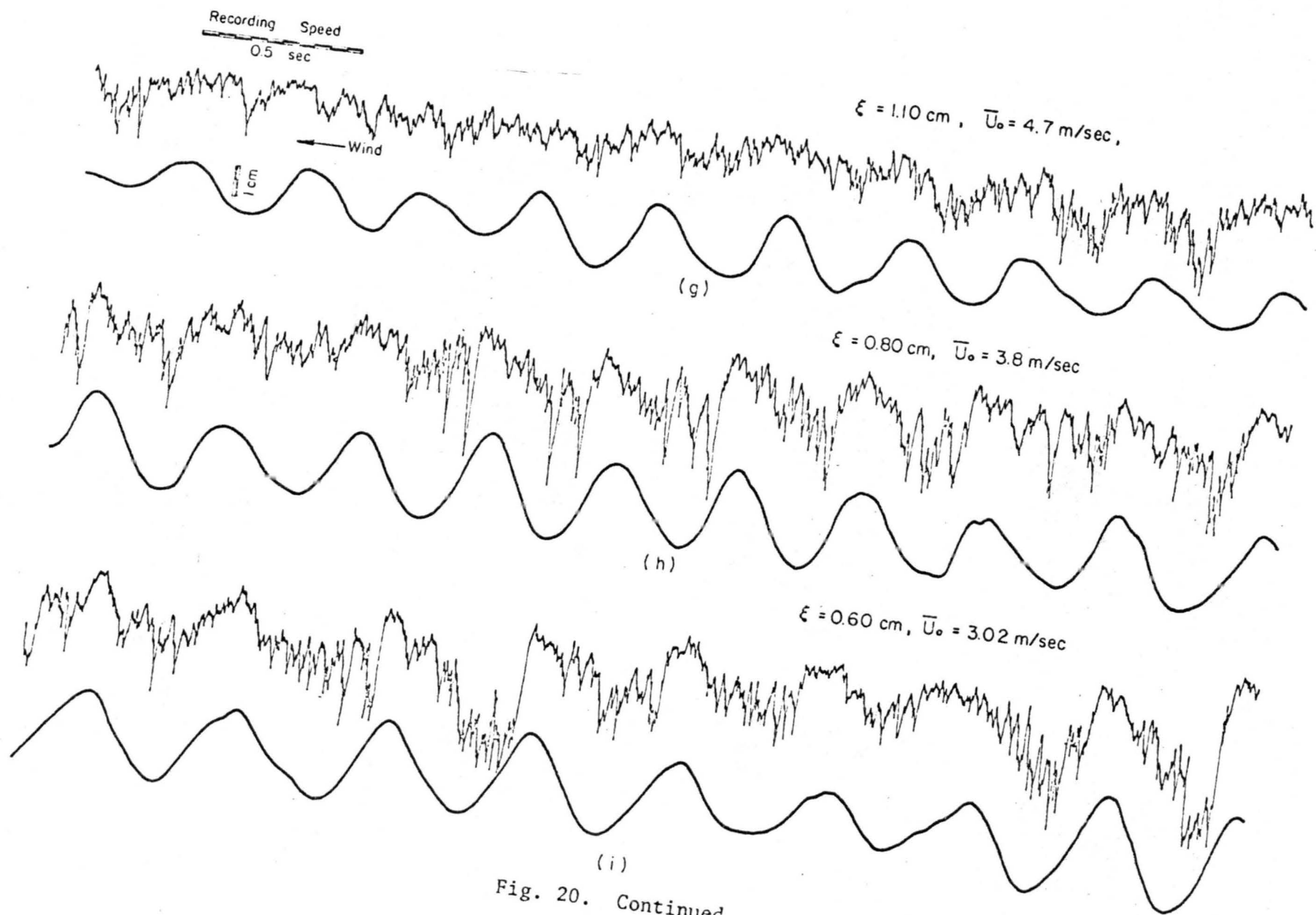


Fig. 20. Continued.

They were recorded in arbitrary D.C. levels so that only the instantaneous velocity fluctuation appears.

At a height well above the air-water interface (about four times the wave height of 2 cm) air flow is completely free from the effect of water surface motion (figs. 20a, 20b) and is characterized by weak irregular oscillations with constant intensity. As the height decreases, the velocity fluctuations become larger, particularly above wave troughs. The instantaneous velocity then begins to reveal its dependence on the relative position with respect to the wave. The mean velocity corresponding to crests is higher than that corresponding to troughs (Figs. 20c, 20d, and 20e). The wave dependence is especially evident in the air flow over higher amplitude waves in the wave train. Thus, the air velocity at a constant height above the water surface shows a velocity field coupled with the wave pattern. With further decrease in height, the coupled appearance becomes more pronounced (Fig. 20f and 20g). The air flow over the windward and leeward side valleys has a completely different character, (Fig. 20h and 20i). A much larger velocity fluctuation occurs over the leeward side of crests. At places just behind the crests (leeward) the air velocity reaches a maximum value and then falls suddenly. The instantaneous velocity behind the crest is apparently lower than that in front of the corresponding crest. These observations give a strong suggestion of flow separation from the wave crest.

From previous qualitative observations, it is seen that the texture of the air flow is considerably altered by the oscillations of the water surface. The properties of the air flow are significantly different from position to position above the wave profile. To

understand the physical processes which occur at the air-water interface, the determination of local turbulent air properties above and around water waves becomes necessary.

4.2.2 Mean velocities

a. Local mean velocity profiles.--The local mean velocity is the sum of the overall time mean value and the fluctuating components associated with wave and probe motions. The local mean velocity profiles along an average dominant wave, at 11 positions in case 1 and at 14 positions in case 2 are shown in Figs. 21 and 22. The corresponding data are also listed in Tables 1 and 2. These profiles are constructed at the corresponding positions with zero velocity axes vertically through the points they represent. The air flow direction is from right to left with reference to the figures. At the lowest elevations, the signal at the lee side of waves was occasionally disturbed by the water droplets, thus those data were not accepted. In case 2, two velocity profiles with different symbols are shown at the lowest trough position (position 4 or position 18). They are estimated independently by using the data in the two troughs on the windward side and lee side. But they actually represent the same position with respect to the wave, thus, illustrating that the consistency between the two profiles is good.

To show the estimated confidence level of the ensemble average of the 20 short time-events, the confidence band; i.e., the standard deviation of 20 data points, of the estimated velocity profiles at position 4 of case 2 is shown in Fig. 23, the corresponding skewness factors, $\overline{u^3}/(\overline{u^2})^{3/2}$, and flatness factor $\overline{u^4}/(\overline{u^2})^2 - 3$, which describe the symmetry and width of data distribution are both

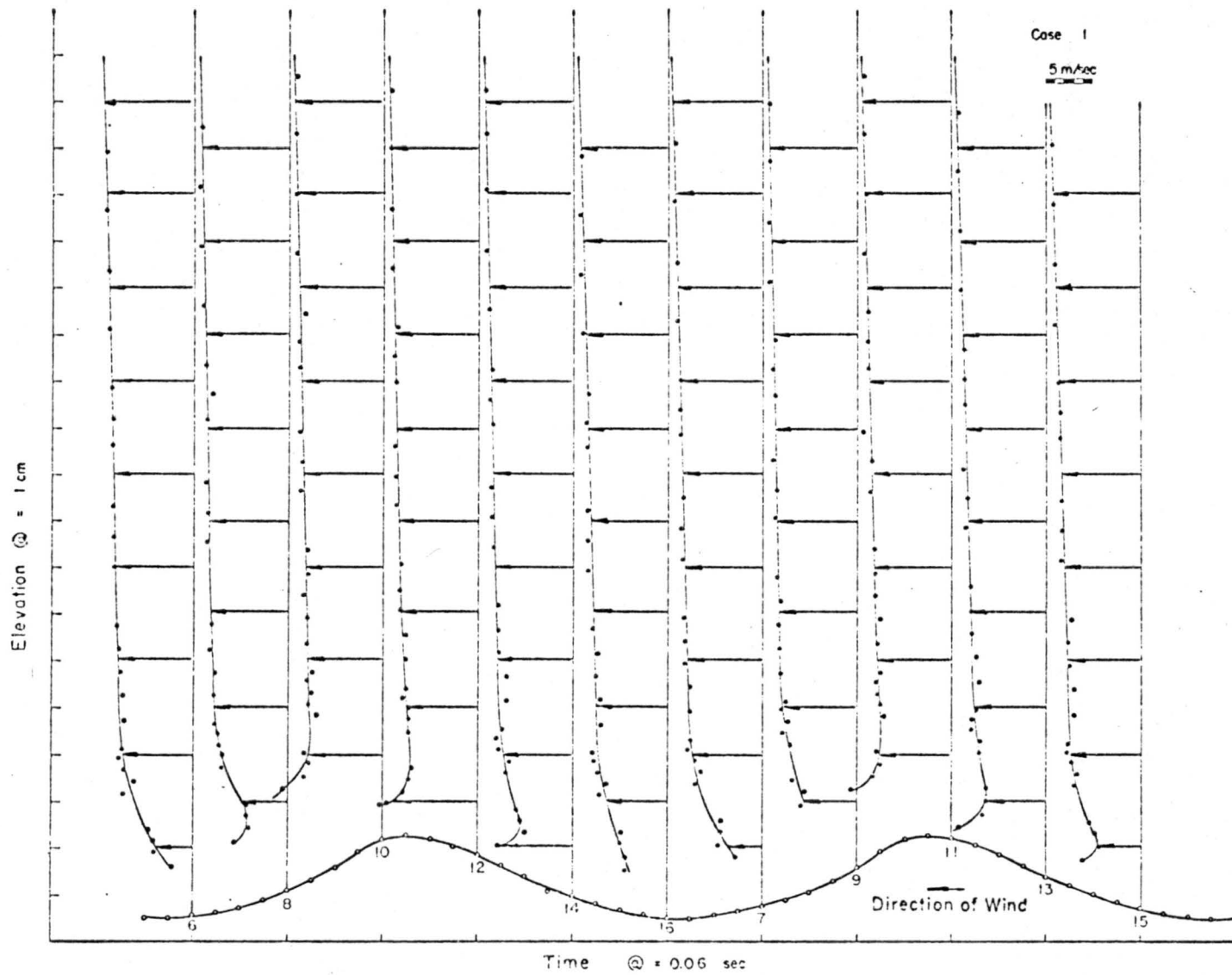


Fig. 21. Local mean velocity profiles (I).

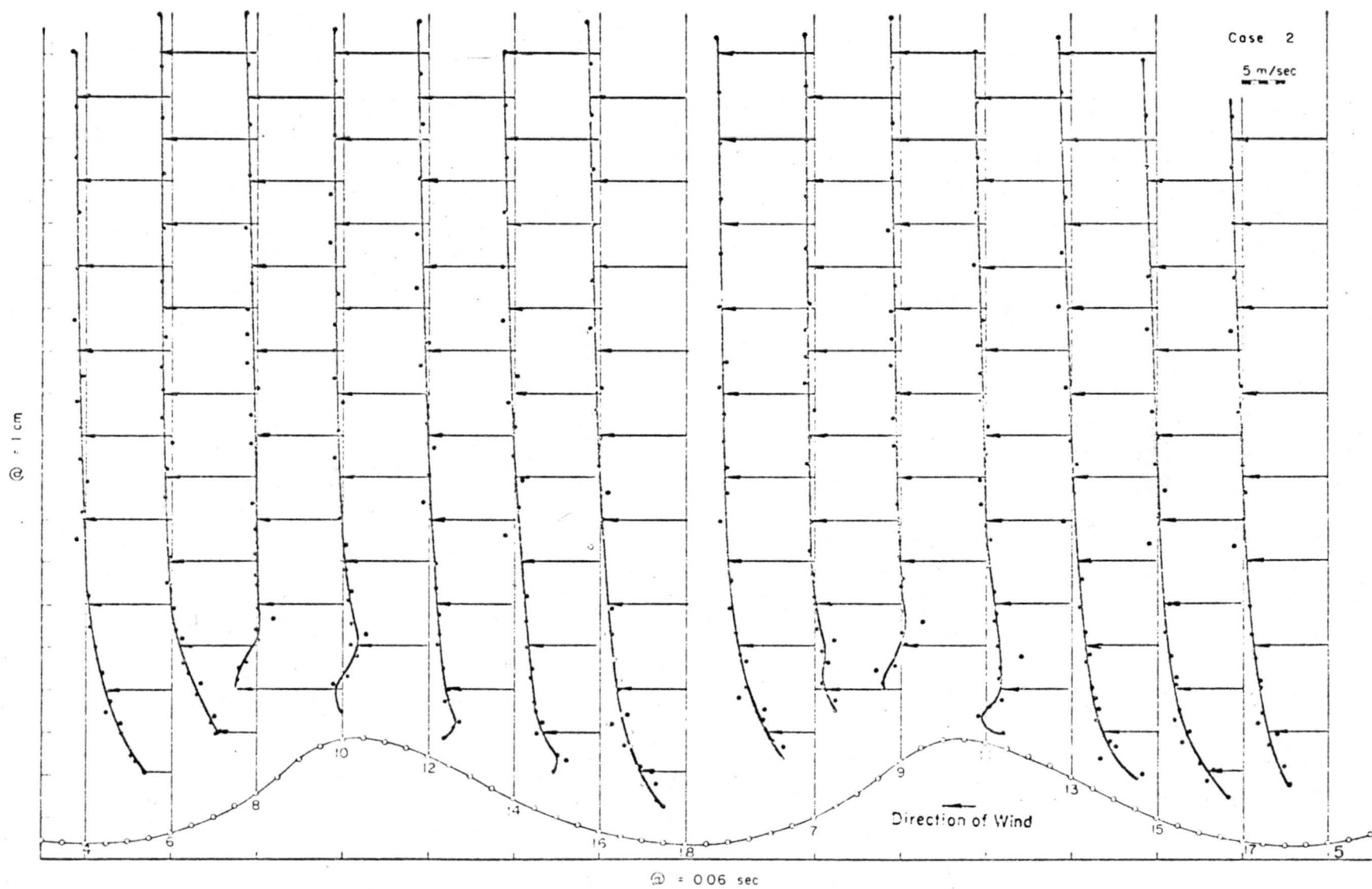


Fig. 22. Local mean velocity profiles (II).

Table 1. Local Mean Velocity Data (m/sec) Case 1. $\bar{U}_{Loc} = 9.26$ m/sec $\bar{H} = 1.8$ cm $\bar{p} = 0.33$ sec

(cm)	16.35	15.10	13.81	12.55	11.28	10.65	10.11	8.74	8.10	7.46	6.20	5.69	5.18	4.68	4.17	3.66	3.40	3.15	2.90	2.64	1.88	1.63	1.37	1.12
6	9.2438	9.2945	9.1559	9.0337	8.6424	8.5255	8.5460	8.6334	8.3852	8.3887	7.9711	7.9220	7.7619	7.4967	7.2993	7.5129	7.7266	7.3395	6.291	7.2964	4.7424	4.1845	4.0462	2.1857
7	9.2706	9.3528	9.1348	9.0375	8.6610	8.6976	8.6223	8.7250	8.5043	8.3662	8.1273	8.0597	8.1295	7.5764	7.6253	7.6468	7.7344	7.2334	6.3890	7.0886	4.3920	4.3847	4.6270	2.7692
8	9.2659	9.3735	9.2946	9.0792	8.8204	8.8133	8.6953	8.7718	8.4927	8.5608	8.3641	8.1138	8.3543	7.7763	7.9836	7.6689	7.4915	7.2989	7.0170	7.1211	4.4370	4.3452	4.2104	5.5517
9	9.3035	9.3454	9.3352	9.2217	8.7725	8.9225	8.7725	8.8534	8.5848	8.6436	8.4072	8.1609	8.3533	8.1399	8.1291	7.5878	7.8619	7.3720	7.8339	7.2297	6.8131	5.5602	5.8011	
10	9.2970	9.3437	9.2703	9.2219	8.8322	8.9670	8.8509	8.8697	8.6620	8.7805	8.4951	7.9546	8.4295	8.0801	8.3083	7.5023	7.9855	7.4064	7.8468	7.1356	8.1952	7.8213	8.2482	
11	9.2508	9.3141	9.2473	9.2679	8.9269	8.8177	8.8841	8.9394	8.5810	8.6706	8.3469	8.1238	8.0531	7.7062	7.9268	7.5744	7.8800	7.2858	7.5821	7.1756	7.9346	7.6374	8.2370	
12	9.2675	9.3140	9.2182	9.1662	8.6459	8.7883	8.6946	8.7489	8.6222	8.6349	8.1117	8.1486	8.1295	7.5889	7.5502	7.5461	7.8002	7.2727	7.2724	7.2864	7.0483	7.2547	7.6650	
13	9.2825	9.3017	9.1554	9.0888	8.7356	8.6859	8.5999	8.6561	8.4597	8.4737	8.0234	7.9107	7.9170	7.3277	7.2279	7.4420	7.8859	7.2900	6.9170	7.0508	6.3823	6.3666	6.6533	
14	9.2097	9.3246	9.0997	8.9408	8.5991	8.6586	8.5074	8.6056	8.4608	8.3904	7.8635	7.9628	7.7628	7.0283	7.0861	7.4883	7.9471	7.3572	6.5507	7.0852	6.0345	5.5830	5.1577	7.6955
15	9.2701	9.2586	9.1599	9.0117	8.5831	8.4888	8.5236	8.4172	8.2736	8.4412	7.8363	7.8457	7.5200	7.0961	7.0863	7.6350	7.6873	7.3566	6.7526	7.1370	5.4111	4.9584	4.3499	6.1169
16	9.2228	9.2939	9.1998	8.9585	8.4360	8.5747	8.5214	8.3905	8.4239	8.3871	7.7939	7.7394	7.4803	7.0311	7.1620	7.7626	7.7443	7.2613	6.4513	7.2334	4.8016	5.0413	4.3223	4.2584

Table 2. Local Mean Velocity Data (m/sec) Case 2. $\bar{U}_{Loc} = 11.48$ m/sec $\bar{H} = 2.7$ cm $\bar{p} = 0.42$ sec

(cm)	18.4	17.1	15.9	14.6	13.3	12.05	10.75	10.15	9.52	8.89	8.26	7.63	6.98	5.57	4.93	4.35	3.84	3.66	3.07	2.82	2.57	2.31	1.61	1.68	1.42	1.04	0.915	
4	11.4912	11.2166	11.1663	10.8660	11.0704	11.2705	10.1500	10.7028	10.0886	10.4301	9.5581	9.6119	11.0210	9.0435	8.8958	8.3271	7.5159	8.1788	6.7188	8.8809	6.2364	6.3507	5.5812	4.7496	4.9227	3.3479	2.6950	
5	11.5105	11.1341	11.1278	10.8106	10.9860	11.1176	10.0186	10.7932	10.2081	10.5717	9.7153	9.7540	10.9270	9.2547	9.0217	8.3242	7.4686	7.6896	7.1536	8.7667	6.1152	6.4899	5.4582	4.6393	4.5307		2.0454	
6	11.4760	11.1362	11.1086	10.7745	10.9391	11.3079	10.2533	11.0080	10.5233	10.6705	9.8414	10.2349	10.8108	9.5824	9.3358	8.8149	7.9328	7.4491	6.9994	8.7501	5.7646	5.7857	4.6546	4.1939	4.5088			2.7912
7	11.4927	11.2240	11.0403	10.8362	10.9741	11.2114	10.3672	11.0602	10.5829	10.6153	10.1200	10.1463	10.9530	9.7428	8.8320	9.1304	8.5438	7.9309	7.9230	8.6850	5.7037	5.8166	4.7211	3.6766	3.9772			
8	11.4543	11.2279	11.1227	10.8396	10.9462	11.1936	10.6118	11.1312	10.8591	11.0125	9.8294	10.3769	10.6524	10.0900	10.3835	9.6997	9.4359	8.6805	8.5238	8.3913	6.4072	6.9836	4.8137	5.2951	4.7467			
9	11.4613	11.1805	11.0727	10.8628	11.1067	11.1207	10.5925	11.0605	11.0183	11.1863	10.1130	10.5231	10.8836	10.1346	10.4994	10.2553	10.0150	9.8207	9.6338	7.6320	9.0596	8.3835	9.0887	10.9987	10.5275			
10	11.4879	11.2355	11.0602	10.8524	10.9861	11.3518	10.7057	11.1612	11.2267	11.2953	10.2323	10.7125	10.6580	10.5036	10.2884	10.1166	10.1056	9.9001	9.8816	8.0080	10.0394	9.8586	11.1413	13.0302	12.2287			
11	11.4548	11.2075	10.9964	10.8854	10.9453	11.4760	10.5645	11.1432	11.0215	11.0462	10.1357	10.8003	10.7328	10.2901	10.2187	10.1360	9.7074	9.8093	9.5941	7.4434	9.7598	9.3369	10.6875	12.7778	12.0084			
12	11.4356	11.1907	10.9407	10.8412	10.9798	11.4773	10.4985	11.0022	11.0324	11.0330	10.0581	10.4675	10.8340	9.9716	9.6486	9.6466	8.9501	9.2704	8.8542	7.2103	9.0056	8.7349	9.3441	11.0500	10.8042			
13	11.5069	11.1575	10.9672	10.8490	11.0741	11.3924	10.2956	10.8594	10.5707	10.6517	9.7700	10.0710	10.7365	9.4976	9.6318	9.1163	8.7176	8.9904	8.5840	6.8178	8.2853	8.4641	8.1322	9.5318	10.7256			7.9395
14	11.5122	11.1826	10.9950	10.7636	11.0115	11.3837	9.9421	10.8536	10.1152	10.2271	9.3631	9.8395	10.6442	9.1248	9.0666	8.7096	8.6948	8.8197	8.2419	7.3086	7.5763	7.9491	6.2366	6.9805	8.1109	4.7053		
15	11.4843	11.1898	11.0534	10.6883	11.1013	11.4088	9.8633	10.6543	10.1118	10.1535	9.3206	9.7107	10.8970	8.6660	8.9345	8.3531	7.7953	8.2514	7.6092	7.1913	6.7344	7.1168	5.4078	4.8023	6.6346	1.7234		
16	11.5125	11.1612	11.0286	10.9124	11.0296	11.3742	9.6892	10.7026	9.9718	10.0916	8.9895	9.4654	10.8280	8.4989	8.5021	8.3674	7.5992	7.9431	7.5621	7.4850	6.6621	7.2398	4.8670	3.7896	5.2806			
17	11.4924	11.1828	11.0662	10.8176	10.9276	11.1842	9.8886	10.5041	9.9105	10.2254	9.0710	9.6870	10.9428	8.5038	8.9364	8.2599	7.7306	7.6628	7.2866	7.8497	6.2411	6.9520	4.9690	3.3141	4.1876	1.6042		
18	11.5114	11.2052	11.0397	10.8140	11.0363	11.1735	9.8587	10.4847	10.0518	10.0786	9.0899	9.6197	10.8885	8.5820	8.5530	8.3316	7.5696	7.7826	7.4013	8.5124	6.3744	7.0522	5.2041	3.9266	3.4050	3.6270		2.9301

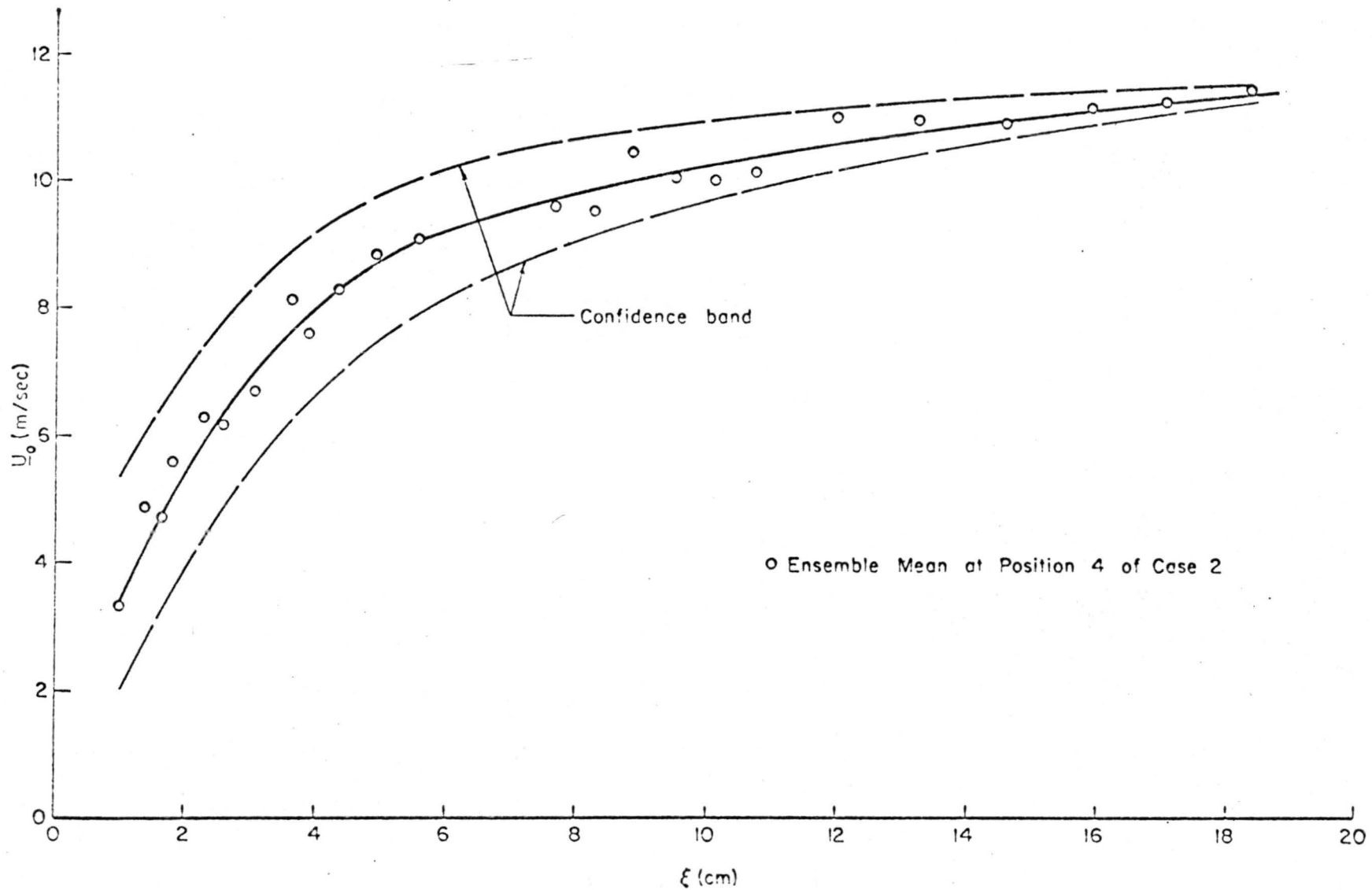


Fig. 23. Confidence band of the local mean velocity profile.

around ± 1 . Therefore, the distribution of data is only approximately Gaussian for which both factors are zero.

The air velocity profiles are plotted over average dominant waves which are assumed stationary. This is not exactly true since the air-water interface is a more complicated boundary than a solid boundary because of (a) the presence of moving waves, (b) water particle motions due to the waves, and (c) wind driven drift currents. The apparent mean air velocities would therefore be modified if they are plotted against a coordinate system moving with the wave celerity so that the wave profile becomes stationary. However the phase velocity and water particle velocity are one order of magnitude smaller than the lowest air velocity measured. Thus, in these cases, they are not significant for our purposes as far as the mean velocity profiles are concerned.

With a single hot wire probe as a sensor, only the magnitude of the velocity vector could be measured. The measured quantities are hence subject to the correction of the attack angle to yield the velocity in the direction of wave propagation. The velocity profiles shown have been corrected for flow direction which was estimated from the streamline pattern. The construction of streamlines will be described in the next chapter (p.105). The angle correction was important only in the layer close to the air-water interface.

The results shown in Figs. 21 and 22, clearly indicate that the mean velocity profiles at heights lower than one wave amplitude from the crests are substantially different from position to position above the water waves. The most evident phenomena is the appearance of a strong "jet" flow around the wave crests. At the windward side

of waves, the air flow begins to be accelerated, and the jet becomes most pronounced at a short distance behind the wave crests. The maximum velocity is even higher than the free stream value.

As was discussed for the visual record, Fig. 20, the dependence of air velocity on the relative positions with respect to wave crests is getting weaker as the heights increase. In order to see quantitatively how the mean air velocity at a given point varies with the passage of underlying water waves, Figs. 24a and 24b have been prepared. In these figures the air velocities at several positions above the average dominant wave of case 2 are superimposed on one another in both moving probe and fixed probe frames of reference. The air velocity (4 times above that of wave height (2.7 cm)) seen by the probes is invariant with time. Below that level, the characteristic of velocity profiles varies from position to position with respect to wave peak, especially from the point of view of the moving probe frame.

b. Mean velocity profiles with reference to the mean water level.--To measure the instantaneous properties of turbulent air flow along water waves is a very elaborate and time consuming task. Field and laboratory measurements are therefore usually restricted to observations with reference to the mean water level.

Before the results of overall mean velocity are presented, the mean velocity profiles of air flow over the aluminum plate are first shown (Fig. 25a). They are logarithmic with height. This assures a well-defined turbulent air flow approaching the water surface.

From the instantaneous local velocity data over average dominant waves in Fig. 22, temporal mean velocities can be inferred by

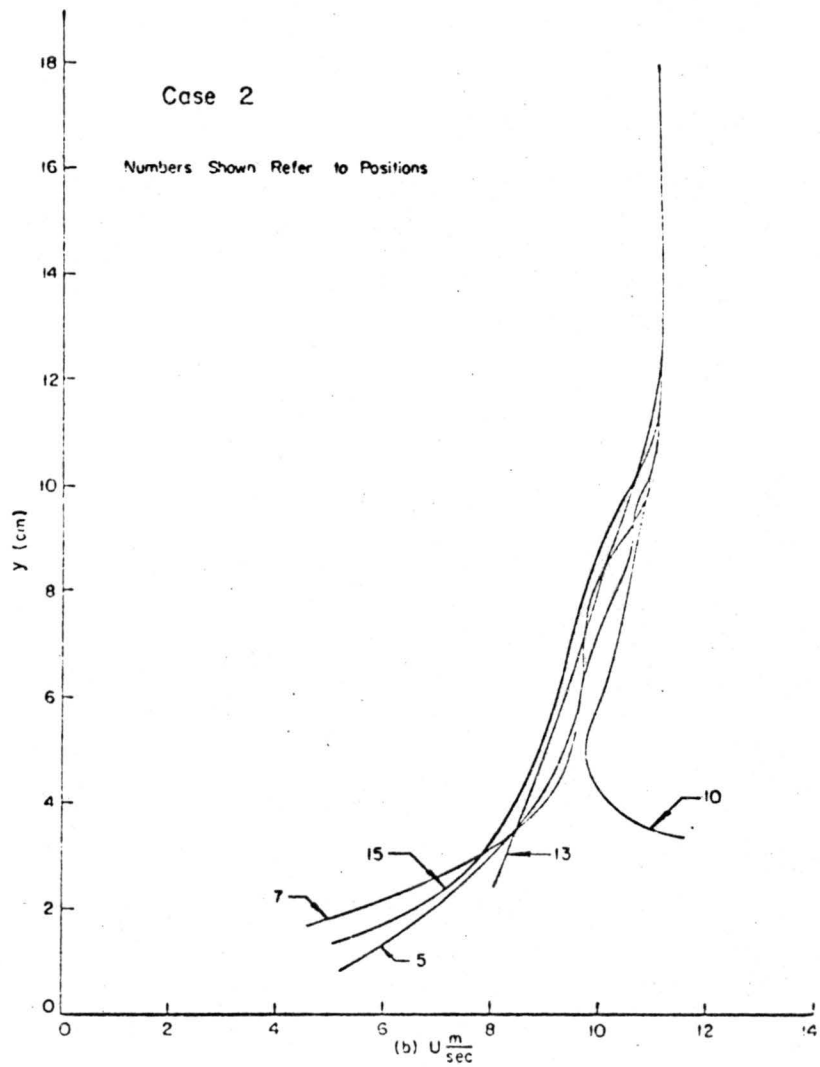
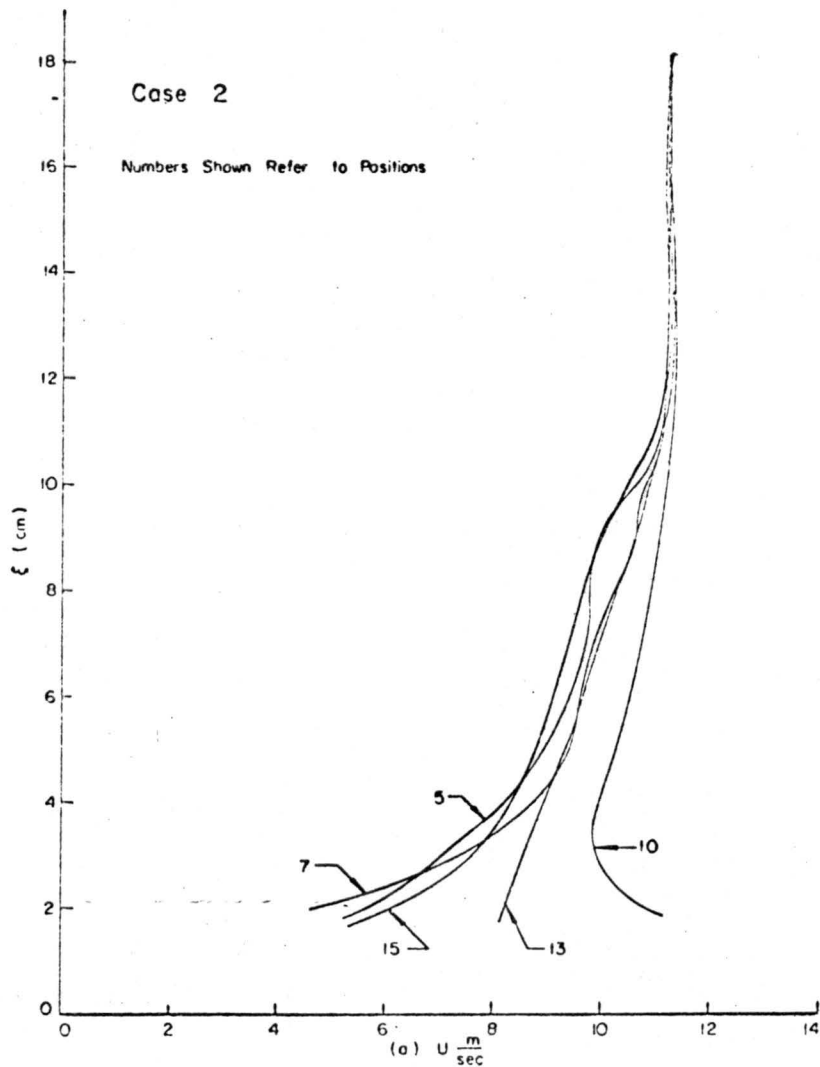


Fig. 24. Comparison of air velocity profiles at different positions along the waves.

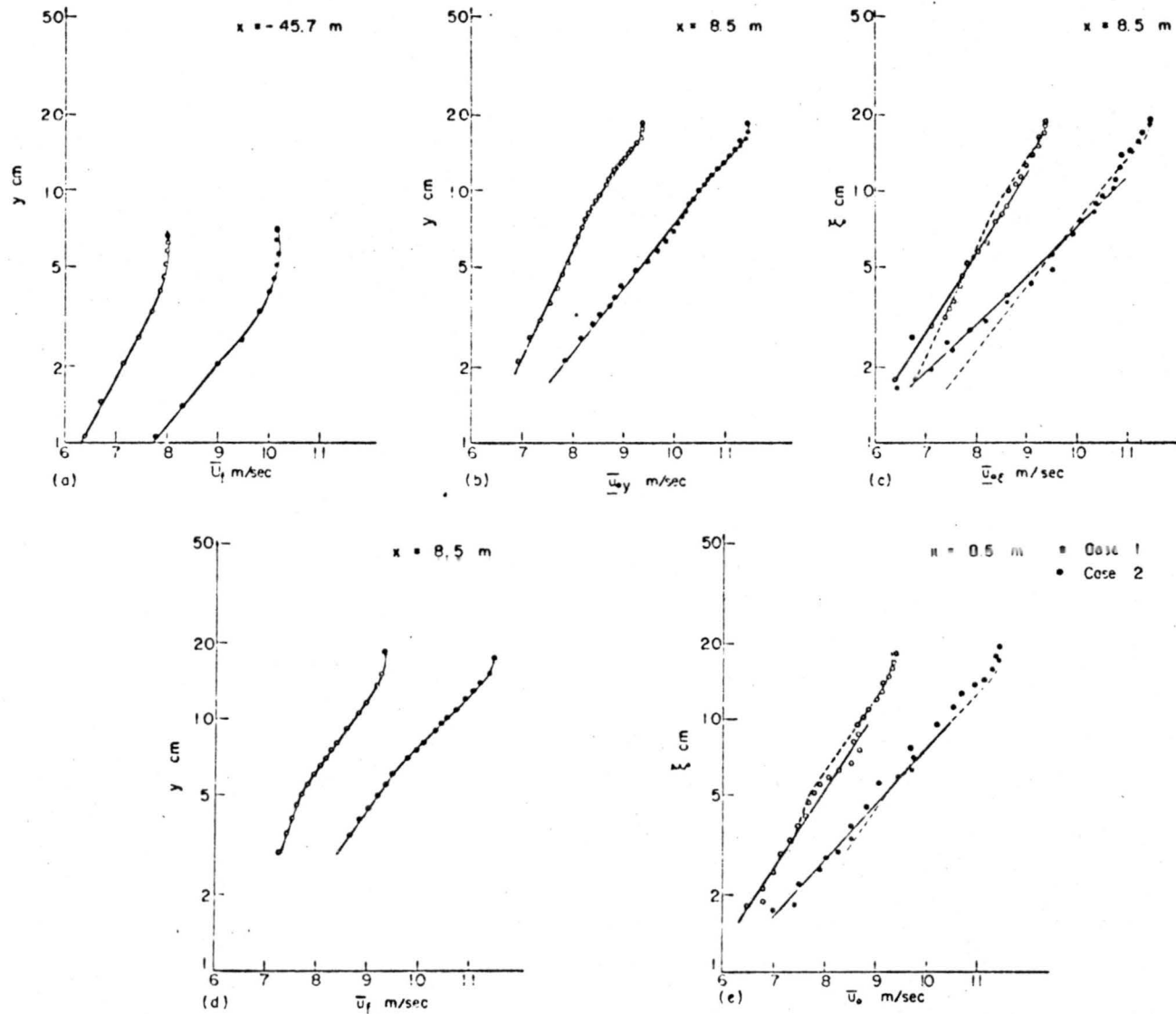


Fig. 25. Mean velocity profiles above the mean water level.

calculating the arithmetical mean of the available local mean velocity data at fixed heights either from the mean water level (constant y 's) or from the instantaneous water level (constant ξ 's). The results correspond to the measurements in fixed probe and moving probe reference frames, respectively. Such results are shown in Figs. 25b and 25c. A weak kink is observed over the mean velocity profiles for fixed probe measurements (Fig. 25b). The data points for moving probe experiments (Fig. 25c) are comparatively scattered, so that only an arbitrary average curve can be drawn. In Fig. 25c, the profiles of fixed probe measurements indicated by a dashed curve, are also shown for comparison. Near the edge of free stream these two sets of data do not show significant differences from each other. Only at heights close to the water surface, the mean velocity at a given ξ is about 5% smaller than the mean velocity at the equivalent y , i.e., at $y = \xi$. Similar results were found for flow over solid wave models by Roll (1949), who compared the result of fixed probe measurement and moving probe measurement with Motzfeld's (1937) data over solid wave model and found the mean wind speed values gained with moving probe reference are about 5% smaller than those determined for the same fixed height at the vicinity of the boundary.

Under the same conditions of case 1 and case 2, the overall mean velocity profiles were also obtained directly from continuous sampling over many different wind waves. The fixed probe measurement was taken with a pitot-static tube and the moving probe measurement was taken with a hot wire probe. The profiles constructed in terms of the logarithmic height above the mean water level are shown in Fig. 25d and Fig. 25e. These results agree fairly well with those inferred from the

velocity data over the ensemble of the highest waves. Again, the data for moving probe measurements are more scattered and show a lower velocity than those obtained by fixed probe measurement at the heights close to the water surface; but the agreement between these two types of measurement still appears satisfactory.

The wind profiles from direct fixed probe measurement show the existence of two distinct logarithmic regions (Fig. 25d), one over the data points at the upper portion of the boundary and the other over the data points near the air-water interface. The inferred fixed probe measurements have a similar tendency but not so evident as observed here. The fact that the velocities near the surface are greater than the corresponding upper logarithmic profile indicates the reduction of the slope $\partial u/\partial y$, i.e., of turbulent shear. This result is consistent with that observed by Hidy and Plate (1966), Plate and Hidy (1967), Hess (1968), Shemdin and Hsu (1966) and Shemdin (1967) over laboratory wind waves, Takeda (1963), Weiler (1966) over ocean waves, and Motzfeld (1937) and Moore and Laird (1957) over solid model waves. However, there has not been any conclusive physical explanation for this kind of behavior.

4.2.3 Longitudinal turbulent fluctuation

a. Local $\sqrt{u'^2}$ profiles.--The local $\sqrt{u'_o{}^2}$ was calculated from the experiments by means of Eq. (2-30). The profiles of longitudinal turbulent fluctuation along an average dominant wave, at 11 positions in case 1 and 14 positions in case 2 are shown in Figs. 26 and 27. The corresponding data are listed in Table 3 and Table 4. These profiles are constructed at the corresponding positions with zero axes vertically through the points they represent. The direction

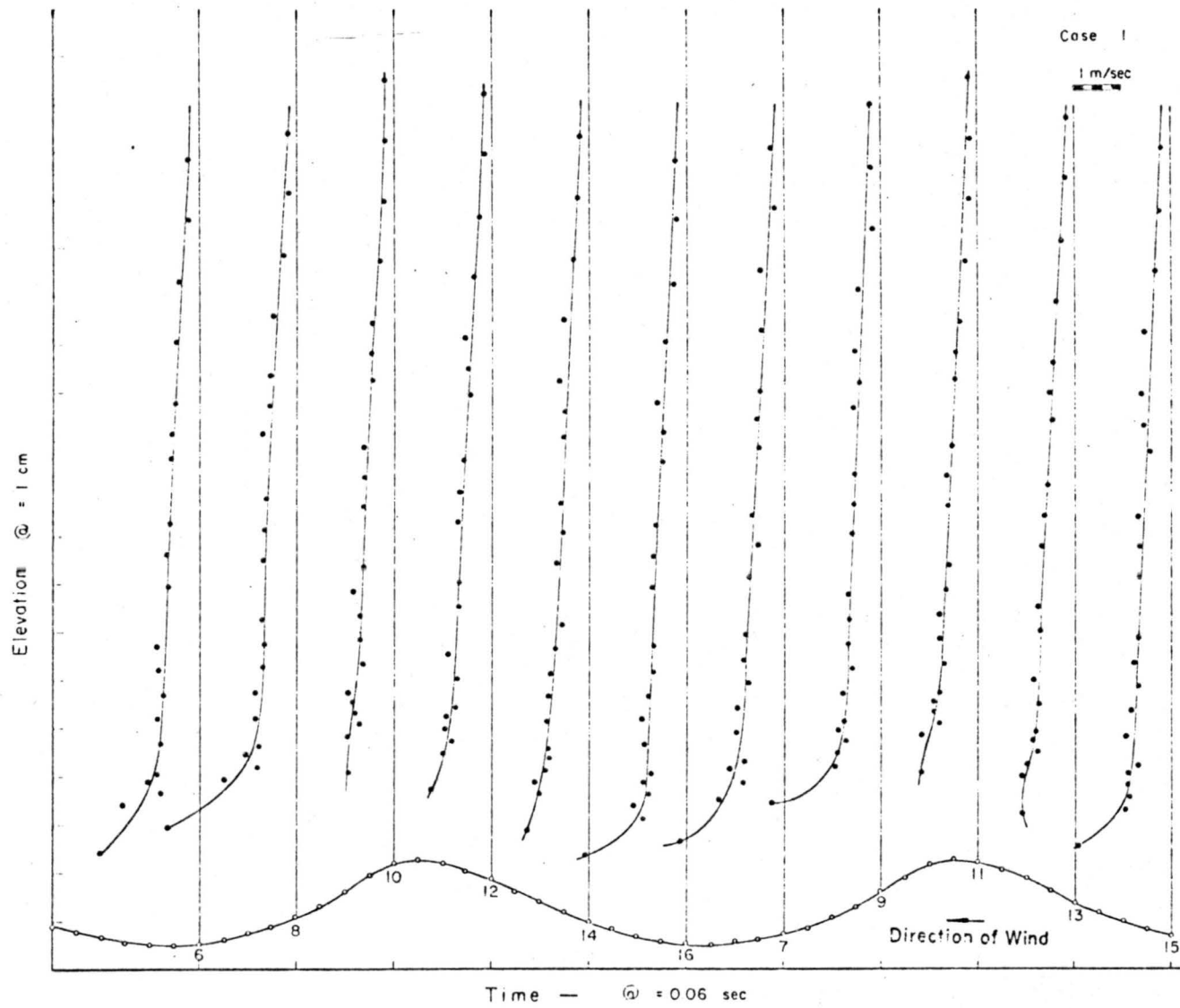


Fig. 26. Local turbulent RMS profiles (I).

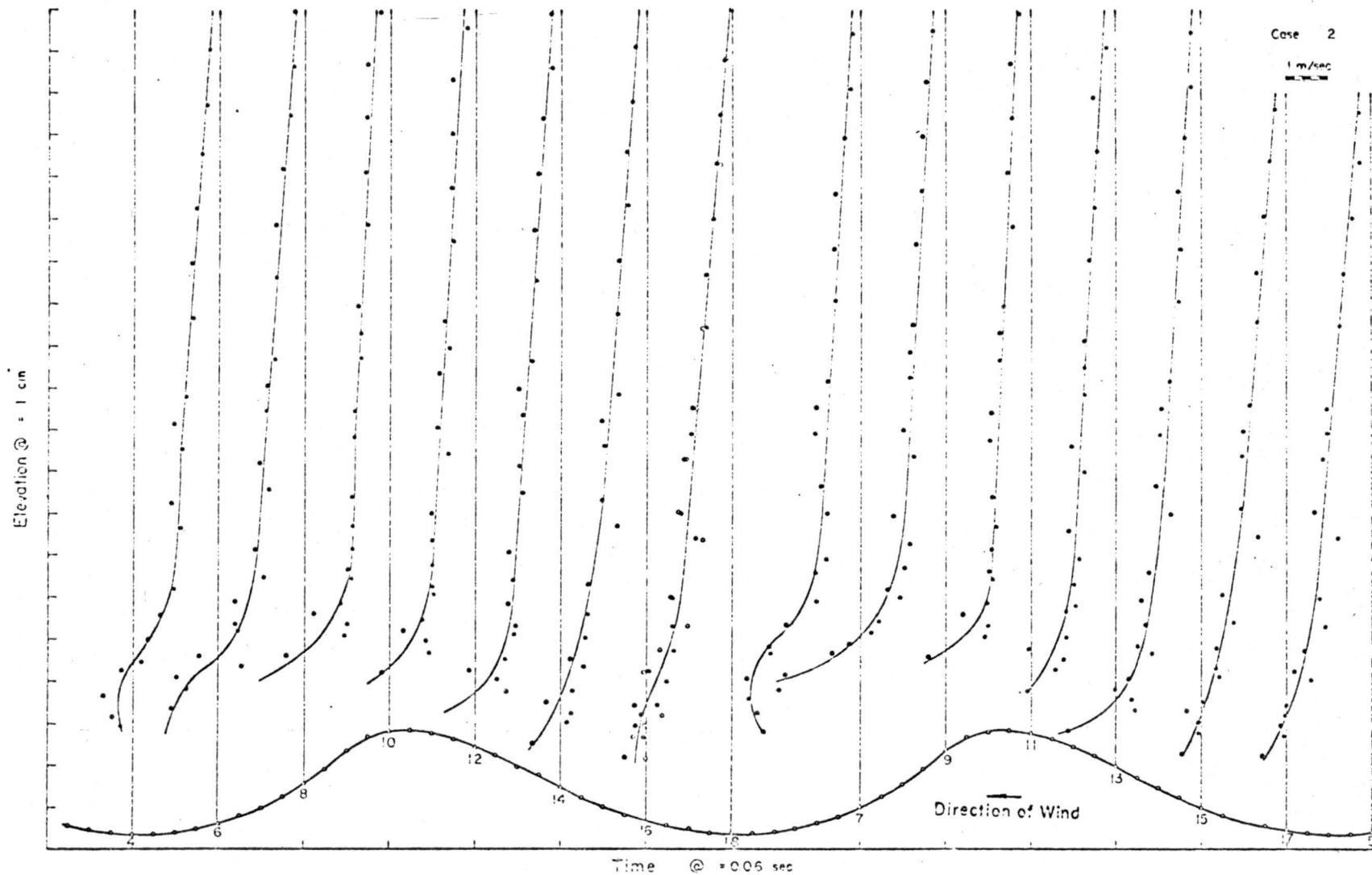


Fig. 27. Local turbulent RMS profiles (II).

Table 3. Local $\sqrt{u'^2}$ Data of Case 1. $\bar{U}_{Loc} = 9.26$ m/sec $\bar{H} = 1.8$ cm $\bar{p} = 0.33$ sec

ξ (cm)																					
Positions along waves	16.35	15.10	13.81	12.55	11.28	10.65	10.11	8.74	8.10	7.46	6.20	5.69	5.18	4.68	4.17	3.66	3.40	2.15	2.90	2.64	1.88
6	0.231	0.213	0.407	0.472	0.492	0.564	0.563	0.605	0.662	0.63	0.856	0.81	0.712	0.819	0.765	0.857	1.064	0.759	1.561	0.856	2.02
7	0.234	0.181	0.471	0.492	0.491	0.539	0.498	0.626	0.523	0.679	0.78	0.797	0.699	0.928	0.951	0.811	1.12	0.840	1.528	1.156	2.135
8	0.178	0.164	0.252	0.476	0.521	0.550	0.692	0.599	0.630	0.67	0.702	0.651	0.693	0.858	2.816	0.780	1.053	0.808	1.461	1.010	2.630
9	0.206	0.200	0.165	0.463	0.528	0.431	0.560	0.539	0.653	0.598	0.673	0.646	0.684	0.585	0.759	0.764	0.887	0.711	0.864	0.932	2.245
10	0.172	0.175	0.208	0.291	0.443	0.458	0.462	0.611	0.608	0.609	0.615	0.818	0.691	0.699	0.635	0.945	0.860	0.795	0.711	0.941	0.930
11	0.188	0.136	0.163	0.230	0.361	0.444	0.468	0.533	0.65	0.602	0.584	0.634	0.790	0.770	0.681	0.770	0.900	0.899	0.786	1.136	1.146
12	0.148	0.129	0.218	0.328	0.525	0.460	0.450	0.551	0.649	0.681	0.643	0.661	0.781	0.875	0.700	0.726	0.919	0.926	0.810	0.978	1.23
13	0.160	0.182	0.280	0.387	0.466	0.525	0.449	0.585	0.609	0.694	0.761	0.699	0.745	0.840	0.733	0.798	0.863	0.771	0.994	1.093	1.073
14	0.193	0.221	0.308	0.496	0.595	0.519	0.549	0.584	0.56	0.689	0.544	0.678	0.752	0.846	0.856	0.839	0.809	0.892	1.118	1.014	1.251
15	0.197	0.206	0.310	0.527	0.605	0.540	0.428	0.678	0.646	0.661	0.676	0.751	0.692	0.822	0.927	0.700	0.898	0.896	0.864	0.945	1.920
16	0.228	0.200	0.273	0.417	0.590	0.489	0.495	0.630	0.666	0.688	0.686	0.661	0.760	0.909	0.851	0.730	0.875	0.792	1.086	0.879	2.062

Table 4. Local $\sqrt{u'^2}$ Data of Case 2. $\bar{U}_{Loc} = 11.48$ m/sec $\bar{H} = 2.7$ cm $\bar{p} = 0.42$ sec

ξ (cm)																					
Positions along waves	18.4	17.1	15.9	14.6	13.3	12.05	10.15	9.52	8.89	7.63	6.98	5.59	4.93	4.35	3.84	3.66	3.07	2.82	2.57	2.31	1.81
4	0.180	0.254	0.281	0.502	0.644	0.695	0.801	0.881	1.097	1.285	0.688	1.381	1.045	1.69	2.085	1.56	2.28	1.62	2.03	2.27	1.98
5	0.233	0.369	0.307	0.502	0.572	0.710	0.867	0.981	1.103	1.30	0.711	1.14	1.298	1.75	1.98	1.92	2.105	1.69	2.165	2.42	2.43
6	0.222	0.276	0.398	0.540	0.626	0.581	0.758	1.051	0.862	1.11	0.870	1.053	1.36	1.64	1.80	2.27	2.69	1.68	2.48	2.29	1.965
5	0.198	0.234	0.376	0.582	0.638	0.603	0.754	1.045	1.068	0.914	0.734	1.014	1.03	1.74	2.145	2.12	2.64	1.91	2.60	2.41	2.235
8	0.231	0.255	0.340	0.518	0.685	0.677	0.693	0.869	0.888	1.06	0.8	1.17	0.95	1.615	1.60	1.53	2.46	1.47	2.96	2.74	3.10
9	0.264	0.286	0.458	0.540	0.575	0.696	0.771	0.824	0.850	1.005	0.75	1.201	0.846	0.972	1.37	1.05	1.575	1.755	2.265	2.66	3.76
10	0.22	0.220	0.507	0.524	0.582	0.521	0.746	0.689	0.679	0.833	0.826	0.883	0.87	0.881	0.965	0.902	1.14	1.78	1.0	1.07	2.42
11	0.254	0.265	0.456	0.421	0.639	0.541	0.642	0.720	0.728	0.914	0.938	0.911	0.801	0.915	0.966	0.917	1.02	1.58	1.01	1.075	2.40
12	0.219	0.198	0.525	0.544	0.587	0.501	0.723	0.630	0.840	0.887	0.659	1.03	1.02	0.996	1.005	1.001	1.247	1.69	1.16	1.071	2.17
13	0.218	0.204	0.527	0.432	0.506	0.626	0.751	0.756	0.726	1.065	0.762	1.13	0.891	0.993	0.97	1.17	1.19	2.055	1.23	1.44	2.08
14	0.212	0.226	0.421	0.574	0.611	0.594	0.671	0.970	0.874	0.965	0.888	1.22	1.12	1.230	1.05	1.09	1.30	2.14	1.48	1.275	2.72
15	0.228	0.252	0.388	0.586	0.470	0.526	0.749	0.930	0.995	1.06	0.688	1.255	1.40	1.32	1.51	1.145	1.84	1.98	1.655	1.55	3.14
16	0.246	0.326	0.444	0.437	0.636	0.693	0.675	1.015	0.975	1.02	0.666	1.330	1.36	1.42	1.77	1.480	1.74	2.33	1.740	1.85	2.64
17	0.195	0.249	0.379	0.546	0.680	0.688	0.85	1.005	1.05	1.09	0.670	1.505	1.245	1.64	1.64	1.580	1.99	2.34	2.07	2.065	2.46
18	0.184	0.293	0.378	0.465	0.619	0.611	0.924	0.934	1.11	1.21	0.840	1.405	1.375	1.35	1.92	1.49	1.73	2.12	2.24	2.05	2.50

of the air flow is from right to left with reference to the figures. In case 2, two $\sqrt{U_0'^2}$ profiles at position 4 and position 18, which correspond to the leeward side trough and the windward side trough, respectively, are expected to be the same since they are actually at the same position with respect to the crests of the water waves. The superimposed profiles are shown with two different symbols. They are in satisfactory agreement with each other.

The local $\sqrt{U_0'^2}$ profiles indicate that the values of intensities increase with decrease in height. This is characteristic of turbulent shearing flows. When the height is lower than about one wave height from the wave crests, the intensity begins to reveal its strong dependence on the relative position with respect to the wave crests. The most evident phenomenon is the appearance of an extremely strong maximum intensity at the place a short distance from the wave crests. This is also the place where the strong jet flow was observed. Following the maximum intensity, the turbulent fluctuation consistently decreases as the air flow moves down to the trough and up to the crest. At the crest, the turbulent intensity in the vicinity of the interface seems to reach its lowest value. This type of turbulent profiles is characteristic of the disturbed turbulent flow over a separation region behind an obstacle, for example, see Arie and Rouse (1956). Plate and Lin (1965) and Plate et al. (1968a). In such flows, the region of maximum turbulence coincides with the onset of the mean streamlines dividing the main flow from that in the zone of separation.

b. Longitudinal $\sqrt{u'^2}$ profiles with reference to the mean water level. --Following the same averaging procedure of obtaining overall mean velocity profiles, the general $\sqrt{u'^2}$ profiles with respect to the mean water level can be inferred from the local turbulent fluctuations above the average dominant waves. Such profiles in fixed probe and moving probe reference frames $\sqrt{\frac{u'^2}{-oy}}$ and $\sqrt{\frac{u'^2}{-o\xi}}$ respectively, are shown in Fig. 28a and Fig. 28b respectively. They have been nondimensionalized with the local friction velocity u_* and plotted against y/δ , where δ , the boundary layer thickness, is defined as the height where the mean air velocity is equal to 99% of the free stream air velocity. The friction velocity was obtained from the following equation:

$$u_* = 0.0185 u_\infty^{3/2} \quad (4-2)$$

where u_∞ is free stream velocity in m/sec, u_* is given in m/sec. This empirical formula was originally given by Hidy and Plate (1966). They derived this relation from a direct momentum balance relating the average slope of the water surface to the pressure gradient in the air towards the downstream direction for a well developed pattern of small wind waves. In these figures the result of Corrsin and Kistler (1954) for flow over a flat plate roughened by corrugated paper is also shown for comparison.

These results based on the two reference frames are in perfect agreement. For $y/\delta > 0.2$, it seems that the profiles reach an equilibrium stage, since they exhibit a close similarity in shapes to that found in the equilibrium shearing layer of Corrsin and Kistler (1954). This result is consistent with that obtained by Hess et al.

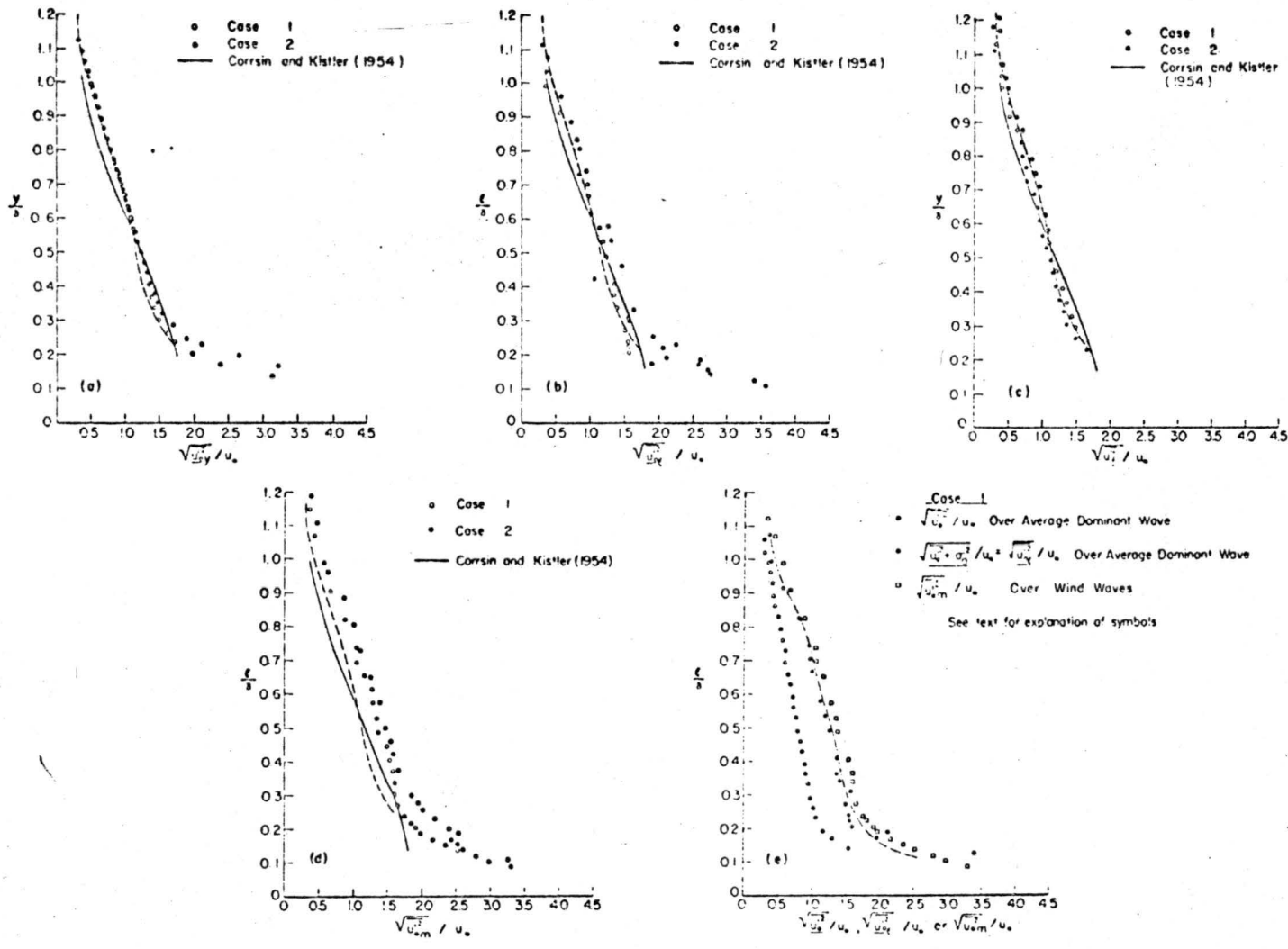


Fig. 28. Turbulent intensity profiles above the mean water level.

(1968), and Plate et al. (1968), in the same facility. They have also found that away from the surface the rates of production and dissipation are very nearly equal. For $y/\delta < 0.15$, the normalized turbulent intensity significantly exceeds the values found in an equilibrium layer. The scaled profiles of longitudinal fluctuation seem to be similar under equilibrium conditions only at heights greater than the height of the roughness elements or wave heights. Since the profiles are nondimensionalized by the average friction velocity over many wave components, one might attribute the increased values to the stronger disturbance in the air flow caused by the dominant waves. Hess et al., and Plate et al., did not observe any anomalous behavior in the longitudinal turbulent intensity near the water surface. However, their data were taken principally above $y/\delta \approx 0.15$.

The results obtained with a fixed probe from the continuous sampling over many different wind waves are shown in Fig. 28c. The fixed probe $\sqrt{u'^2}$ profiles are consistent with those inferred from the local data over average dominant waves. Unfortunately, the fact that the lowest level the data extended to is $y/\delta = 0.2$, does not permit a check of the anomalous behavior that was noticed in the inferred profiles. The average curve of this result is also shown with a broken line over Figs. 28a and 28b. The agreement between these results is remarkable.

The moving probe $\sqrt{U_{om}'^2}$ profiles, shown in Fig. 28d where the subscript *om* denotes the uncorrected quantities obtained directly from moving probe measurement, are consistently higher than those obtained directly with the fixed probe. This is due to the fact

mentioned in Section 2 of Chapter II, that measured turbulent energy obtained with a moving probe through continuous sampling is the sum of true turbulent energy and the contribution from probe and wave motions.

The effect of wave and probe motions can be further explained by the curves shown in Fig. 28e. The curves represented by open circles and solid circles were obtained from the instantaneous data over average dominant waves. Open circles denote $\sqrt{\overline{U_o'^2}}(\xi)$ which is the square root of the ensemble mean of the 20 variances of velocity fluctuations with respect to their corresponding sample mean. Solid circles show the $\sqrt{\overline{u_{o\xi}'^2}}$ which is the square root of the sum of $\overline{u_o'^2}(\xi)$ and the variance, σ_a^2 of the 20 sample means with respect to their ensemble mean. The open square shows the combination of turbulent fluctuations and the fluctuations due to wave and probe motions, which is consistently higher than the inferred turbulent intensity.

It should be pointed out that the effect of wave and probe motions on turbulent fluctuation, the quantity \hat{u} , does appear in continuous fixed probe measurement also, although the extent is comparatively smaller. This is illustrated with Fig. 29, where the velocity at a given point at a fixed height from mean water level or moving water surface are drawn as a function of positions with respect to wave peaks and troughs. The results were obtained under the experimental conditions of case 2.

A method of separating u_o' from \hat{u}_o through linear correlation of air motion and water waves has been developed in Chapter II. The correlation coefficients of the water surface displacements and wave-probe induced air motions are defined and calculated by the following equation

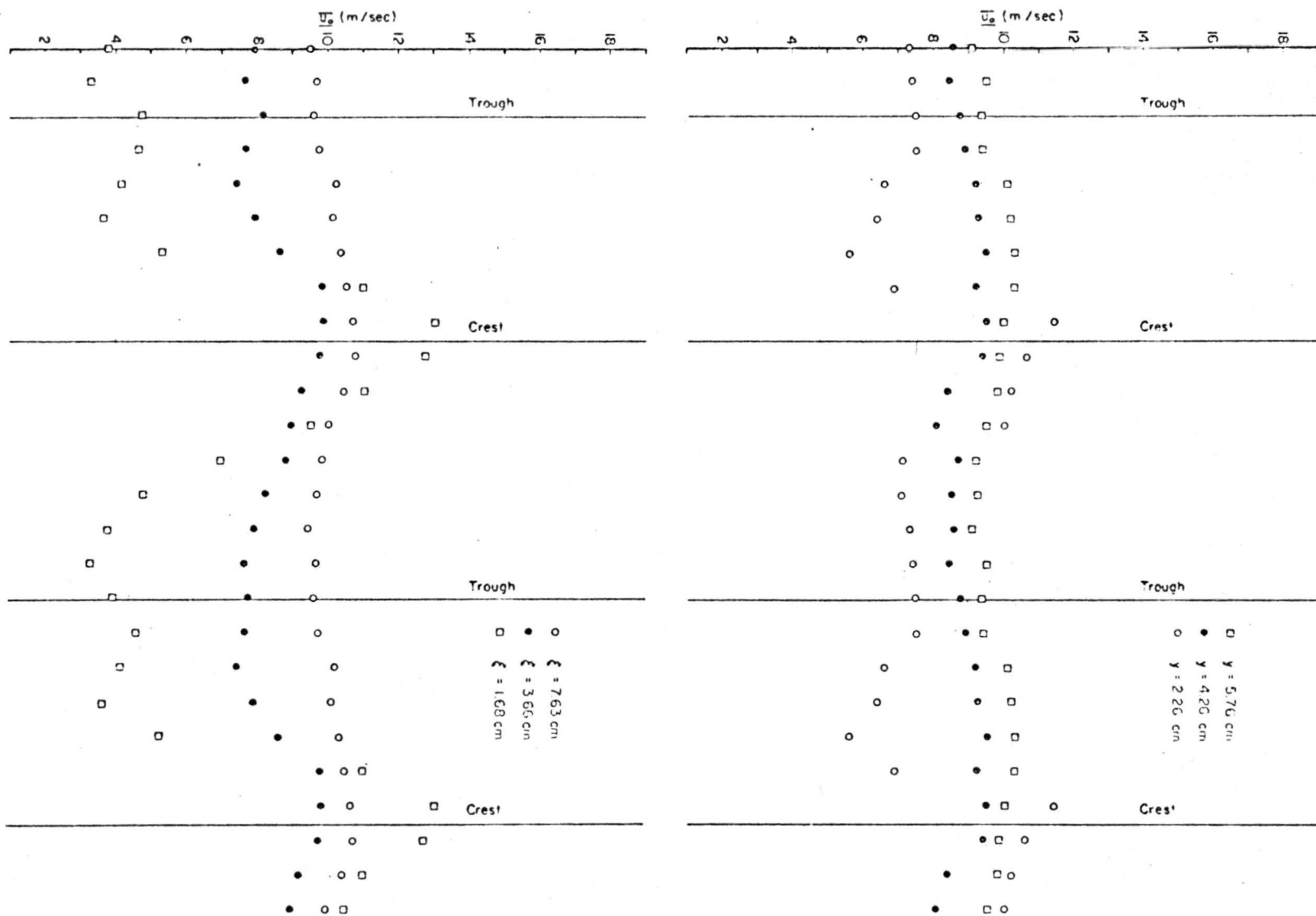


Fig. 29. Variation of mean velocity at a given point along the water waves.

$$R_{\hat{u}_0\eta}(\xi, t) = \frac{\hat{u}_0(\xi, t)\eta(0, t+\tau)}{\sqrt{(\hat{u}_0 + u'_0)^2} \sqrt{\eta^2}} \quad (4-3)$$

Some calculated correlation coefficients are shown in Fig. 30, where the normalized autocorrelation coefficient $R_{\eta\eta}(\tau)$ is also shown for reference. Again, we see that the variation of mean velocity at a given point is wave like and in phase with water waves within small errors.

By applying Eq. 2-33, the true turbulent rms value can be determined from the measured value, $u'_{0m}{}^2$, and the correlation coefficient $R_{\hat{u}_0\eta}(\xi, 0)$. The results are shown with a broken line in Fig. 28e. The calculated turbulent rms values are close to the inferred profile, although the calculated values are in general some 5% higher. The difference can be attributed to the nonlinear relation between air motion and water displacement. The velocity variation due to probe motion \hat{u}_0 , at the height greater than $4\bar{H}$, obtained experimentally from $R_{\hat{u}_0\eta}$, is in good agreement with that calculated from Eq. 2-8; for example, at $\xi = 13.8$ cm, the values $\sqrt{u_0'^2}$ obtained from two methods are 6.5 cm/sec and 5.8 cm/sec respectively.

4.2.4 Turbulent energy spectra

a. Local energy spectra.--A set of ensemble average spectra over various heights and positions above average dominant waves are shown in Fig. 31. The data were obtained under the flow conditions of case 2. The positions of the spectra are identified in the figure. The solid lines are the best fit curves with the slope of $-5/3$ in the double logarithmic plots.

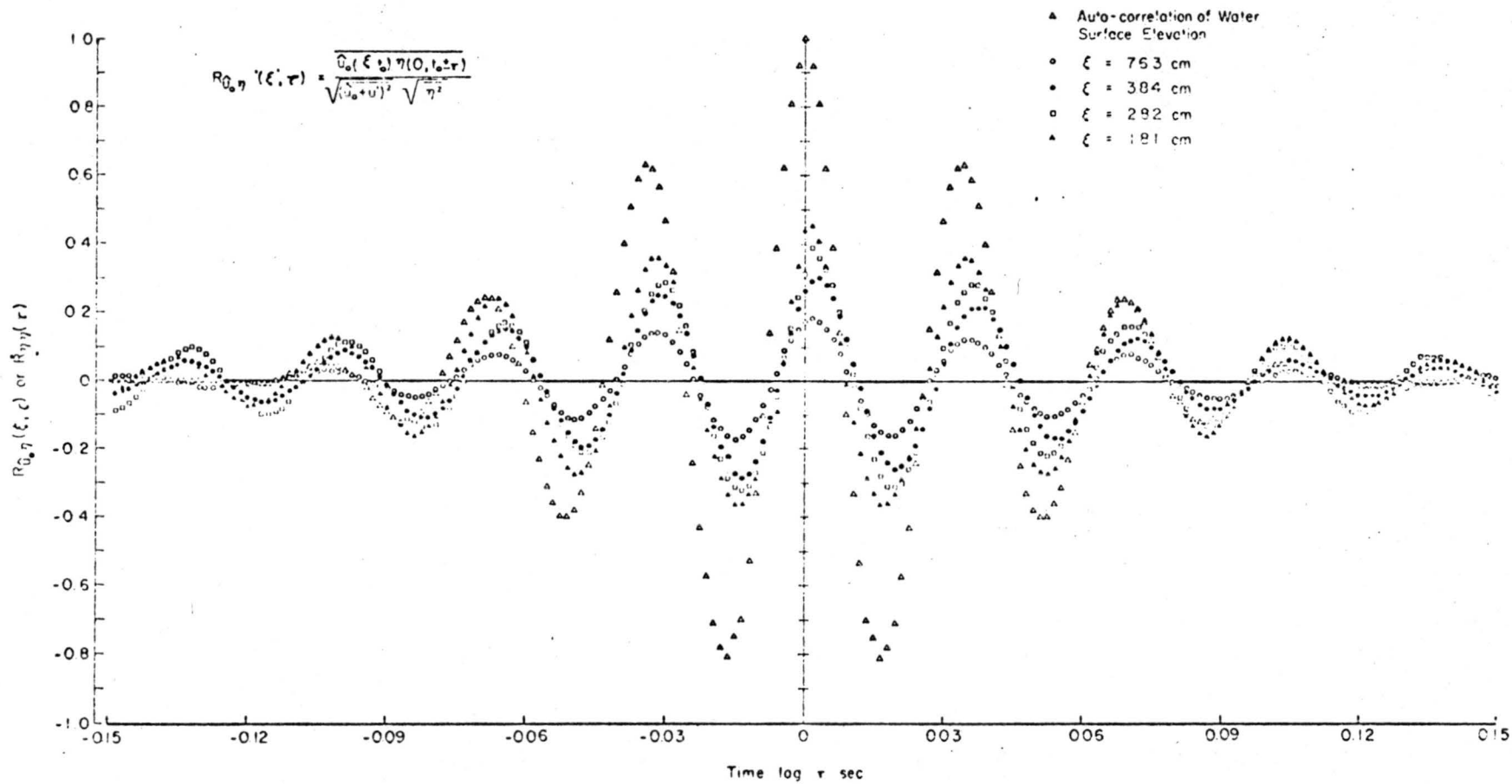


Fig. 30. Correlation of air and water motions.

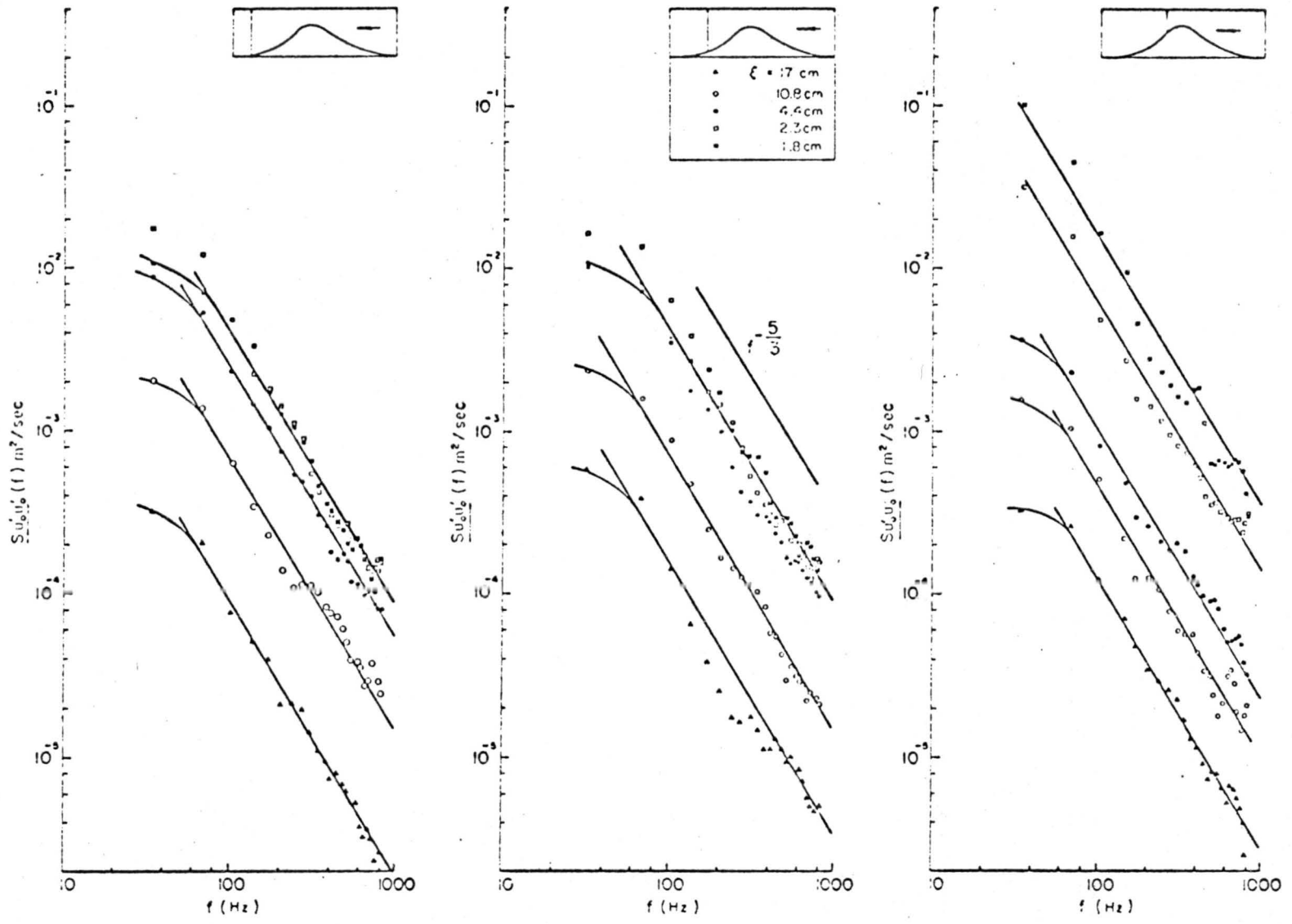


Fig. 31. Local turbulent energy spectra.

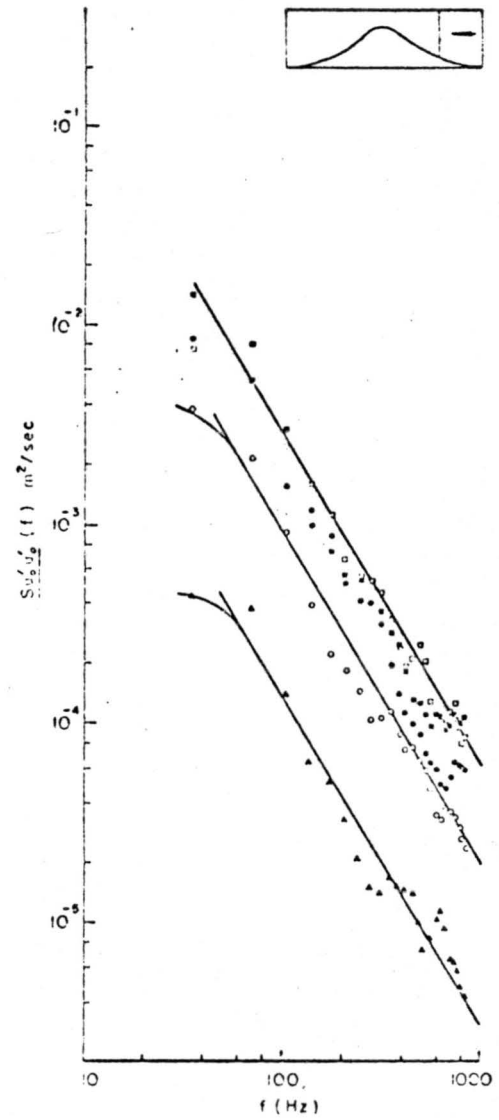
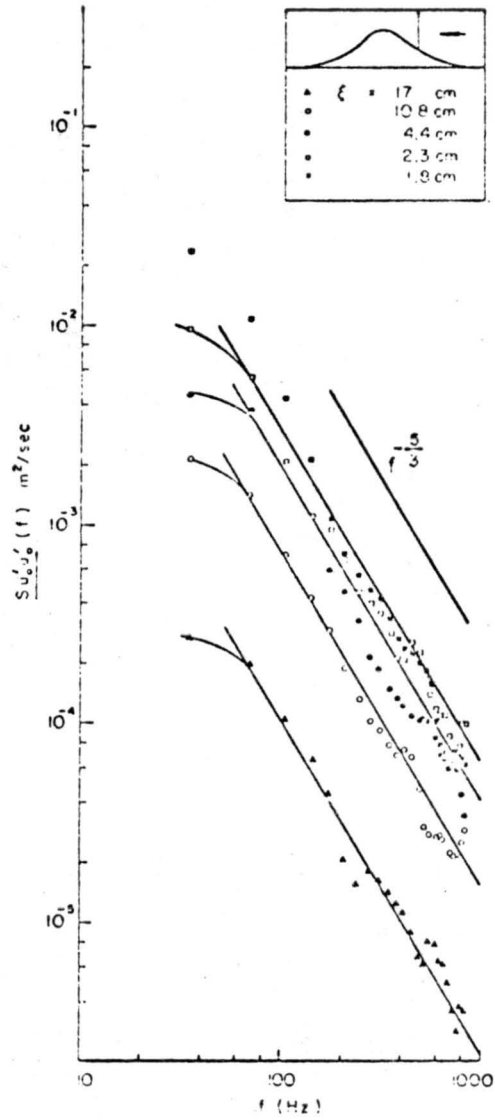
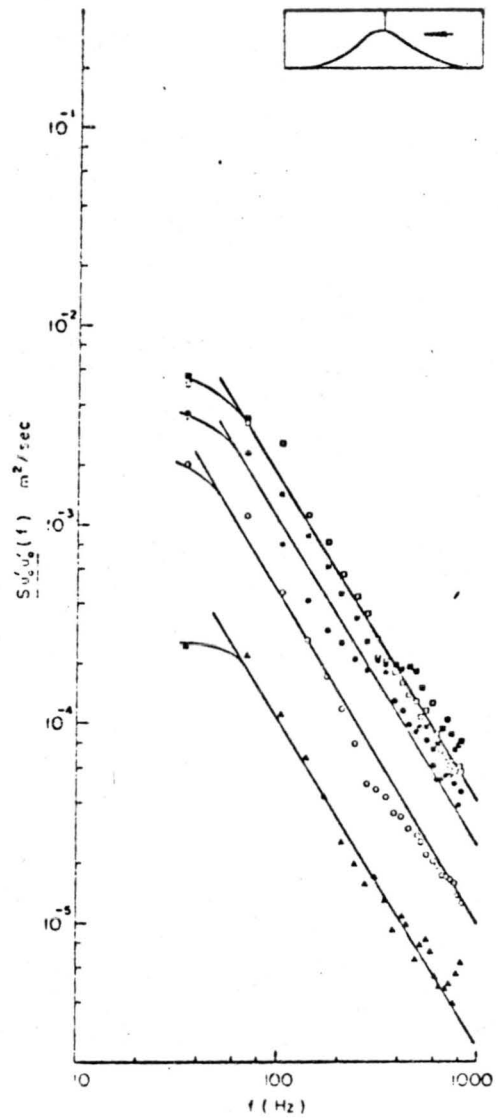


Fig. 31. Continued

In the very short pieces of sample record, the velocity fluctuations were measured with respect to their own sample mean $\bar{u}_{oi}[\xi, T_{pi} \pm (2n+1)\Delta t]$ so that sample spectra might be considerably different from one another. The average local spectra shown were obtained by averaging the 20 values of sample spectral density $S_{u'_{oi}u'_{oi}}[\xi, T_{pi} \pm (2n+1)\Delta t]$ at the corresponding frequencies. Considering the possible effects of the different sample variance $\overline{u''_{oi}^2}$ another averaging process was also taken. The alternate method first normalized every sample spectrum with its sample variance $\overline{u''_{oi}^2}$, and then averaged the 20 values of normalized sample, spectral density at the corresponding frequencies. In this fashion, the scattering due to different sample variances, $\overline{u''_{oi}^2}$, can be eliminated and only the normalized spectrum shape will be counted in averaging. The final local spectrum was obtained by multiplying the average normalized spectrum with its local variance $\overline{u''_{oi}^2}$. Put into a mathematical equation, the procedure corresponds to:

$$\begin{aligned}
 & \overline{u'_{oi}u'_{oi}}[f, \xi, T_p \pm (2n+1)\Delta t] = \\
 & = \overline{u''_{oi}^2}(\xi, T_p \pm (2n+1)\Delta t) \left\{ \frac{1}{20} \sum_{i=1}^{20} \frac{S_{u'_{oi}u'_{oi}}[f, \xi, T_{pi} \pm (2n+1)\Delta t]}{\overline{u''_{oi}^2}[\xi, T_{pi} \pm (2n+1)\Delta t]} \right\} \quad (4-4)
 \end{aligned}$$

The results obtained by these two methods did not show any distinct difference.

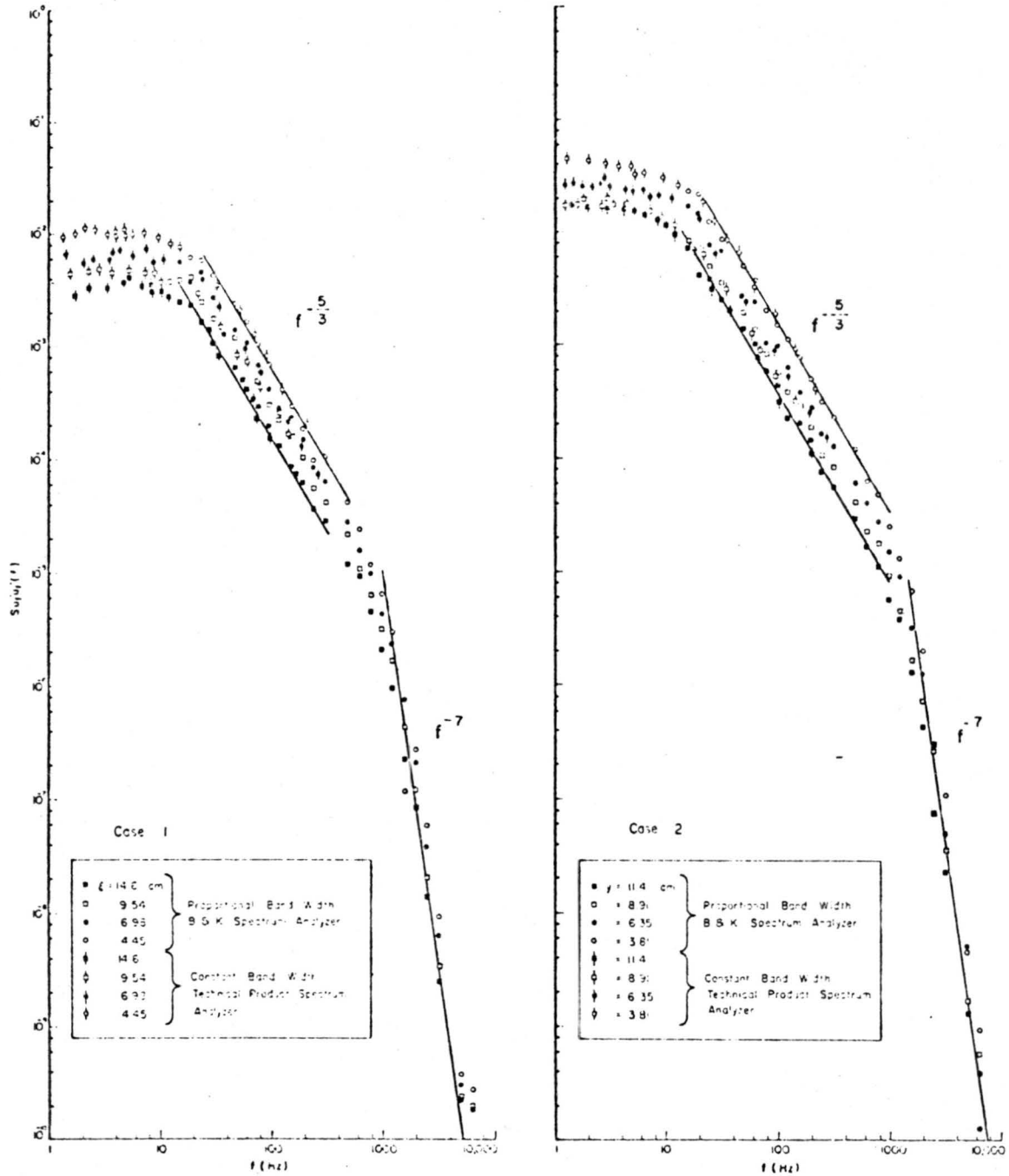


Fig. 33. Turbulent energy spectrum measured with a fixed probe.

Surprisingly, the results indicated that Kolmogoroff's inertial subrange exists almost everywhere. According to Kolmogoroff's hypothesis, (Hinze, 1959), the non-viscous inertial subrange varies as $f^{-5/3}$. Only at the lowest height, the spectra have the tendency to be steeper at the low frequency end. This tendency could be due to a slight trend in the data even though the sampling time was chosen as small as 0.03 sec. The region of inertial subrange covers almost the whole frequency domain obtained from the digital data. This behavior may be associated with the relatively high Reynolds number of the flow (Hinze 1959), and the complete mixing of air caused by the water surface undulation. By this mixing, the turbulence loses its identity with the origin and the motion evidently becomes locally isotropic.

Although the limitations on sample length and digitizing rate restrict the frequency range of local spectrum, it is still possible to infer the whole spectrum, from which the important turbulent parameters like micro-scale and dissipation rate can be estimated. Since the most important portion of spectrum has been provided, the inference of the low frequency end and high frequency end can be made without too much uncertainty. Evidently the energy at the low frequency end should be equal to the variance of the 20 sample mean, σ_a^2 , with respect to their local (ensemble) mean. As a first approximation, it can be assumed that the energy or the variance σ_a^2 is equally distributed over this frequency range, i.e.,

$$\int_0^{f_\ell} S_{u'_o u'_o}(f) df = S_{u'_o u'_o}(f) f_\ell = \sigma_a^2 \quad (4-5)$$

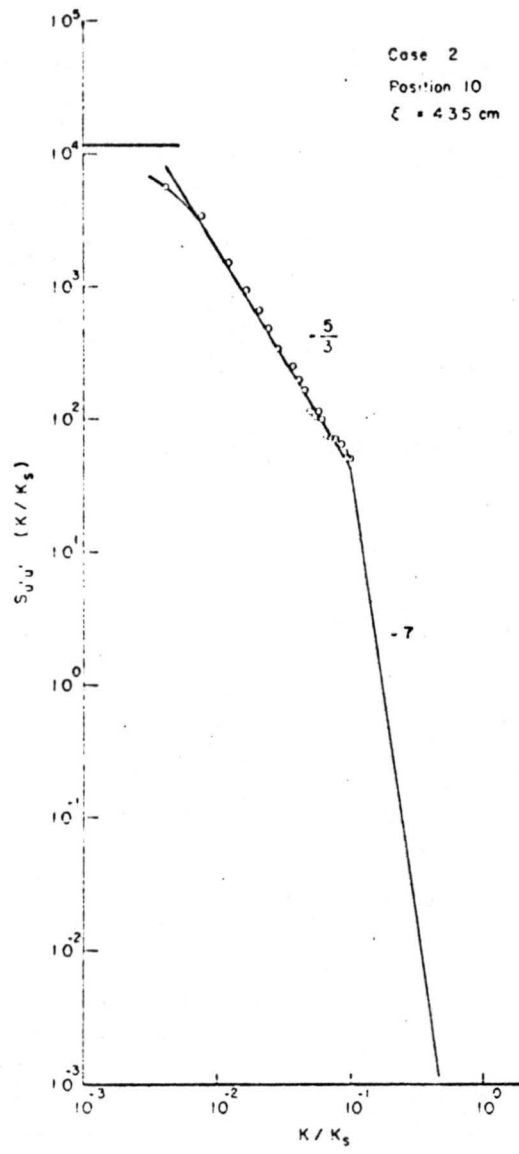
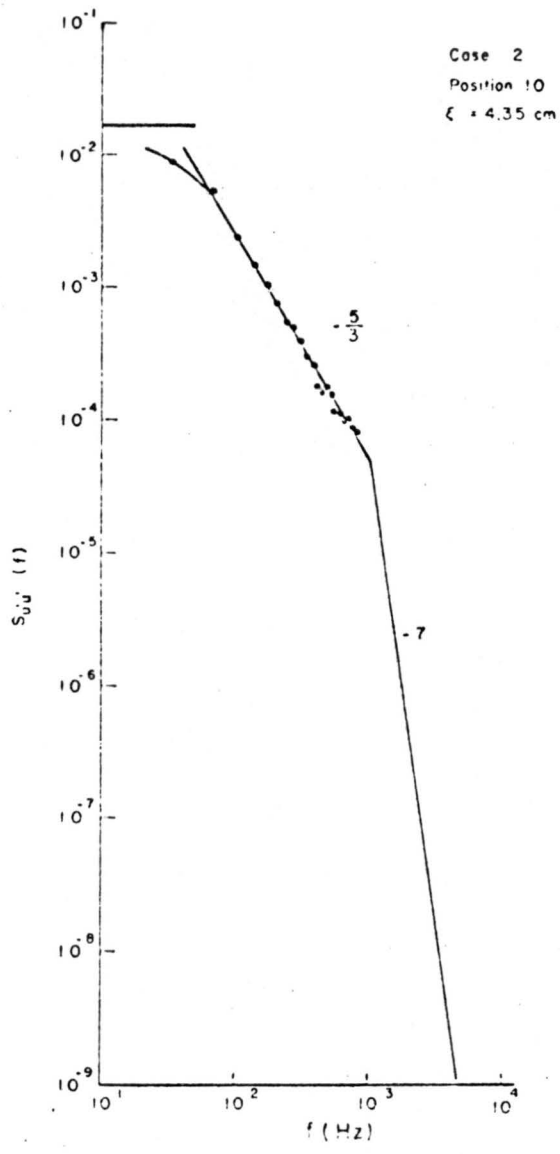


Fig. 32. Inferred energy spectrum

where f_g is the cut-off frequency and is equal to 33 Hz here. The spectral shape at the high frequency end also can be inferred from spectra obtained from a long continuous record. Since the effect of wave and probe motion does not appear over the high frequency range, the characteristic of local and overall spectra should be identical there. The results of overall spectra which will be presented in the next section, show the high frequency end follows an f^{-7} law very well. This behavior controlled solely by the viscous dissipation has been well established in many other turbulent shearing flows also; for example, see Sandborn and Marshall (1965).

The complete inferred spectrum at position 10 and $\xi = 4.35$ cm, is shown in Fig. 32a where $-5/3$ region and -7 region are assumed to intersect at 1000 Hz. This spectrum has also been nondimensionalized to see whether it follows a similarity profile reported by other investigators. The scaling parameters were those required by Kolmogoroff's inertial subrange. This dimensionless spectrum is given by

$$\underline{S_{u'u'}}\left(\frac{k}{k_s}\right) = \frac{\bar{u}}{2\pi} (\epsilon \nu_a^5)^{-1/4} \underline{S_{u'u'}}(f), \quad (4-6)$$

where $k = 2\pi f/\bar{u}$ is the wave number, $k_s = (\epsilon \nu_a^{-3})^{1/4}$ is the reference wave number of the inverse of Kolmogoroff's length, ν_a is kinematic viscosity of air and ϵ is the rate of energy dissipation. If the turbulence is assumed to be isotropic at the frequencies responsible for dissipation, the dissipation rate ϵ could be evaluated from the inferred spectrum with the following relation:

$$\epsilon = 15 \overline{u'^2} v_a \int_0^{\infty} k^2 S_{u'u'}(k) dk \quad (4-7)$$

The nondimensional spectrum is shown in Fig. 32b. The Kolmogoroff's constant C_k as defined by

$$S\left(\frac{k}{k_s}\right) = C_k \left(\frac{k}{k_s}\right)^{-5/8} \quad (4-8)$$

is found to be 0.88 which deviates from the value of 0.46 reported by Pond et al. (1963). However, Plate et al. (1968a), found that Kolmogoroff's constant could vary from 0.46 to 1.2 over the laboratory wind waves of limited fetches.

b. Energy spectra of longitudinal velocity fluctuations over mean water surface.--The energy spectra of longitudinal velocity fluctuations were calculated from magnetic tape recordings of the hot wire signal. By combining the results from the Bruel and Kjaer analog spectrum analyzer and the Technical Products spectrum analyzer, or the digital computer, the frequency domain of spectrum was extended from 1 Hz to 7000 Hz. In Fig. 33 are shown the energy spectra of longitudinal velocity fluctuations from fixed probe measurements; i.e., turbulent energy spectra. These spectra are still in arbitrary analog units. They could easily be put into a nondimensional similarity profile by using suitable scaling parameters. All spectra indicate the existence of a viscous dissipation region varying as f^{-7} at the high frequency end. Adjacent to the low frequency extreme of f^{-7} range, an extensive nonviscous subrange varying as $f^{-5/3}$ appeared. The results also indicate the increase in the length of $-5/3$ region with

increasing air velocity or Reynolds number (Hinze 1959). From Fig. 29 it is noticed that the air motion seen by a fixed probe is wavy. Therefore, an increase in energy near the frequency of dominant wave in the spectrum may be anticipated. However, no significant modification of the energy spectrum is discerned. The band width of the analog filter, 2Hz, may be still too wide to detect a spectral peak around 2 to 3 Hz.

Turbulent energy spectra from moving probe measurements are shown in Fig. 34. Since the probe was following the waves the component \hat{u}_0 was also found in the spectral density. This component however should concentrate its energy distribution around the dominant frequency of water wave spectrum and cause a distortion of air velocity spectrum at the low frequency end only. The shape of spectrum at frequencies, say, higher than 20 Hz should remain unaltered and should reveal the same characteristics of "pure" turbulent spectrum. As the experimental spectra show, this is indeed the case.

At the heights close to the water surface, the distortion caused by the motion of the probe and the water surface is particularly profound and a peak appears at the frequency corresponding to dominant waves which are 3.0 Hz and 2.3 Hz for case 1 and case 2 respectively. At larger heights from the water surface, the distortion can still be found, but the energy distributes itself more uniformly over the low frequency end and no energy peak directly associated with dominant wave frequency can be discerned. At the highest position, the contribution from \hat{u}_0 seems to be so weak that the whole spectrum reveals only the characteristics of an ordinary turbulent energy spectrum over fixed boundary.

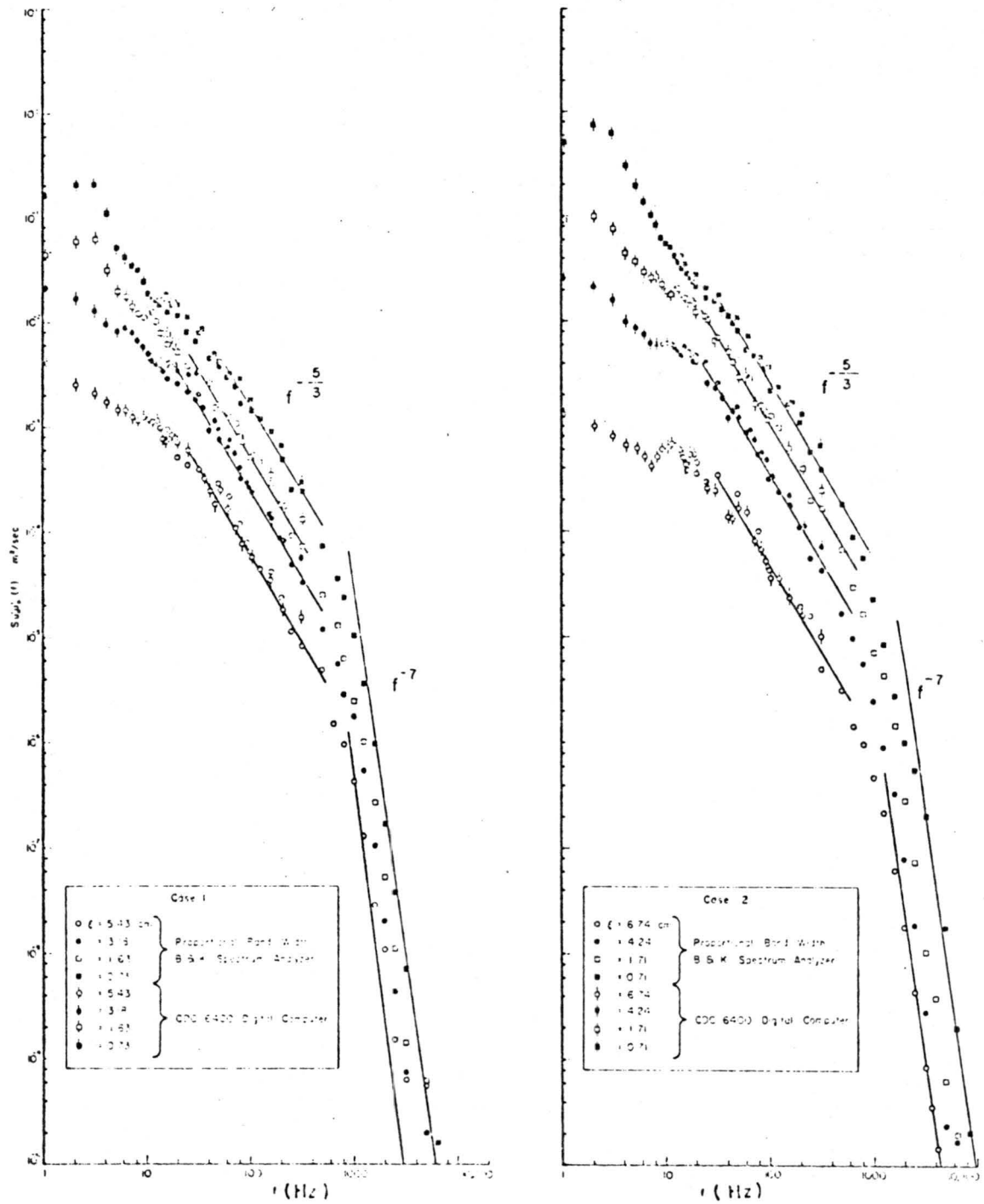


Fig. 34. Turbulent energy spectrum measured with a moving probe.

By applying the linear correlation method developed in Chapter II, the turbulent spectrum has been estimated. The result is shown in Fig. 35. The measured spectrum, or the uncorrected spectrum, is denoted with open circles and the estimated turbulent (t) spectrum, or the corrected spectrum, is denoted with solid circles. Comparing the estimated turbulent spectrum with that obtained directly with a fixed probe, it seems the technique can only correct for the component of the dominant wave peak. The correction to the other low frequency components is apparently too small. Again, this can be attributed to the appearance of nonlinear effect between surface wave and the fluctuation components of \hat{u}_o .

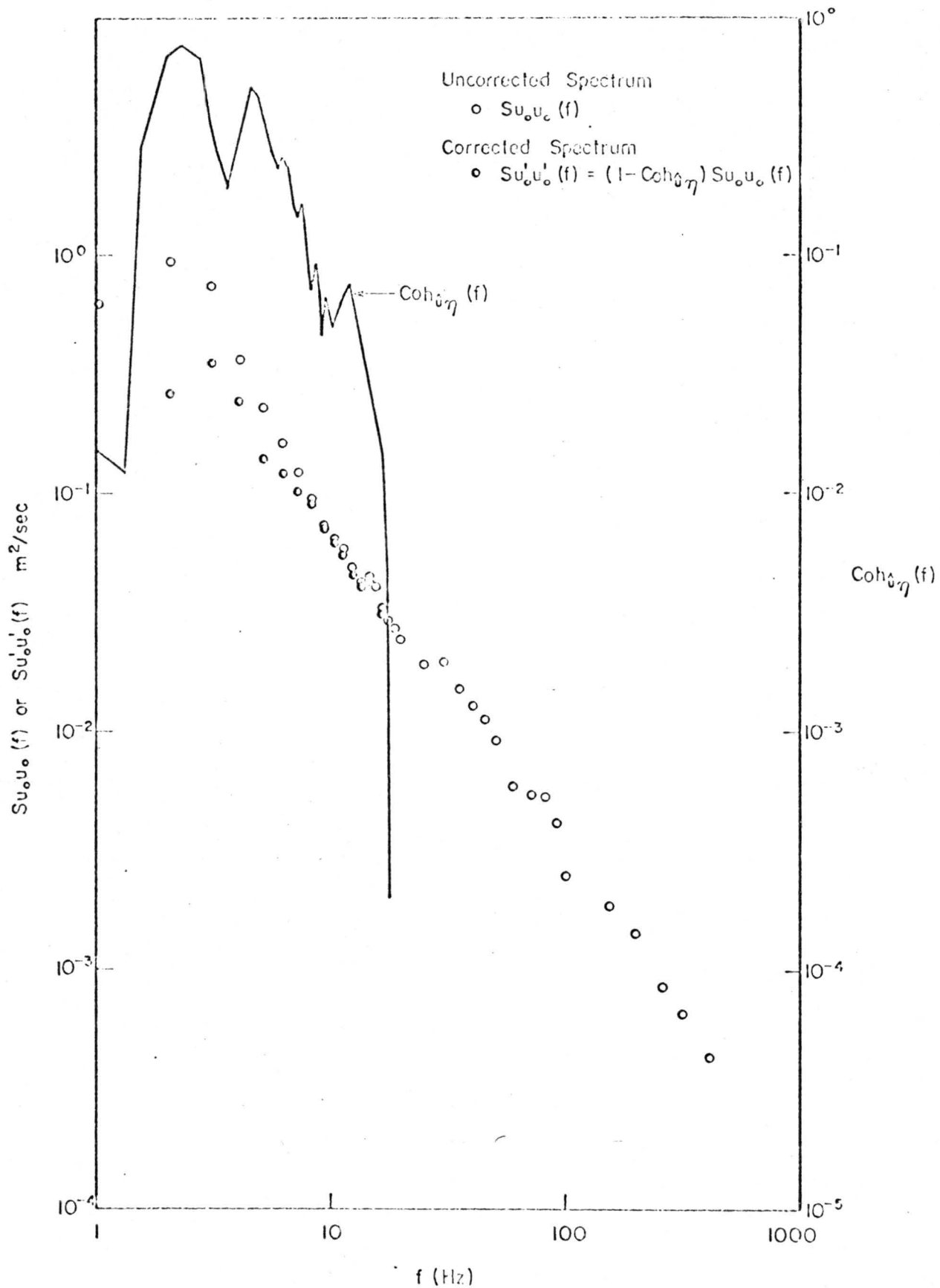


Fig. 35. Turbulent energy spectrum corrected for wave-probe induced fluctuations.

Chapter V

DISCUSSION

In this chapter the physical picture of the air flow over fully developed wind generated waves will be inferred from the experimental results described in the previous chapter. The applicability or the effectiveness of the existing theoretical wave generation mechanisms at this stage of development will be discussed in the light of the deduced physical process for energy transfer from wind to waves.

5.1 General Characteristics of the Water Surface Serving as the Lower Boundary of Air Flow

The turbulent boundary layer over water differs in many respects from the commonly encountered boundary layers. "Here the nature of the boundary is not prescribed but is essentially part of the solution." (Stewart 1967). Due to the deformability of water surface, there is energy transfer from air to water. Energy is partitioned between random surface waves and drift currents. Thus the resulting boundary is not only changing its shape irregularly but it is also moving. In the coordinate system which is stationary relative to the form of the waves, the zero wind speed occurs at the critical height where $u(y) = c$, which plays an essential role in energy transfer from air to water.

In this study, the resulting phase velocity and surface current that cause the critical height occurred on the average in the viscous sublayer of the air flow. Although this distance is small, the dissimilarity in energy transfer still may make the air flow over water essentially different from that over a solid boundary.

5.1.1 Symmetry of wind wave shape

From the calculated probability distributions of the water surface displacements and their time rates of change (see 4.1.1), it is found that waves have a tendency to form sharp crests and shallow troughs. The waves are also skewed, with longer and smoother upwind sides than downwind sides.

The above properties can also be seen from the comparison of the average dominant waves and theoretical wave forms. In Fig. 36 the average dominant waves are nondimensionalized by their corresponding average wave amplitudes and wave lengths and compared with a sine wave and a trochoidal wave profile ($\bar{H}/\bar{\lambda} = 0.09$) from finite amplitude theory. The trochoidal wave or Gerstner-Rankine wave is the only gravity wave which satisfies the constant pressure, surface dynamic boundary condition exactly, rather than approximately. Its sharper crests and longer, flatter troughs, appear to be a little more realistic than the sinusoid as a description of water surface waves. The equations of wave shape in dimensionless form with the origin of the coordinates at the crest and the vertical dimension measured negatively downward are (Wiegell 1965 p. 58):

$$\eta/\bar{H} = 1/2 (1 - \cos \theta) \quad (5-1)$$

$$x/\bar{\lambda} = t/T = 1 - (\text{rad } \theta/2\pi - H/2\bar{\lambda} \sin \theta) \quad (5-2)$$

In Fig. 36, waves are superimposed on one another in such a way that their troughs are coincident. The sine wave apparently has a broader crest than an actual wind wave and significantly over-estimates the water elevation at the windward side (positive x). The theoretical trochoidal form over-estimates the water elevation at the windward

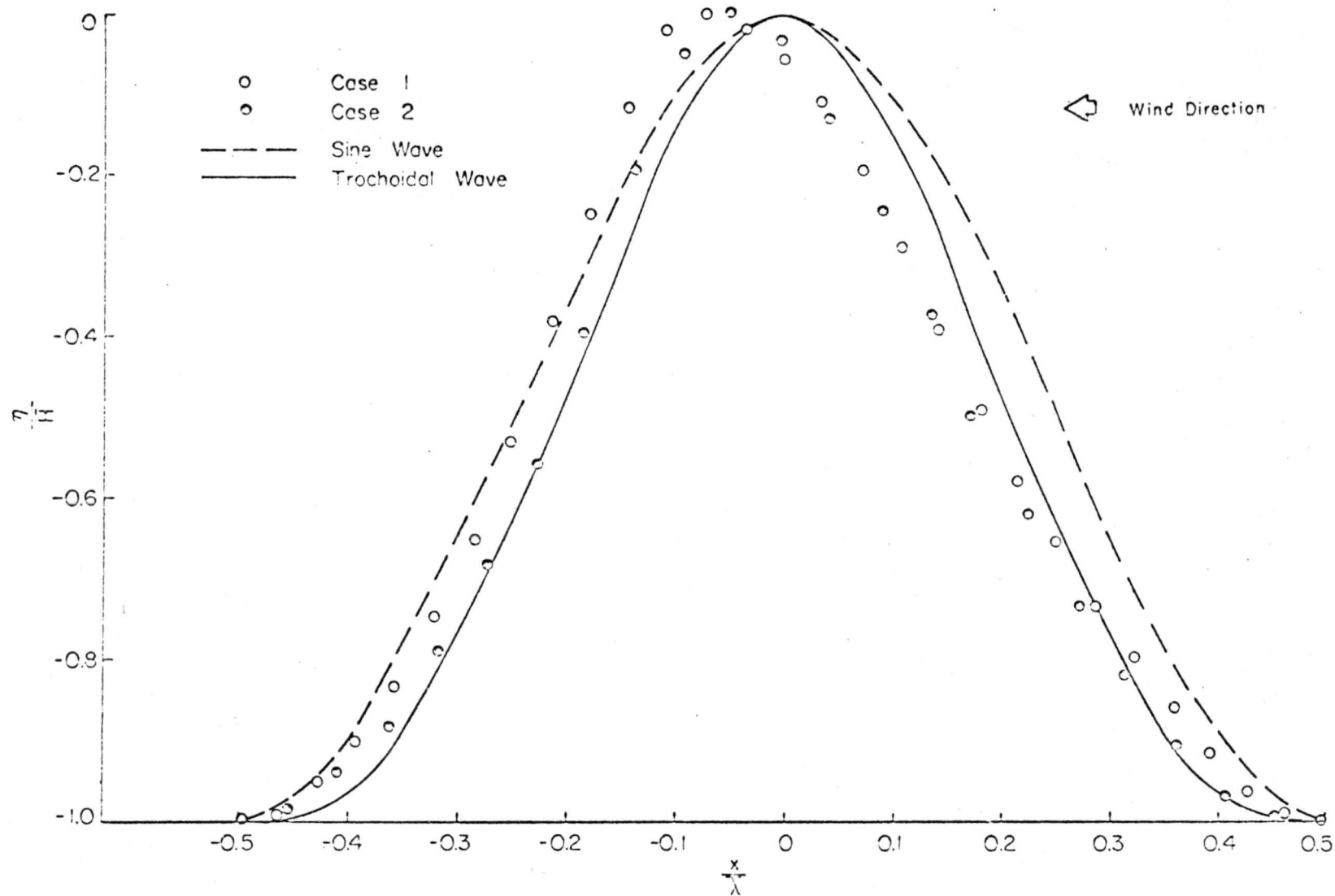


Fig. 36. Comparison of normalized average waves with sine wave and trochoidal wave.

side and under-estimates the water elevation at the other side. The experimental data are skewed in contrast to a simple sine wave and the theoretical trochoidal shape. It was noticed in the last chapter that the leeward face is 25% steeper than the windward one. This asymmetry seems to favor a separation of the air flow on the leeward face of the crests. All theoretical simple wave forms are symmetrical, but if non-zero skewness can be taken into account, a better description of wind waves should be obtained.

5.1.2 Properties of the frequency spectra of wind waves

Phillips (1958), considering the breaking of waves, found that the spectrum of the gravity waves has an equilibrium range denoted by

$$S_{ww}(f) = \gamma g^2 f^{-5} \quad (5-3)$$

over the high frequency end of the spectrum. Here, g is the gravity acceleration, f is frequency given in Hz, and constant γ has been found empirically equal to approximately 7.5×10^{-6} . In contrast, Hicks (Phillips, 1958) has pointed out that the equilibrium range for pure capillary waves is, on dimensional grounds, of the form

$$S_{ww}(f) = \gamma' (T/\rho)^{2/3} f^{-7/3} \quad (5-4)$$

where T is the surface tension, and ρ is the mass density of water.

The results shown in Fig. 15 indicate Phillips equilibrium range holds only for $2f_m \leq f \leq f_c$. Considering the equation of motion to second order, Pierson (1958) qualitatively predicted that Phillips equilibrium is valid for $2f_m \leq f \leq f_c$. This prediction is consistent with the experimental result.

At $f_m < f < 2f_m$, the slope of wave spectra is close to -9 or -8. This trend was also found by Sutherland (1967) and Plate et al. (1968a). Phillips equilibrium range apparently cannot be applied to this range.

For $f > f_c$, it is doubtful that there exists a stable equilibrium range for "pure" capillary waves as predicted by Hicks. The capillary waves which emerged on both the windward and leeward sides of the dominant waves, may not be free from the influence of gravity. Thus, there would be a region which displays the joint effects of gravity and capillary. The experimental slope for $f > f_c$ approximately proportional to f^{-3} tends to be the consequence of these effects. In other words, the Phillips' -5 law and Hicks' -7/3 law are respectively the upper and lower limits of the wind-generated waves in this region; but, in the frequency range of the present experimental data, the exact -7/3 law has not shown up.

5.2 Turbulent Air Flow over Water

5.2.1 Separation and the streamline pattern

With the velocity profiles over a series of positions along average dominant waves, as shown in Figs. 21 and 22, the areas $\psi = \int u dy$ enclosed by these profiles can be calculated graphically as the function of vertical distance from the water surface. This calculation, hence, permits the determination of successive streamlines for a selected increment $\Delta\psi$ by employing mass continuity.

Since the flow pattern near the air-water interface was not known, a horizontal line at a height y , that equaled four times the wave height was selected as a reference streamline. This was the place where the measurement of the integral $\psi = \int_{y'}^y u dy$ was started. It has been seen (Fig. 24) that the flow at such a height is free from the effect of surface undulation and is parallel to mean water level, thus the location of the reference streamline is well defined.

With a single hot wire probe as a sensor, only the magnitude of the velocity vector normal to the hot wire could be measured. This measured velocity was at first assumed to be indicative of the longitudinal component only. The streamlines evaluated by the measured quantities yield the inclination of the velocity vector as a first approximation, from which the horizontal velocities could be determined to a second approximation. With this second approximation the streamlines were determined again, and the resulting horizontal velocities compared with the second approximation. They were found to be in close agreement. The velocity profiles shown in Fig. 21 and Fig. 22 have all been corrected for flow direction which was important only at the points below the wave crests.

In Fig. 37 and Fig. 38 are shown the streamline patterns obtained by this technique. The increment Δq is $0.048 \text{ m}^3/\text{sec}$. The streamlines were constructed as if the boundary were stationary. The results indicate the presence of a stationary eddy or a separated region behind the wave crests. The construction of the streamline pattern inside the bubble was not attempted due to insufficient data. The flow evidently separates just behind the crests but not right at them.

Just like the well known separation process, the fluid particles in the boundary layer, after passing the wave crests are retarded by the adverse pressure gradient that develops along the surface. At the separation point the particles can no longer penetrate into the region of increased pressure owing to their small kinetic energy. The fluid in boundary layer thus separates from the water surface and moves into the main stream. Considering the effect of the critical layer on the flow configuration, Stewart (1967) has postulated a

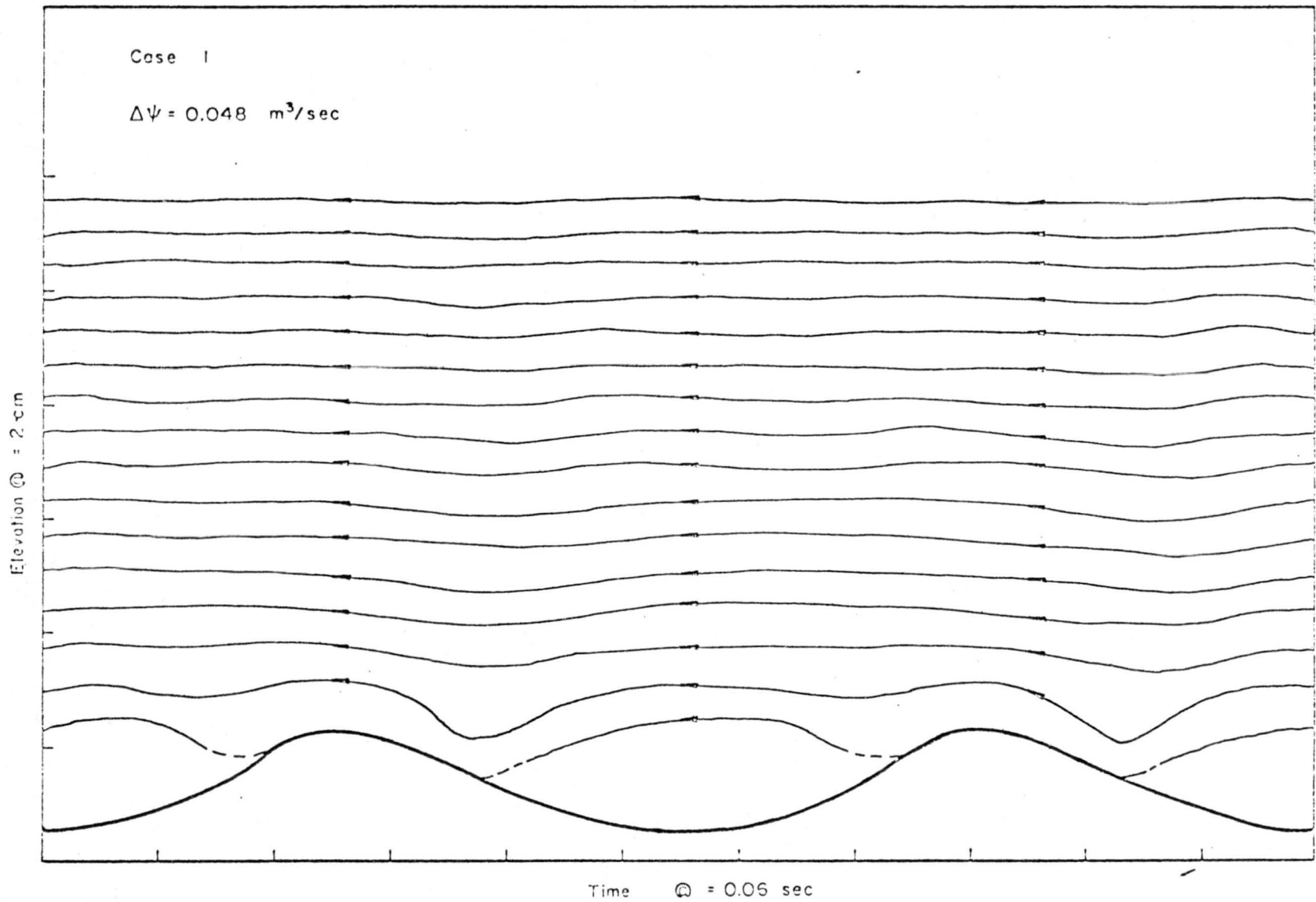


Fig. 37. Streamline pattern over wind generated waves (I).

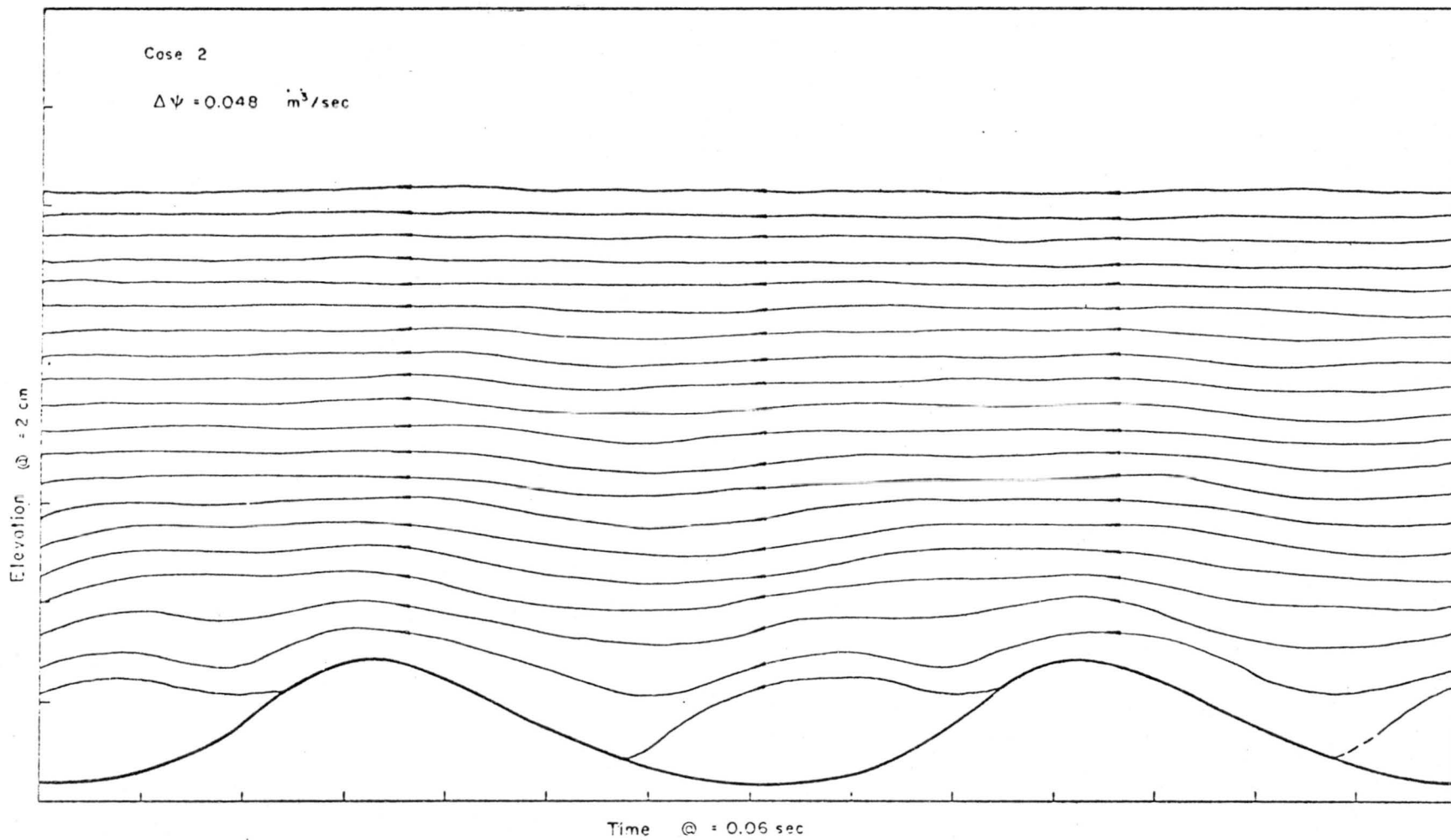


Fig. 38. Streamline pattern over wind generated waves (II).

streamline pattern in $u-c$ coordinate system, very similar to what has been observed.

From the previous observation, one may anticipate that the separation eddy occurs on the average on the lee side of large wave crests and stays stationary with respect to wave motion. If this is the case, the separation eddy accompanying a particular wave will grow in size as the wave travels downstream. This growth will result from the entrainment of air into the layer formed along the bubble boundary through turbulent mixing with the higher velocity flow. In this fashion, one may speculate the same growth rate for both waves and their associated separation bubbles.

It is interesting to consider the possible configuration of streamlines if the motion of the boundary is taken into account. In fact, for the water waves where the interface is in motion, a basic question arises about the proper definition of separation to be applied. The conventional definition of separation involves a boundary point where shear stress vanishes. This is no longer sufficient. If the coordinate system moves with the phase celerity c , the surface configuration becomes stationary, the water particles at the boundary may move relatively upstream or downstream depending upon the magnitude of the wind driven drift current U_s , and the water particle motion due to wave U_p . If $c > U_s + U_p$, the boundary is moving upstream in $u-c$ coordinate system, which is the generally encountered case. Moore (1958) has formulated a criterion of separation for a wall moving downstream and a wall moving upstream. According to him, if the wall is moving downstream, it is expected that the separation bubble will be lifted off the surface and its leading edge will be signified

by the simultaneous vanishing of shear and velocity at some point in the boundary layer away from the surface. If the wall is moving upstream, it appears that the velocity profile, where it crosses through zero, should decay to zero over an extensive portion of the boundary layer, yielding a bubble with a "shoulder" which may be identified as a separation point (see Fig. 39b). The upstream end of this "shoulder" is a long, thin bubble fully embedded within the boundary layer and to be regarded as part of the boundary layer. If the picture Moore proposed is correct, then the streamline pattern of the separation of air flow over wind waves would be as shown in Figs. 39a and 39b, where some velocity profiles at typical positions are also shown. For the case $c > U_s + U_p$, corresponding to a wall moving upstream, two types of separation bubble appear, one over the troughs and the other over the crests. For this case, another possibility for the development of a separation point is in the manner as shown in Fig. 39c where the separation bubble is lifted off the surface. This picture is indeed similar to that proposed by Stewart (1967).

a. The consequences of separation.--With the flow pattern shown, the pressure distribution should be in such a fashion that the high pressure is on the windward side of the wave and the low pressure is on the leeward side. The existence of this difference of normal pressure will allow an energy transfer from air to water.

The presence of separation leads to the conclusion that the process of interaction between the turbulent shearing flow and underlying water waves is nonlinear. Many features observed in the air flow above water can now be explained in the light of flow separation.

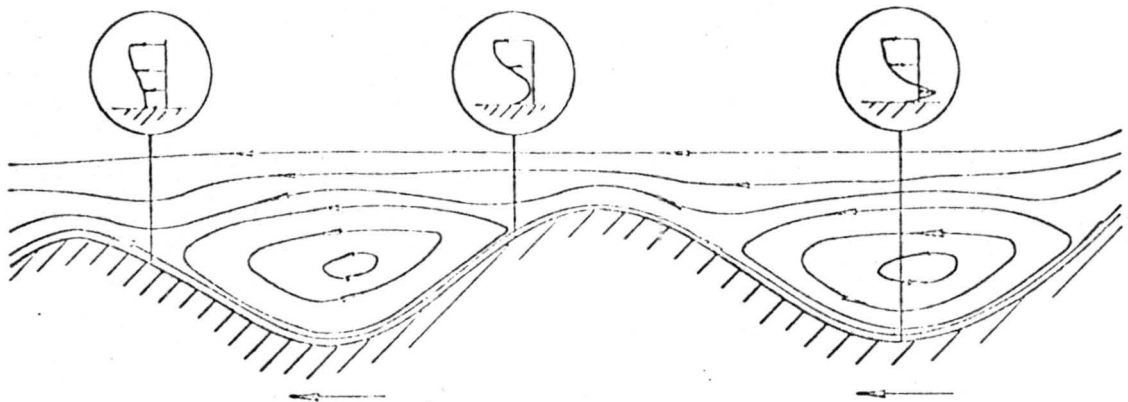
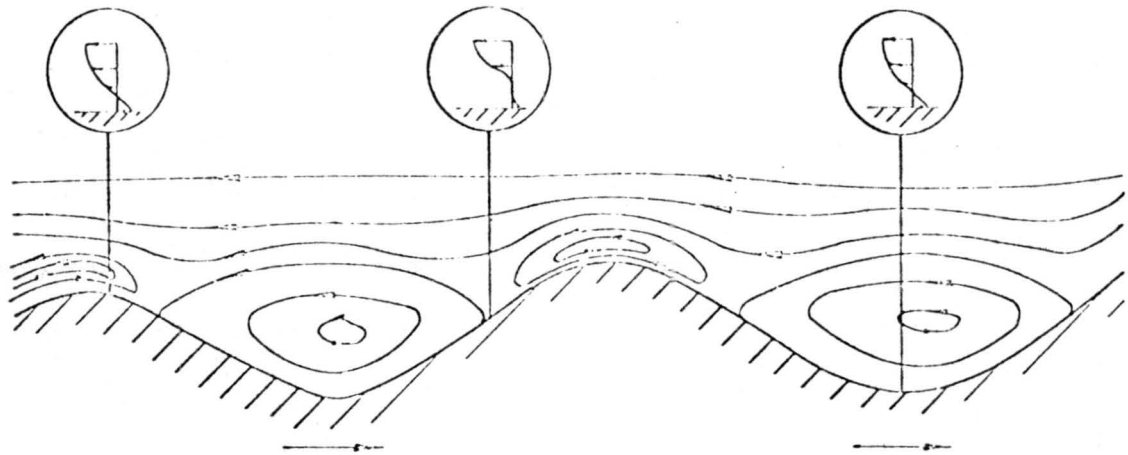
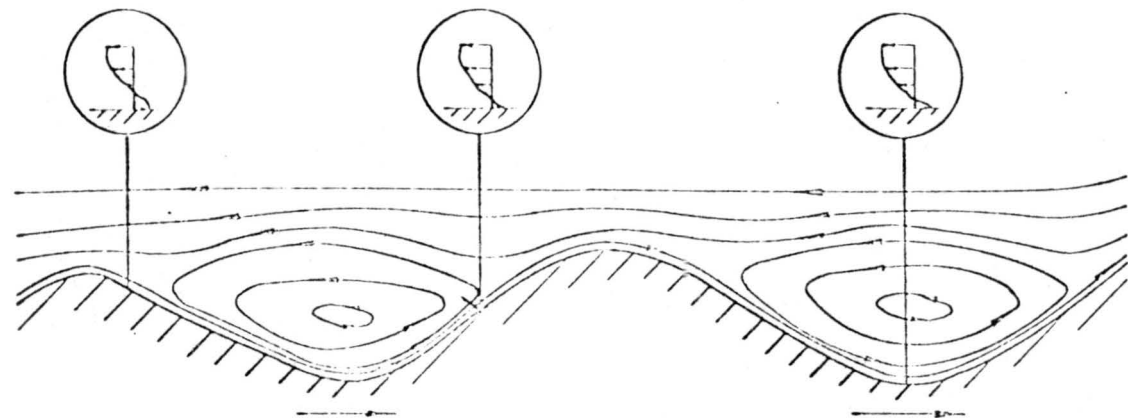
(a) $c < u_s + u_p'$ (b) $c > u_s + u_p'$ (c) $c > u_s + u_p'$

Fig. 59. Possible configuration of streamlines above progressive water waves.

Hess et al. (1968) have discussed the role of separation in the modification of air flow above small water waves. For example, the measurements of the mean flow indicate that the lower portion of the air velocity profile deviates from the logarithmic profile drawn over the data points at the upper portion of the boundary. In the presence of separation, the air flow in the separation region is decelerated by an adverse pressure gradient. Most of the drag then becomes form drag, the corresponding skin friction stress evidently becomes smaller than that without separation. Thus the velocity gradient in layers of air nearest the surface becomes less intensive.

Although the experimental program has been limited to measurements of mean velocity and longitudinal turbulent fluctuation of the air flow, we can still infer the shearing stress distribution qualitatively from the air flow pattern just described. By comparison of the sequence of mean velocity profiles and turbulent intensity profiles along water waves with those of a separated air flow (Arie and Rouse, 1956, and Chang, 1966), it was found that similarity exists between the air flows over water waves and solid obstacles. Arie and Rouse's and Chang's measurements of the turbulent intensity $\overline{u'^2}$ and shearing stress $\overline{u'v'}$ behind a normal plate or a ridge, indicate the profiles $\overline{u'^2}$ and $-\overline{u'v'}$ are similar in shape; i.e., the higher the values of $\overline{u'^2}$, the higher the absolute values of $\overline{u'v'}$, and the region of maximum turbulence and maximum shear coincide near separation with the mean streamline dividing the main flow from that in the zone of separation. Although the difference in geometric boundary makes the quantitative comparison of the turbulent data of this study and their data difficult, they still suffice to infer that the shearing stress is high around the wave crests and small in the troughs.

Liu et al. (1966) have shown that the calculated shearing stress profile over a rough solid surface where flow was known to be separating agrees with Klebanoff's result. Directly measuring $\overline{u'v'}$ over wind waves, Hess et al. (1968), and Karaki and Hsu (1967), however, found that the measured shearing stress was somewhat smaller than that over solid surfaces. Perhaps this dissimilarity is associated with the property of momentum and energy exchange between air and water. For further exploring the local Reynolds stresses along a particular wave, in principle, the technique developed in this study can be applied by fixing a crossed hot wire anemometer on the self-adjusting positioner.

Despite the fact that the dynamic nature of the water surface is different from that of a solid boundary, there are still many similar features between the air flows over the two types of boundary. The structure of mean air flow has been studied extensively over solid wavy models. In the following section, the measured local velocity profiles are compared with those obtained over water and over solid boundaries which simulate wind generated waves.

5.2.2 Comparison of measured local velocity profiles with other experiments

Schooley's (1963) measurements seem to be the only available local wind profiles along the actual wind waves. He measured the wind profiles above various places along waves generated by a 9-to 10-meter-sec⁻¹ wind in a short-fetch water-wind tunnel by evaluating photographs of small, neutrally buoyant soap bubbles. Schooley's data for the horizontal wind profiles at four points along an average wave are reproduced in Fig. 40a. He drew the average wave profile from the profiles of 30 individual waves, but the detailed description of

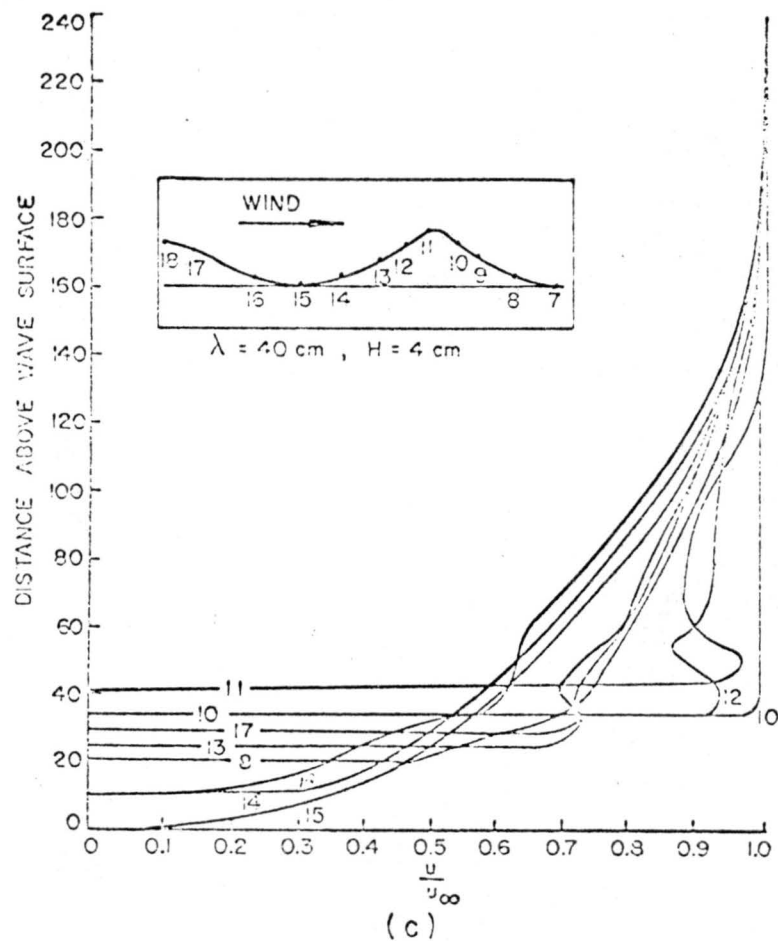
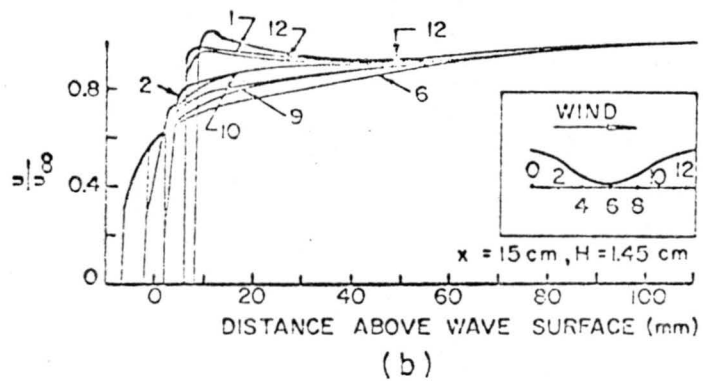
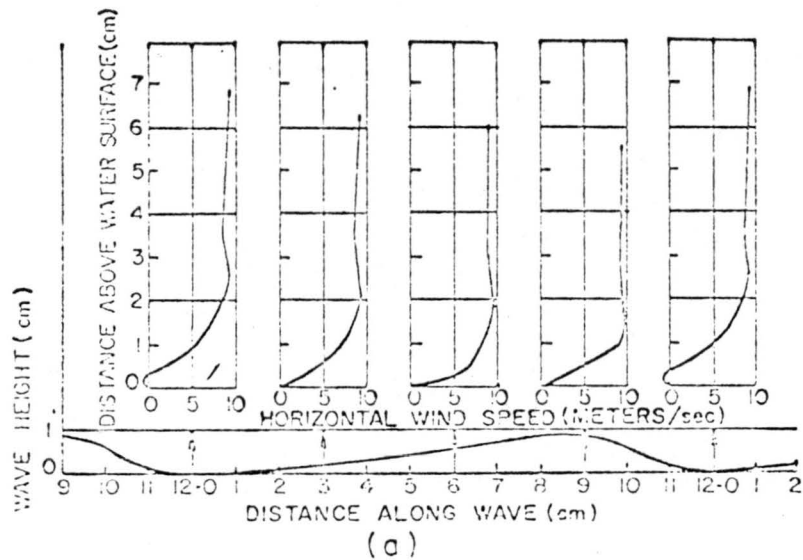


Fig. 40. Air velocity profiles above wavy surface (from Schooley, Motzfeld and Bonchkovskaya).

sampling and averaging process was not given. His ratio of H/λ is approximately equal to 0.08 which is slightly smaller than the values of average design waves adopted in this study. The ratio of average slopes on the windward side and lee side, in our notation that is \bar{p}_W/\bar{p}_L , is equal to 2.43; this is significantly different from the value of 1.25 for this study. At the level of about two wave heights from the mean water surface, Schooley found a maximum velocity "jet" at all points along the water waves. This result is not quite the same as the observations of this study. Here a stronger jet was found in the layer very close to the air-water interface, which only appears around the wave crests in contrast to Schooley's case. This difference may be the result of the different character of average wave form and a different method for analyzing the data. Despite these differences, the fact that he found separation of air flow behind the wind crests (leeward) is at least qualitatively consistent with the present observations.

Experiments over solid models were primarily designed to measure the pressure distribution along a wavy boundary and were performed by Stanton et al. (1932), Motzfeld (1937), Thijsse (1952), Bonchkovskaya (1955), Larras and Claria (1960), and Zagustin et al. (1966).

Zagustin et al. simulated the moving deformed boundary conditions in a flume with running water and a moving flexible boundary. This seems to be the closest simulation of flow over progressive water waves. Unfortunately, there are not enough velocity profiles along wave form available for detailed comparison. Among the quoted experiments, Motzfeld's and Bonchkovskaya's measurements on velocity profiles are most complete. Fig. 41b reproduces the air velocity profiles over

Motzfeld's nearly trochoidal wave model. Motzfeld's waves had a height of 1.45 cm and a height to length ratio of 0.096. His experiments were performed in a wind tunnel 20 cm high, 60 cm wide, and 600 cm long. The number of waves was 6 and the ambient velocity was 2 m-sec^{-1} . In Fig. 41b, Bonchkovskaya's result over trochoidal wave profiles with a wave height of 4 cm and a height to length ratio of 0.1 is also reproduced. Her experiments were made in a wind tunnel of hexagonal cross section with a width of 160 cm and a length of 14 m. There were seven waves and the ambient velocity was 5 m/sec.

Both of these results taken over solid boundaries reveal the existence of a strong jet around the crest of the waves. At the leeward side of crest, Motzfeld found that the maximum velocity of the jet was higher than the ambient value. This jet flow is very similar to the present findings over wind waves which resemble a trochoidal wave. Even with such qualitative correspondence, Motzfeld found no separation of air flow behind the wave crest as has been observed in this study. This difference may well be due to the symmetry of the solid model, and the low free stream velocity used in his study. Although Bonchkovskaya's model shows the existence of jet flow around the crest and separation behind the crest, the similarity between her mean velocity profiles along the wave and those observed over actual wind waves in this study is still far from complete.

5.3 Comparison of Experimental Results with Existing Theoretical Models

With the experimental results and the inferred physical picture of air flow over the waves, the applicability of the existing theoretical models for the energy transfer from turbulent air to small water

waves is examined. Since the measurements were made at a fixed fetch, the effort will be concentrated on checking the basic assumptions of the models rather than checking the actual growth rate. The comparison then can only be made on a qualitative basis.

In Phillips' model, there is no coupling between air and water motion and the statistical properties of the pressure fluctuations inherent in a turbulent wind are assumed to be independent of the wave generated and statistically homogeneous over the water surface. The experimental results indicate that the turbulent air in the vicinity of air-water interface responds to the appearance of the waves. Thus the basic assumption of neglecting all interactions between the pressure fluctuation in the air and water surface fails for the waves studied. This confirms other results found by different methods; for example, by Plate et al. (1968).

Since the air flow separates from the wave crests and the velocity profiles referred to the instantaneous water surface are substantially different from position to position, the flow configuration differs completely from that assumed by Miles (1957, 1962) in his calculations. Hence, Miles' linear theory now must be modified to accounting for the nonlinear effect associated with flow separation. The flow separation may also explain the discrepancy between the other observations and Miles' theoretical predictions. Indeed, the results of Hamada (1963), Hidy and Plate (1966), Snyder and Cox (1966) and Bole and Hsu (1967) suggest that the Miles theory systematically underestimates the input of energy from air to water compared with observed rates of growth. Hess (1968) measured the turbulent air flow over small water waves and found the effect of air flow by the

presence of the waves were not in any way predictable quantitatively if Miles' (1957) mechanism was assumed to be responsible for the disturbances added to the air turbulence already present.

Jeffrey's separation model has in the past been considered inapplicable because there was not any real proof of his postulate of separation of air flow, and the laboratory experiments on solid wave models, gave values of the pressure difference across the wave which are much smaller than Jeffrey's estimate for the sheltering coefficient s for the case of the smallest wind-velocity capable of raising waves. Since the present experimental results give evidence for separation of flow near the crest of wind waves, the pressure difference on the windward side and leeward side of waves can certainly produce wave growth. Unfortunately, no reliable pressure distribution along waves can be inferred as yet so no quantitative evaluation of the amount of energy transferred by this pressure difference can be made. However, the fact that separation would cause a larger phase shift and hence a larger exponential growth rate than Miles (1962) result predicts, seems to be consistent with the observations of growing wind waves by Hamada (1963), Hidy and Plate (1966), and Bole and Hsu (1967). At any rate, the importance of Jeffrey's theory in the stage of fully developed water waves cannot be overlooked.

Although Stewart's (1967) flow configuration is the consequence of the appearance of a critical layer which is the order of wave height away from mean depth, the basic mechanism drawn seems to be the same as Jeffrey's proposal. The streamline pattern suggested by Stewart is similar to that observed in this study over the waves with critical height in the sublayer. The experimental data thus at least

appears to favor Stewart's concept, though it is difficult to tell from Stewart's first paper what he really means by his form of leeward eddy, as compared with Jeffreys' idea or Miles' model.

Chapter VI

CONCLUSIONS

This investigation is a first direct attempt to measure the detailed structure of turbulent air flow above and between crests of progressing wind waves. A specially designed self-adjusting positioner allowed a velocity sensor to measure instantaneous air velocities at a fixed distance from a water surface with waves of a dominant frequency of 2 to 3 Hz. With the aid of a high speed digital computer, a special statistical technique was developed to sample and average simultaneous recordings of instantaneous air velocities and water waves. The mean velocity profiles, turbulent intensity profiles, and turbulent energy spectra above various positions along a defined average wave were obtained through ensemble averaging.

The measured mean velocity profiles were significantly different from position to position along water waves, but were substantially the same as the characteristics of turbulent air flow over a bluff body. A well-defined streamline pattern was obtained from the measured mean velocity profiles, the configuration clearly indicated the presence of a separation region below the crests. The air flow separated on the average from the water surface at a short distance behind the crest and reattached to the water surface somewhere on the windward face of the next crest. The observed flow configuration suggests that the well known shear flow mechanism proposed by Miles needs revising to be applicable for predicting the growth of fully developed small water waves where $U_* \approx c$. The experimental results seem to support the validity of flow configurations proposed by Jeffreys (1925) and more recently by Stewart (1967).

The profiles of $\sqrt{u'^2}$ show that the maximum intensity appears near the separation point. The region of maximum turbulence coincides with the onset of the streamline dividing the main flow from that in the zone of separation. The measured turbulent energy spectra at various points above water waves show that Kolmogoroff's inertial subrange exists everywhere.

In addition to finding the local properties above waves, two kinds of overall average properties of turbulent wind with reference to the mean water level also were obtained. One consisted of averages of the air properties at a fixed distance from the mean water level (fixed probe measurements) and the other was obtained by averaging the air properties at a fixed distance from the moving water surface (moving probe measurements). The results of fixed probe measurement are in agreement with what has been observed by previous investigators for both solid surfaces and water waves. The mean velocities obtained by the two methods are comparable, but the moving probe yields measurements of the fluctuations seen by the probes, which differ somewhat from those obtained with the fixed probe. The fixed probe measurements also yield lower spectral densities at low frequencies than the measurements from moving probe. A linear correlation method was applied to separate the turbulent velocity fluctuations from those due to probe and wave motions. Except for an apparently weak nonlinear effect, the linear correlation technique was fairly successful. In view of the experimental feasibility and the measurement error, the fixed probe measurement seems to be a better method to measure the overall air flow properties, through continuous sampling.

The water surface was found to consist of random asymmetrical waves with sharp crests and shallow troughs as determined from probability distributions of water elevation and its time derivatives. The experimental wave spectra indicate that Phillips equilibrium range holds only for $2 f_m < f < f_c$, where f_m is the dominant peak, and f_c is the frequency where surface tension and the dissipation caused by viscosity become important. The range is succeeded by an f^{-3} region characterizing the joint effect of gravity and capillary waves. The slope of spectral density between dominant and secondary peaks is close to -9 or -8.

This study showed that the self-adjusting positioner is a useful device for observing the local properties of air in the vicinity of the air water interface. In principle, the technique developed can readily be applied to measure the pressure or shear stress distributions above and around progressive wind waves, by fixing a fast response pressure sensor or a crossed hot wire anemometer on the self-adjusting positioner. This technique could also be applied to the surface layer in the water. Such measurements should greatly aid the understanding of the mechanics of air-water interaction.

REFERENCES

- Arie, M., and H. Rouse (1956); "Experiments on Two-Dimensional Flow over a Normal Wall," J. of Fluid Mech., Vol. 1, pp. 129-141.
- Benjamin, T. B. (1959); "Shearing Flow over a Wavy Boundary," J. of Fluid Mech., Vol. 6, pp. 161-205.
- Blackman, R. B. and J. W. Tubey (1958); "The Measurement of Power Spectra," Dover Publications, Inc., New York.
- Bole, J. B., and E. Y. Hsu (1967); "Response of Gravity Water Waves to Wind Excitation," Stanford University, Department of Civil Engineering, Tech. Rept. No. 79, Stanford.
- Bonchkovskaya, T. V. (1955); "Wind Flow over Solid Wave Models," Akademia Nank SSSR, Movskoi Gidrofizicheskii Institute, 6, pp. 98-106.
- Chang, S. C. (1965); "Velocity Distributions in the Separated Flow Behind a Wedge Shaped Model Hill," M.S. Thesis, Colorado State University, Fort Collins, Colorado.
- Corrsin, S., and A. L. Kistler (1954); "Free Stream Boundaries of Turbulent Flow," Natl. Adv. Comm. Aero., Tech. Note 3133.
- Cox, S. C. (1968); "Measurements of Slopes of High-Frequency Wind Waves," J. Mar. Res., Vol. 16, pp. 199-225.
- Deacon, G. E. R. (1963); "Present Status of Wave Research," in Ocean Wave Spectra, Prentice-Hall, New York.
- Drake, R. L. (1967); "Wind Generation of Waves on Open Channel Flow," Unpublished Ph.D. dissertation, Colorado State University, Fort Collins, Colorado.
- Eckart, C., (1953); "The Generation of Wind Waves in a Water Surface," J. of Appl. Physics, Vol. 12, No. 12, pp. 1485-1494.
- Grant, H. L., R. W. Stewart and A. Moillicet (1962); "Turbulence Spectra from a Tidal Channel," J. Fluid Mech., Vol. 12, pp. 241-263.
- Hamada, T. (1966); "An Experimental Study of Development of Wind Waves," Port and Harbour Tech. Research Institute, Rept. No. 2, Yokosuka, Japan.
- Hamblin, P. F. (1965); "Cup Anemometer Wind Observations over the Sea," M.S. Thesis, University of British Columbia, Vancouver.
- Helmholtz, H. (1868); "Uber Discontinuirliche Flussigkeitsbewegungen," Sober. Preuss. Akad. Wiss., pp. 215-228.

- Hess, G. D. (1968); "Turbulent Air Flow over Small Water Waves," Unpublished Ph.D. dissertation, University of Washington, Seattle.
- Hess, G. D., G. M. Hidy and E. J. Plate (1968); "The Structure of Turbulence in Air Flowing over Small Water Waves," Submitted to J. of Fluid Mech.
- Hidy, G. M. and E. J. Plate (1966); "Wind Action on Water Standing in a Laboratory Channel," J. of Fluid Mech., Vol. 26, pp. 651-687.
- Hinze, J. O. (1959), Turbulence, McGraw-Hill, New York.
- Holmes, P. (1963); "Wind Generation of Waves," Ph.D. thesis, University of Wales, Swansea.
- Jeffreys, H. (1925); "On the Formation of Water Waves by Wind," Proc. Roy. Soc. A., Vol. 107, pp. 189-206.
- Karaki, S. and E. Y. Hsu (1967); "An Experimental Investigation of the Structure of a Turbulent Wind over Water Waves," TRNo. 88 Dept. of Civil Engineering, Stanford University, Stanford.
- Kelvin, W. (1871); "The Influence of Wind and Waves in Water Supposed Frictionless," Phil. Mag., Vol. 4, pp. 368-374.
- Kinsman, B. (1960); "Surface Waves at Short Fetches and Low Wind Speed--A Field Study," Chesapeake Bay Inst., The John Hopkins University, Tech. Rept. No. 19.
- Kinsman, B. (1965); Wind Waves. Prentice-Hall, Inglewood Cliffs.
- Larras, H., and W. Claria (1960); "Wind Tunnel Research on Relative Wave and Wind Action." La Houille Blanche, Vol. 6, pp. 647-677.
- Lighthill, J. J. (1962); "Physical Interpretation of the Mathematical Theory of Wave Generation by Wind," J. of Fluid Mech., Vol. 14, pp. 385-398.
- Lock, R. C. (1954); "Hydrodynamic Stability of the Flow in the Laminar Boundary Layer between Parallel Streams," Proc. Camb. Phil. Soc., Vol. 50, pp. 105-124.
- Miles, J. W. (1957); "On the Generation of Surface Waves by Shear Flow," J. of Fluid Mech., Vol. 3, pp. 185-204.
- Miles, J. W. (1959); "On the Generation of Surface Waves by Shear Flow, Part 2," J. of Fluid Mech., Vol. 6, pp. 568-582.
- Miles, J. W. (1962a); "A Note on the Inviscid Orr-Sommerfeld Equation," J. of Fluid Mech., Vol. 13, pp. 427-432.

- Miles, J. W. (1962b); "On the Generation of Surface Waves by Shear Flow, Part 4," J. of Fluid Mech., Vol. 13, pp. 433-448.
- Miles, J. W. (1965); "A Note on the Interaction between Surface Waves and Wind Profiles," J. of Fluid Mech., Vol. 22, pp. 823-827.
- Miles, J. W. (1967); "On the Generation of Surface Waves by Shear Flow, Part 5," J. of Fluid Mech., Vol. 30, pp. 163-175.
- Moore, F. K. (1958); "On the Separation of the Unsteady Laminar Boundary Layer," International Union of Theoretical and Applied Mechanics, Boundary Layer Research, Symposium, Springer, Berlin.
- Motzfeld, H. (1937); "Die Turbulente Strömung an Wallingen Wänden," Z. Angew. Math. Mech., Vol. 17, pp. 193-212.
- Phillips, O. M. (1957); "On the Generation of Waves by Turbulent Wind," J. of Fluid Mech., Vol. 2, pp. 417-445.
- Phillips, O. M. (1966); The Dynamics of the Upper Ocean. Cambridge University Press, Cambridge.
- Plate, E. J. (1965a); "A Research Facility with Concurrent Air and Water Flows," La Houille Blanche, Vol. 6, pp. 595-598.
- Plate, E. J., and C. W. Liu (1965b); "The Velocity Field Downstream from a Two-Dimensional Model Hill, Part 1," Tech. Rept. CER65EJP-CWL14, Fluid Dynamics and Diffusion Laboratory, Colorado State University, Fort Collins, Colorado.
- Plate, E. J., and G. M. Hidy (1967); "Laboratory Study of Air Flowing over a Smooth Surface onto Small Water Waves," J. Geophys. Res., Vol. 72, pp. 4627-4642.
- Plate, E. J. (1967); The Analysis of Experimentally Determined Stationary Time Series, Unpublished Lecture Notes, Dept. of Civil Engineering, Colorado State University, Fort Collins.
- Plate, E. J., P. C. Chang and G. M. Hidy (1968a); "Experiments on the Generation of Small Water Waves by Winds." To be published in the J. of Fluid Mech.
- Plate, E. J., F. F. Yeh, and R. J. Kung (1968b); "Approximate Joint Probability Distributions of the Turbulence along a Hypothetical Missile Trajectory Downwind of a Sinusoidal Model Ridge," Tech. Rept., Fluid Dynamics and Diffusion Laboratory, Colorado State University, Fort Collins.
- Pond, S., R. W. Stewart and R. W. Burling (1963); "Turbulence Spectra in the Wind over Waves," J. Atmos. Sci., Vol. 20, pp. 319-324.

- Pond, S., S. D. Smith, P. F. Hoblin and R. W. Burling (1966); "Spectra of Velocity and Temperature Fluctuations in the Atmospheric Boundary Layer over the Sea," J. Atmos. Sci., Vol. 23, pp. 376-386.
- Roll, H. U. (1949); "Vergleichende Betrachtung und kritik von Windprofilmessungen an See." Ann. Meteorol., Vol. 2, pp. 71-78.
- Sandborn, V. A., and R. D. Marshall (1965); "Local Isotropy in Wind Tunnel Turbulence," Tech. Rept. CER65VAS-EDM71, Fluid Dynamics and Diffusion Laboratory, Colorado State University, Fort Collins.
- Schooloy, A. H. (1963); "Simple Tools for Measuring Wind Fields above Wind-Generated Water Waves," J. of Geophys. Res., Vol. 68, pp. 5497-5504.
- Shemdin, O. H., and E. Y. Hsu (1966); "The Dynamics of Wind in the Vicinity of Progressive Water Waves." Stanford University, Department of Civil Engineering, Tech. Rept. No. 66, Stanford.
- Shemdin, O. H. (1967); "Experimental and Analytical Investigation of the Air Velocity Profile above Progressive Waves." Stanford University, Department of Civil Engineering, Tech. Rept. No. 82, Stanford.
- Shemdin, O. H., and E. Y. Hsu (1967); "Direct Measurement of Aerodynamic Pressure above a Simple Progressive Gravity Wave," J. of Fluid Mech., Vol. 30, Part 2, p. 403.
- Snyder, R. L., and C. S. Cox (1966); "A Field Study of the Wind Generation of Ocean Waves." Sears Foundation; J. Marine Res., Vol. 24(2), pp. 141-178.
- Stanton, T. E., D. Marshall, and R. Houghton (1932); "The Growth of Waves on Water Due to the Action of Wind," Proc. Roy. Soc., Sec. A., Vol. 137, pp. 283-293.
- Stewart, R. W. (1967); "Mechanics of the Air-Sea Interface," Physics of Fluids, 10, 547-555.
- Takeda, A. (1963); "Wind Profiles over Sea Waves," J. Ocean. Soc. Japan, Vol. 19, pp. 16-22.
- Thijsse, J. T. (1951); "Growth of Wind Generated Waves and Energy Transfer," Gravity Waves, National Bureau of Standards, Circular No. 521, Washington, pp. 281-287.
- Ursell, F. (1956); "Wave Generation by Wind," Survey in Mechanics (ed. G. K. Batchelor and R. W. Davies), Cambridge University Press, Cambridge, 216-249.
- Weiler, H. S. (1966); "Direct Measurements of Stress and Spectra of Turbulence in the Boundary Layer over the Sea," Ph.D. Dissertation, University of British Columbia, Vancouver.

- Wiegel, R. L. (1964); Oceanographic Engineering, Prentice Hall, Englewood Cliffs.
- Wiegel, R. L., and R. H. Cross (1966); "Generation of Wind Waves," J. Waterways and Harbours Div., ASCE, Vol. 92, pp. 1-26.
- Wuest, W. (1949); "Beitrag zur Entstehung von Wasserwellen durch Wind," Z. Angew. Math. Mech., Vol. 29, pp. 239-252.
- Zagustin, K., E. Y. Hsu, R. L. Street, and B. Perry (1966); "Flow over a Moving Boundary in Relation to Wind-Generated Waves," Stanford University, Department of Civil Engineering, Tech. Rept. No. 66, Stanford.